EFFECT OF ADHESIVE STIFFNESS AND CFRP GEOMETRY ON THE BEHAVIOR OF EXTERNALLY BONDED CFRP RETROFIT MEASURES SUBJECT TO MONOTONIC LOADS

by

Benjamin Zachary Reeve

Bachelor of Science in Civil Engineering, University of Pittsburgh, 2003

Submitted to the Graduate Faculty of

School of Engineering in partial fulfillment

of the requirements for the degree of

Master of Science

University of Pittsburgh

2005

UNIVERSITY OF PITTSBURGH

SCHOOL OF ENGINEERING

This thesis was presented

by

Benjamin Z. Reeve

It was defended on

November 21, 2005

and approved by

Dr. Christopher J. Earls, Chairman and Associate Professor,
Department of Civil and Environmental Engineering

Dr. Amir Koubaa, Academic Coordinator and Lecturer,
Department of Civil and Environmental Engineering

Dr. Kent A. Harries, Assistant Professor,
Department of Civil and Environmental Engineering
Thesis Advisor

EFFECT OF ADHESIVE STIFFNESS AND CFRP GEOMETRY ON THE BEHAVIOR OF EXTERNALLY BONDED CFRP RETROFIT MEASURES SUBJECT TO MONOTONIC LOADS

Benjamin Z. Reeve, MS

University of Pittsburgh, 2005

Nine 10" (254 mm) deep, 6" (152 mm) wide and 186" (4730 mm) long concrete beams having three #4 longitudinal steel reinforcing bars as primary flexural reinforcement, were tested monotonically to failure under mid-point bending. Eight beams were strengthened with various arrangements of soffit-mounted externally bonded carbon fiber reinforced polymer (CFRP) and one beam was left as an unretrofit control specimen. A commercially available 4" (102 mm) wide, 0.055" (1.4 mm) thick preformed unidirectional high strength carbon fiber (CFRP) strip system was used in this study. Additionally, two commercially available adhesives, with significantly different moduli, were used to apply the CFRP strips to the concrete substrate. In order to investigate the effect of the CFRP strip width-to-soffit width ratio (b_f/b), four different strip arrangements were used.

All specimens tested in this program exhibited intermediate crack induced debonding behavior. The observed failures were generally bond-induced although concrete crushing was also observed in all cases. Increased flexural capacity and decreased flexural ductility was observed with increasing CFRP retrofit material area.

Observations indicate retrofit geometry has an influence on the overall retrofit performance. The FRP width-to-substrate width ratio (b_f/b) is shown to affect intermediate crack induced debonding behavior – an increase in strain at debonding is seen for specimens having a smaller b_f/b ratio. Additionally, superior performance in the form of higher general yield and

maximum loads, and higher deflections at these loads, was observed for the specimens having the lower modulus of elasticity adhesive.

The current American Concrete Institute (ACI) recommendation intended to mitigate debonding failure by limiting the allowable strain in the FRP (the limiting strain is referred to as ε_{fub}) is shown to be non-conservative, overestimating the strain where debonding becomes likely by two fold for the high modulus adhesive and less so for the low modulus adhesive. The equation for estimating ε_{fub} recommended by Teng et al. (2001), including the modifying k_b term, appears to provide appropriately conservative estimates of debonding for the specimens having low modulus adhesive although remains unconservative for the high modulus adhesive. This indicates that the nature of the adhesive should be included in the calculation of limiting strain. Proposed values for the coefficient k_b which accounts for the b_f/b ratio were found to generally underestimate the effect of the width ratio for the test specimens. Therefore, not only is the ratio b_f/b (as represented by k_b) a contributing factor to bond behavior, its contribution may be underestimated. Cover delamination (end peel debonding) was effectively mitigated in all specimens by extending the CFRP close to the support along the relatively long shear span.

TABLE OF CONTENTS

LIST OF TABLES

LIST OF FIGURES

NOMENCLATURE

Abbreviations

ACI	American Concrete Institute
CAA	conventional adhesive applied [FRP system]
CFRP	carbon fiber-reinforced polymer
FRP	fiber-reinforced polymer
LVDT	linear variable displacement transducer
NSM	near-surface mounted [FRP system]
PC	personal computer
RC	reinforced concrete

Notation

a	shear span of beam
A_c	concrete cross-sectional area
A_f	FRP cross-sectional area
A_s	steel reinforcement cross-sectional area
b	width of RC member (tension face)
b_f	width of FRP strip
E	modulus of elasticity
E_f	FRP modulus of elasticity
E_s	steel modulus of elasticity
f_c	compressive concrete strength
f_c'	28 day concrete compressive strength
f_u	ultimate strength of steel reinforcement

f_y	yield strength of steel reinforcement
G_a	adhesive shear modulus
$G_a t_a$	adhesive shear stiffness (modulus multiplied by thickness)
G_f	critical fracture energy
h	depth of concrete section
k_b	factor accounting for b_f/b in design
k_{b2}	value of k_b calculated for H2 or L2 (as appropriate)
$k_{bspecimen}$	value of k_b calculated for the specimen considered
k_L	factor accounting for $L_b < L_{bmax}$ in design
L	beam clear span length
L_b	provided anchorage bond length
L_{bmax}	effective anchorage bond length
n	number of plies of FRP
P	applied load at midspan
s	FRP spacing in slab retrofit
t_a	adhesive thickness
t_f	FRP thickness
V_c	shear strength
α	empirical constant
ε_{fu}	*in situ* rupture strain of FRP
ε_{fub}	strain in FRP when debonding occurs
$\varepsilon_{fubspecimen}$	debonding strain for the specimen considered
ε_{fub2}	debonding strain for H2 or L2 (as appropriate)
κ_m	ACI 440.2R strain reduction factor
$\rho_{equivalent}$	equivalent steel ratio

1.0 INTRODUCTION

1.1 INTRODUCTION

The need for repair and retrofit in infrastructure is a growing field. In most cases, repairing or retrofitting a deficient structure is more economically efficient than demolishing the existing structure and erecting a whole new structure, especially in cases where only a fraction of the structure is deficient.

Fiber Reinforced Polymer (FRP) composite materials have found uses in the repair and retrofit of concrete elements (Buyukosturk et al., 2004): (1) to increase axial, flexural or shear load capacities; (2) to increase ductility for improved seismic performance; (3) to increase stiffness for reduced deflections under service and design loads; (4) to increase the remaining fatigue life; and, (5) to improve durability against environmental effects.

Reinforced concrete (RC) members can be strengthened in flexure by bonding FRP to the tension face of the member. The FRP is applied with its fibers running longitudinally along the member, parallel with the greatest tensile forces, and is understood to be augmenting the capacity of the existing tension steel reinforcement. FRP strips should be fully bonded to members to engage composite action between the FRP and adjacent concrete. For the strengthening system to work at its utmost efficiency, there should be full composite action between the concrete and

FRP, causing the FRP to be fully engaged. This FRP to concrete bond is critical because this is where the transfer of stress will occur.

One of the benefits of using FRP to strengthen a concrete structure is that it is an environmentally durable material. It is non-corrosive and also has a high tensile capacity (8-10 times that of steel). It also has outstanding ratios of stiffness and strength to weight. FRP is lightweight which adds to its ease of handling and application. And due to the ease of the application process, extensive training is not required. Closures of structures during retrofit is also generally not required. FRP retrofit measures result in a minimum size and weight increase of the members it is applied to and therefore, has a minimal impact on a member's dead load and aesthetics. Externally bonded FRP composites have been shown to improve a structural member's performance under both monotonic and fatigue loading conditions by increasing ductility, load carrying capacity, and stiffness of the member (Buyukosturk et al., 2004). In applying FRP to a member these results can be achieved whether the member is initially cracked or uncracked.

FRP applied RC beams can fail by the crushing of concrete (before steel reinforcement yields), steel yielding followed by concrete crushing (before FRP rupture), steel yielding followed by FRP rupture, concrete cover delamination (in the plane of steel reinforcement), or FRP debonding at the concrete/FRP interface. Shear failure, resulting from increased flexural capacity is also a concern (Buyukosturk et al., 2004). Concrete crushing, cover delamination, FRP rupture and shear failure would be brittle failures. Concrete cover delamination and FRP debonding are undesirable failures which don't allow a retrofitted member to reach its potential flexural capacity. FRP materials remain relatively expensive so it is important to fully utilize the FRP strengthening system.

Debonding of the FRP can take place in or between any of the systems components. It can occur in the concrete at a weakened plane (such as at the level of internal reinforcement) or in a thin layer just next to (adjacent to) the adhesive line (cover delamination). Debonding failure could also occur at the concrete/adhesive interface (adhesion failure), in the adhesive itself (cohesion failure) or at the adhesive/FRP interface (adhesion failure). And because the FRP is a composite material itself, failure could occur through the FRP between the resin and the fibers (interlaminar shear failure). However, assuming proper selection of materials for the strengthening system, and proper surface preparation, the weakest part of the system should be in the concrete very near the adhesive line (fib, 2001).

Problems occur with FRP when debonding occurs. The FRP/adhesive/concrete region is a multi-component laminate system usually subject to mixed mode loading and eventual failure; thus debonding is a complicated phenomenon. FRP plate end debonding is not a consideration in the present work since the FRP will be extended nearly the full length of the beam, ending just short of the supports where the moment in the beam is negligible. Therefore plate end debonding will be mitigated and "midspan debonding" is expected to be the mode of failure in the experiments described in this work. Shear stresses at the concrete/FRP interface will control midspan debonding, although out of plane peeling stresses are recognized to severely cripple the shear capacity of the interface region.

Applying FRP to the soffit of a beam, or other tension face of a member, is a mechanically efficient method of retrofit. The FRP will be located at the furthest possible location from the compression zone, which will increase the member's stiffness and flexural strength. However, due to the additional reinforcing provided, tension face plates also result in a decline in member ductility, which can limit the ultimate strength of an FRP strengthened

member (Oehlers, 2001). FRP can also be applied to the sides of structural members for an increase in flexural and/or shear strength. In theory, deep side plates can increase a flexural member's flexural strength indefinitely without a loss in member ductility (Oehlers, 2001). Combinations of applying FRP to more than one face of a member can also be used (Oehlers, 2001).

The present study is "explicitly concerned only with soffit plating of simply-supported beams for simplicity in description, although the conclusions are applicable to tension face plating of beams in general" (Smith and Teng, 2001). Numerous studies have proposed strain (or stress) limits for FRP with the intent of mitigating debonding failures. Smith and Teng (2001) report that generally these models only show good predictive capacity of the data from which they were derived. Therefore, this study will focus on established consensus guidelines. It will be shown that the available consensus for mitigating debonding failures is weak and requires considerable further study. This thesis focuses on a few specific aspects of the work required to improve the understanding and design of bond.

1.2 SCOPE AND OBJECTIVE OF PRESENT WORK

The present study is one part of a larger study of factors affecting the bond behavior of adhesively bonded FRP flexural retrofit measures. Parameters addressed in this work are:

1. stiffness of the adhesive system.
2. geometry of the CFRP retrofit measures as measured by the ratio of CFRP width to soffit width (b_f/b).
3. the effects of fatigue loading conditions.

The former two parameters are the focus of this thesis. Additionally, the data presented here will form the control dataset for an ongoing study involving fatigue loading (Zorn, 2006). This study will also contribute significantly to an existing database of similar tests of FRP-strengthened system and will provide "control" specimens for future investigations carried out by Dr. Harries at the University of Pittsburgh and Dr. Kotynia at the University of Lodz in Poland.

1.3 OUTLINE OF THESIS

Chapter 2 of this work provides a detailed discussion of the background material necessary for the study of FRP bond in the context of flexural retrofit and a literature review of relevant material. The experimental program and fundamental results are presented in Chapter 3. Comparisons between specimens and assessment of effects of the parameters studied are presented in Chapter 4. Additionally, the data and findings of the present work are placed in the context of other international efforts. Finally in Chapter 5 the work is summarized, and recommendations (including those for future work), are presented.

1.4 NOTATION

The terms *retrofit*, *repair*, and *strengthening* are used interchangeably throughout this thesis in association with the application of the FRP to the beams in question. The author acknowledges that there is a difference in technical meaning of these three terms, however in the context of the present experimental study, these terms are interchangeable. The objective of a specific "real world" application provides the differentiation in the terms. When used in this writing, these three terms refer solely to the process of applying FRP to the specimens in question. Abbreviations and symbols used in this thesis are given on page ix.

1.4.1 Conversion Factors

This thesis reports all values in US units throughout and reports SI units in a secondary fashion. The following "hard" conversion factors have been used:

1 inch = 25.4 mm

1 kip = 4.448 kN

1 ksi = 6.895 MPa

Reinforcing bar sizes are reported using the designation given in the appropriate reference. A bar designated using a "#" sign (e.g.: #4) refers to the standard inch-pound designation used in the United States where the number refers to the bar diameter in eighths of an inch.

2.0 BACKGROUND AND LITERATURE REVIEW

The use of fiber reinforced polymer (FRP) materials for infrastructure rehabilitation is an exceptionally broad topic. The scope of this study and literature review addresses the use of FRP strips that are adhesively bonded to the soffits of RC flexural members. The application is intended for flexural strengthening and/or rehabilitation only and is referred to generically as conventional adhesive applied (CAA) FRP. The scope is further refined by restricting the discussion to the effects of monotonic loads. Fatigue loading is the subject of a companion work (Zorn, 2006) and is beyond the scope of this work. Nonetheless, much of this work can be applied to the repair and retrofit of RC members using FRP in general.

2.1 LIMIT STATE OF CAA FRP SYSTEMS

Reinforced concrete beams having CAA FRP retrofits may exhibit a number of limit states (Buyukozturk et al., 2004) as shown in Figure 2.1:

1. crushing of concrete (before steel reinforcement yields) resulting from the addition of FRP making the beam over reinforced in flexure;
2. steel yielding followed by concrete crushing (before FRP rupture);
3. steel yielding followed by FRP rupture;
4. concrete cover delamination (along the plane of steel reinforcement); or,
5. FRP debonding at the concrete/FRP interface.

Shear failure (Figure 2.1) may also occur due to the beam's increased flexural capacity, resulting from the addition of FRP flexure reinforcement and must be considered (Buyukozturk et al., 2004). Steel yielding followed by FRP rupture usually results when a relatively low FRP reinforcement ratio is used, while concrete crushing results from a relatively high FRP reinforcement ratio. Concrete crushing, cover delamination, FRP rupture and shear failure are all relatively brittle failures. Concrete cover delamination and FRP debonding are undesirable failure modes which occur prior to a retrofitted member reaching its full expected flexural capacity as governed by concrete crushing, steel yielding or FRP rupture.

Debonding of the FRP can take place in or between any of the FRP strengthening systems' components. It may occur in the concrete along a weakened plane such as at the level of internal reinforcement, or along a thin layer (so called "covercrete") adjacent to the adhesive line. Such failures are cohesive failures in the concrete substrate. Debonding failure may also occur at the concrete/adhesive interface (adhesive failure), in the adhesive itself (cohesive failure) or at the adhesive/FRP interface (adhesive failure). But because the FRP is a composite material itself, failure may also occur through the FRP between the resin and the fibers (interlaminar shear failure). However, assuming proper selection of materials for the strengthening system, and proper concrete surface preparation, the weakest part of the system should be in the concrete cover very near the adhesive line (fib, 2001). This limitation results from the fact that most retrofitting cases will deal with existing concrete. Therefore, to obtain the most efficient retrofit, all variables of the strengthening system which can be controlled should be made superior to the one variable that cannot be controlled: the existing concrete.

2.2 DEBONDING

In experimental studies, debonding is observed to be a dominate failure mode (Smith and Teng, 2001; Kotynia and Harries, 2006; Sebastian 2000, for example, all provide reviews of extensive experimental programs). Once the FRP strip begins to debond from the member it can no longer fully contribute to the member's load carrying capacity. Therefore debonding is an undesirable failure because the retrofitted member is not allowed to reach its full flexural capacity. Thus, FRP strengthening systems are often used inefficiently. Efficiency of the FRP can be measured as the ratio of the FRP strain that may be obtained *in situ* to the rupture strain of the FRP. FRP rupture would be considered 100% efficiency of the FRP strip. Debonding failures greatly limit the strains observed in the FRP (Kotynia and Harries, 2006). Thus it is important to understand, and hopefully mitigate debonding failures. There are two main areas where debonding can initiate: at the end (curtailment) of the FRP reinforcement, or within the span of FRP reinforcement. Smith and Teng (2001) report that while end debonding is more commonly observed in the experimental literature, intermediate crack induced debonding (often referred to as "midspan debonding") will, for the most part, determine beam flexural strength in practical applications where flexural elements will typically have relatively long shear spans (as discussed below).

FRP debonding will occur in sudden bursts and not as a continuous process (Harries et al., 2003). It will usually initiate in areas of stress concentrations, which are commonly due to material inconsistencies and/or the location of existing cracks in the concrete substrate. Mixed mode (Modes I and II) loading conditions on FRP strengthening systems has been found to initiate debonding in flexural members anywhere that a moment gradient is present (non-zero shear) (Task Group on Bond, 2005). Debonding will then propagate along the length of the beam following the path of least resistance. Propagation is dependant on loading conditions, material

properties (strength and elasticity), and the fracture properties at the debonding crack tip. Therefore, failure in the FRP/RC beam system can take place through materials or at the interface of two materials and may "jump" from one "plane" to another. Less than adequate surface preparation or FRP application is the usual cause of interface failure. Assuming specimens are carefully prepared, then most of the failures should propagate through the concrete substrate. However, combinations of material failures and interface failures can be found in a single debonded member (Buyukozturk et al., 2004). Such a failure is reported in the present work and, as discussed in Chapter 3 (shown in Figure 3.29), is attributed to flaws (insufficient resin wet-out) in the FRP product.

2.2.1 Plate End Debonding

Plate end debonding initiates at the end (curtailment) of the FRP strip and propagates toward midspan (Figure 2.2). This debonding can be characterized as interfacial debonding or concrete cover delamination (although, cover failure is not exactly a "debonding" failure, as it occurs away from the bond line, it is referred to as such). Both of these plate end debonding types are caused by high stresses at the end of the FRP strips.

2.2.1.1 Interfacial Plate End Debonding

Interfacial debonding occurs at the interface between the RC substrate and the FRP strip. This is caused by high normal stresses that occur at the end of the plate which cause a tension failure in the system's weakest component (usually concrete). A thin layer of concrete will usually come off with the FRP strip indicating that the adhesive-to-concrete bond is stronger than the concrete tensile capacity (Smith and Teng, 2001).

2.2.1.2 Concrete Cover Delamination

Experiments by Smith and Teng (2001) found that concrete cover delamination is the more common end debonding failure, as opposed to interfacial debonding. Concrete cover delamination is initiated by cracks forming in the concrete, on the beam soffit, at the end of the FRP strips. These cracks form because of the sudden termination of the FRP strip which causes high normal stresses and high interfacial shear in the flexural tension region of the beam. At the soffit of a beam in flexure, an axial strain exists in the beam, which increases with distance from the supports. The end of the FRP strip is "free" and has zero axial strain at its curtailment. The adhesive and FRP strip then try to "catch up" and achieve the same strain as that of the directly adjacent concrete substrate. So even when there is a very small distance between the end of the FRP strip and the support, there may still be significant stresses being imparted in the adhesive and FRP. This stress will cause a Mode II failure in which the opposing sides of a crack will slide against each other (in the plane of the crack) in opposite directions. The "free" ends of the FRP strip also have zero curvature, unlike the concrete beam which does have curvature under loading. As the beam bends, the FRP attempts to remain straight and a vertical stress (normal to the FRP) is put on the adhesive which pulls on the concrete substrate cover (Sebastian, 2001). This will cause Mode I cracking in which the opposite sides of a crack open and separate away from the crack plane, and each other. An element of peeling stress (Mode I) is present throughout a member and is proportional to the shear to moment ratio (i.e.: increasing near supports) (Kotynia and Harries, 2006).

These two types of stresses at the end of the FRP strip induce the mixed mode failure of end debonding (Sebastian, 2001). A crack will propagate vertically at first to the elevation of the steel reinforcement (a weak plane) and then continue horizontally away from the beam end (toward midspan), separating the concrete cover from the rest of the beam (Smith and Teng,

2001) as shown in Figure 2.2. These cracks propagate towards midspan as this is where the highest induced moment occurs (Kotynia and Harries, 2006). This flexural peeling will eventually detach the entire FRP strip along with the cover concrete and leave the beam unretrofit (Oehlers, 2001). Such debonding is found to occur in beams with low span to depth (a/h) ratios or in beams where the FRP is not terminated close to the supports (Kotynia and Harries, 2006). It should be noted that "concrete cover delaminations can also occur at other points along the beam besides the FRP termination point" (Harmon et al., 2003).

The overall level of stress causing plate end debonding is proportional to flexural induced stress, thus, this effect is mitigated very near the supports where the axial strain at the soffit is very low. Therefore, one method of mitigating end plate debonding is to simply extend the FRP very close to the support (Sebastian 2001). It has also been shown that the addition of mechanical anchors (Brosens and Van Gemert, 2001; Buyukozturk et al., 2004) or transverse FRP "straps" (Maeda et al., 2002; Kotynia and Harries, 2006) also effectively mitigate plate end debonding by resisting the dominating normal stresses of Mode 1 loading.

2.2.2 Midspan Debonding

Midspan debonding occurs in the shear span of the beam and is initiated at locations of high moment-to-shear ratio and propagates in the direction of decreasing moment (toward the support) as shown in Figure 2.3. Large shear stresses are developed along the interface in order for tensile stresses to be transmitted from the FRP through the adhesive and concrete substrate to the internal reinforcing steel. The satisfactory transmission of stresses through the strengthening system must be reliable in order to ensure the continued participation of the FRP in the force-resisting system and to ensure the desired failure behavior. Failure will occur in one of the systems layers, usually in the concrete as it has a lower ultimate strength than the FRP or

adhesive. This failure through concrete will be brittle, propagating rapidly with little warning (Sebastian, 2001).

In the beam shear span, near the location of the maximum moment, diagonal flexural cracks or flexural-shear cracks will form in the concrete substrate (Figure 2.3). Midspan debonding will initiate at the toes of these cracks. Cracking in the concrete will cause axial stress variations in the areas of uncracked concrete and consequently in the attached FRP (higher stresses at the cracks, with stresses decreasing away from the cracks). These stress variations must be transferred across the interface as shear (Mode II) stresses.

There are other factors that can cause crack-inducing stress variations in the system. Axial stress variations may also result from the following:

1. spreading of a load path in the beam span;
2. corroded steel reinforcement which will have a smaller effective cross-sectional area and less of a bond with surrounding concrete; and,
3. yielded steel reinforcement in portions of the FRP-debonded region.

All of these stress variations may result in debonding, and because debonding causes additional stress variation, midspan debonding is a self-propagating process (Sebastian, 2001). It was also reported by Sebastian that the beam will become more flexible as steel reinforcement begins to yield and FRP debonding propagates. This will result in higher deformations of the beam, which will lead to further debonding through a combination of Mode I and Mode II failure.

FRP debonding will initiate at the base of diagonal flexural/flexural-shear cracks and propagate in the direction of decreasing moment (towards the nearest support) as shown in Figure 2.3. This debonding begins where FRP strips span over a shear and/or flexure crack in the

concrete member. Where these cracks intersect an FRP plate, a Mode I-induced crack will propagate away from midspan right next to and parallel to the FRP strip. This will usually occur as a brittle failure through the concrete (Oehlers, 2001). While plate end debonding (cover delamination) will involve the full depth of the concrete cover, midspan debonding typically will not. The crack will propagate through the "covercrete" so close to the concrete/FRP interface that usually no concrete aggregate will be in the fracture plane (Kotynia and Harries, 2006). When this horizontal fracture occurs through the concrete cover, the part of the concrete cover that has debonded will remain with the adhesive and FRP strip, while the concrete substrate on the other side of the fracture will remain an integral part of the beam (Sebastian, 2001).

Midspan debonding is categorized as occurring in two steps: initiation and propagation. During initiation, at the toes of the beam's flexural cracks, inclined cracks begin to appear through the concrete cover. As the beam continues to deflect due to an increasing loading, the inclined cracks open and the bonded FRP is stretched across the opening. As the inclined cracks continue to open, the concrete cover on the side of the inclined cracks closest to the span center will be at an increasingly lower elevation relative to the concrete cover on the side of the crack furthest from the span center. Therefore, local bending begins to occur in the FRP at the inclined crack opening as shown in Figure 2.3. The concrete cover on the side of the crack closest to center span will continue to drop in elevation relative to the other side of the crack and the FRP will be pushed in front of the dropping concrete cover. The section of the FRP being pushed will pull the FRP on the other side of the crack, and cause a stress in the adhesive interface that is normal to the FRP (Mode I). This normal stress, in conjunction with the large shear stresses (Mode II) induced by shear transfer between FRP and concrete will eventually peel the FRP and a thin layer of the concrete cover away from the beam as described above. This will create a

horizontal crack, starting at the inclined crack, which will propagate towards the end of the FRP. At first, the crack will propagate relatively steadily, with a steady increase in load. Since fracture initiation requires greater energy than fracture propagation, the debonding may be arrested as the stress falls or even as the debonding passes across another crack in the concrete substrate. Thus with increasing applied load, the debonding propagation appears somewhat intermittent. Eventually, a critical condition is reached and the debonding crack will instantly propagate along the remaining length of the FRP, completely detaching it from the beam, taking with it a thin layer of concrete and sometimes even the concrete wedges between the flexural and inclined cracks (Sebastian, 2001).

As described, there is a peeling stress (Mode I) associated with midspan debonding in addition to the shear stress (Mode II). It has been shown (Wan et al. 2004; Aidoo 2004) that Mode II bond toughness, as measured by the critical fracture energy (G_f) at the concrete/FRP interface, is significantly reduced in the presence of even a small amount of Mode I stress. Thus, the presence of very low peeling stresses will still have a very significant effect on bond performance (Kotynia and Harries, 2006).

2.3 SYSTEM COMPONENT MATERIALS

The adhesive stress distribution between the FRP and the concrete substrate is dependant on the relative stiffness of: the concrete, the FRP, and the bond transfer mechanism between the concrete substrate and the FRP. The bond transfer mechanism is a function of the shear stiffness of the bond (adhesive) layer and the effective shear stiffness of the concrete shear layer that transfers forces from the FRP to the concrete substrate. In this system, concrete is typically the limiting factor in stress transfer (Harmon et al., 2003).

2.3.1 Concrete

Concrete strength (f_c) is a factor affecting bond capacity; however it is generally the tensile strength of the concrete and not necessarily the compressive strength of the concrete that affects bond behavior. Various researchers have identified different relationships in terms of how concrete strength affects bond behavior and there is presently no consensus (Task Group on Bond, 2005). Concrete strength is not a parameter considered in the present study.

2.3.2 Adhesive

For the desired performance of a member to be realized, the FRP retrofit must be effectively bonded to a member's tension face. Stiffer adhesives are generally viewed as being superior (Saadatmanesh and Ehsani, 1990) although these are now beginning to be associated with debonding failure in FRP applications. Maeda et al. (2002) report experiments using a highly flexible adhesive, termed "flexible layer" which has a modulus, E = 1 MPa (145 psi)[1]. They conducted bending tests and found that this flexible layer helped to increase the overall maximum bending load by relieving stress/strain concentrations in the retrofit. The flexible layer improves the bond between the FRP retrofit and concrete substrate, and adequately transmits stresses between the two. Stresses were distributed more uniformly thru the adhesive to the concrete substrate, so extreme stress variations, which could lead to debonding, were not as prevalent as with a more traditional, stiffer adhesive layer. As a result, the entire strengthening system is much more efficient due to improved bond behavior. The more flexible the adhesive layer is the less likely debonding is to occur, while stiffer adhesive layers are more prone to debonding (Kotynia and Harries, 2006). The Task Group on Bond (2005) reports that adhesive shear stiffness ($G_a t_a$) affects bond behavior in a complex manner. Increasing the shear stiffness

[1] Material properties for the flexible layer were reported by Maeda et al. (2002) as Elastic Modulus: 1N/mm^2 = 1 MPa. These properties are very soft relative to available commercial epoxy systems.

results in a higher strength capacity, but a lower interfacial ductility and lower fracture energy which results in poor stress transfer and a poor distribution of stresses. Sebastian (2001) stated that a more flexible adhesive layer will allow shear deformation of the adhesive to occur. This will allow the plate to "slip" slightly in relation to the beam, which allows for a more gradual axial stress/strain gradient and results in improved FRP efficiency. In the present study, two adhesive systems, having shear moduli differing by about a factor of two, are used as discussed in Chapter 3.

2.3.3 Retrofit Laminate

Steel plates have been used for repair and retrofit of tension faces on RC members for some time (Brosens and Van Gemert, 2001; Ali et al., 2001; Smith and Teng, 2001; Sebastian, 2001). However, unidirectional FRP is now favored due to its greater strength, greater resistance to corrosion, and increased ease of transportation and application (Sebastian, 2001). "Recently, steel plates are increasingly being replaced by FRP plates due to their superior structural tailorability, high resistance to environmental degradation, high stiffness to weight, and high strength to weight ratios" (Ali et al., 2001). Ali et al. performed tests of RC beams with different retrofit plate materials. Through theoretical calculations and test observations, the materials with lower moduli (values of E), i.e. the "less stiff" materials, achieved higher ultimate moments than did those with higher moduli. Therefore, it was concluded that FRP strips (which have a lower modulus than steel) are more desirable when compared to steel plates, in terms of a retrofit beam's flexural capacity. A less stiff laminate will act similarly to a less stiff adhesive in that a lower modulus of elasticity will help alleviate stress/strain concentrations. "Laminates with greater stiffness are prone to delamination" (ACI, 2002). This means the danger of delamination is lower for FRP than for steel plates (Brosens and Van Gemert, 2001). FRP laminates are also

less intrusive on the structure as they are thinner and may cover less area than steel retrofit due to the FRP's higher tensile strength.

The effect of retrofit laminate modulus discussed above essentially demonstrates that material discontinuity results in stress concentrations and thus potential debonding failure. Basic mechanics indicates that a retrofit material is best suited to a substrate when their moduli (and other properties such as coefficient of thermal expansion) are most similar. In cracked RC, however, the tensile behavior is controlled by the reinforcing steel, thus a repair material having similar properties as the reinforcing steel represents an efficient alternative. This argument appears to contradict the findings discussed above, underlining the uncertainty, even within the research community, about the nature of debonding behavior. In the present study, FRP modulus is not a parameter of study.

2.4 EXPERIMENTAL STUDIES OF DEBONDING BEHAVIOR

Many empirical models have been developed which can be applied to debonding of FRP strengthened RC beams. Smith and Teng (2001) report a large number of models which are classified into three types: shear capacity based models, concrete tooth models, and interfacial stress based models. The shear capacity based models appeared to provide the most accurate predictions of debonding behavior, the concrete tooth models were next, and finally the interfacial stress models were found to provide the least helpful predictions. It is noted that all of the models reported were empirically calibrated against specific experimental data and were thus reported to be very accurate at predicting the behavior against which they were calibrated. The accuracy of all reported models degraded considerably when applied to other experimental data.

Some of the models reported by Smith and Teng were taken from strength models using steel-plated RC beams. “It is not unreasonable to expect that models developed for steel-plated beams may well be applicable to FRP-plated beams” (Smith and Teng, 2001). In fact, the most universally accurate beam models were those developed or adapted from steel-plated beam models. It is suggested that the reason for the improved accuracy of steel-plated models is that steel-plated RC beams are recognized to be governed by bond behavior, with the steel plate generally remaining elastic. Smith and Teng (2001) reported that while only simply supported beams with plates or strips applied to their soffits were considered, the conclusions can be applied to the strengthening of a member’s tension face in general.

Buyukozturk et al. (2004) performed experiments in which the cross-sectional area (A_f) of the FRP strip was kept constant while the thickness of the strip (t_f) was varied. Consistent with fundamental mechanics, it was observed that “debonding potential was shown to increase significantly with increasing FRP thickness”. This observation reflects two issues: 1) a thinner plate of the same area is wider and thus has a larger bonding surface resulting in lower bond stress; and 2) the thicker plate results in a larger moment arm between the resultant FRP force and the interface stress transfer; this moment arm induces additional stresses at the interface.

Ahmed et al. (2000) also conducted experiments using FRP of varying thicknesses. The width of the FRP and area of internal reinforcing steel (A_s) were kept constant while the FRP thickness, and therefore area (A_f), varied. It was found that an increase in strength did not directly correlate with an increase in the FRP area. That is, greater flexural capacities were found with greater A_f/A_s ratios, but only to a ratio of about 0.08, after which an appreciable increase in capacity was not observed. An increase in the A_f/A_s ratio was also found to cause an increase in the shear stress at the end of the FRP laminate. This ratio of 0.08 should not be taken as a

standard of optimum FRP performance for all cases; it is merely the optimum for the given test parameters[2]. For the general case of optimum performance from an FRP strengthened RC beam, much more should be taken into account then merely the A_f/A_s ratio.

"ACI Committee 440's guide for surface-bonded fiber-reinforced polymer (FRP) reinforcement limits the allowable strain in the surface-bonded FRP to a value that is inversely proportional to the stiffness of the FRP. This limit is intended to prevent bond failure between the surface-mounted FRP reinforcement and the concrete substrate. The guide does not, however, consider the properties of the resin system bonding the fiber to the concrete, the concrete strength, or the extent to which the concrete is subjected to flexural cracking in ensuring adequate bond performance. These properties are critical to bond performance" (Harmon et al., 2003). These critical characteristics of design have not been included because an all-encompassing bond behavior model has not yet been developed. Design of reinforcing with FRP is based on a FRP threshold stress or strain, inversely related to the FRP stiffness. However, threshold strain is dependant on more than just FRP stiffness. It is proposed that stress-based models which include the parameters of bond layer properties, concrete strength, extent of flexural cracking, FRP stiffness and shear and bending moments at critical sections be developed. While modeling of steel reinforcement is based on anchorage (development length), these FRP reinforcement models should be stress-based models due to the brittle failure behavior of the FRP and the adhesive (Harmon et al., 2003).

[2] In the case presented, the modular ratio E_f/E_s was approximately 1.27.

2.5 MITIGATION OF DEBONDING

Mitigation of debonding is difficult in that the behavior of the concrete/FRP interface is complicated by the specific characteristics of the composite strengthening system and the prevalence of mixed mode failures (Task Group on Bond, 2005).

Plate end debonding is brittle but easily prevented, so it is important to take steps to mitigate such failures. “Hence, it is suggested that although much research effort to date has been invested on end peel [end plate debonding], in practice midspan debond may be critical in many single span simply supported FRP-plated concrete bridges” (Sebastian, 2001). A review of experimentally observed debonding behavior clearly indicates that midspan debonding is critical for beams whose FRP retrofitted shear span-to-depth ratio exceeds 2.7 (Kotynia and Harries, 2006). CAA FRP retrofit should therefore extend at least 2.7 times the beam depth along the shear span beyond the location of maximum moment in order to mitigate plate end debonding. Most practical RC beams will permit this retrofit length as most efficiently designed flexural members will have a shear span-to-depth ratio ranging from 5 to 10.

2.5.1 Poor Mitigation of Debonding

U-shaped anchorages (lateral reinforcement) can be used on beams by way of wrapping the sides and soffit of a beam in an attempt to hold the longitudinal FRP retrofit tight against the beam soffit and resist Mode I failures. Maeda et al. (2002) tested this practice and found that such anchoring to the beam hinders the performance of the flexible layer (adhesive) by limiting its deformation qualities and thereby limiting the full benefits of the flexible layer. RC beams with U-shaped anchorage were found to have lower strains in the retrofit material at the time of retrofit failure than when no U-shaped anchorage was provided. Additionally, smaller deformations were observed due to the U-shaped anchoring not allowing full deformation of the flexible layer, which also limits the benefits of the flexible layer.

Contrary to the findings of Maeda et al. (2002), Kotynia and Kaminska (2003) observed an improvement in debonding behavior when transverse FRP was applied to "clamp" the longitudinal CAA FRP system (in this study, a traditional stiff adhesive system was used). On average, FRP strains at debonding failure increased 21% when transverse FRP was applied. However, the overall load carrying capacity of the beams was only nominally improved.

Another disadvantage of providing transverse FRP reinforcement is that in order for it to be engaged, deformation must be present in the member. But by the time the transverse reinforcement is engaged, peeling stresses will have already developed at the concrete/FRP interface. A study of plate end debonding failures (where Mode I stresses are dominate) in FRP reinforced beams with transverse FRP reinforcement indicated only a 20% increase in FRP strains and beam capacity prior to the initiation of plate end debonding. In no reported cases did the provision of transverse FRP at the curtailment of the longitudinal FRP actually mitigate eventual plate end debonding (Kaminska and Kotynia 2000).

It is therefore recommended that lateral FRP reinforcement be neglected as a form of debond mitigation because even very low peeling stresses will have a very high effect on bond performance (Kotynia and Harries, 2006). According to Brosens and Van Gemert (2001), "In most cases, it is strictly speaking not necessary to provide an anchoring system when (FRP) sheets are used for concrete strengthening."

Along these same lines, internal stirrups (shear reinforcement) are also equally ineffective in mitigation of debonding. Similar to the lateral FRP reinforcement, the stirrups cannot be engaged until deformation due to cracking has occurred. Stirrups may be used to increase a beam's resistance to debonding associated with shear load; however tests have shown that stirrups do not significantly accomplish this (Ali et al., 2001; Oehlers, 2001). The stirrups cannot

be engaged until they are stretched, at which point a diagonal crack will have already formed and debonding will have already begun. In general the effect of stirrups may be neglected in analysis of FRP strengthened RC beams. However, some FRP retrofit measures that have low axial stiffnesses, may be flexible enough that the stirrups can somewhat engage before shear crack induced debonding begins (Oehlers, 2001).

2.5.2 Effective Mitigation of Debonding

The effective bond length (different from internal reinforcement development length) of the FRP is important because there is a limit (L_{bmax}) at which increasing the bonded length is no longer beneficial to bond strength (Task Group on Bond, 2005). As discussed above, it is important to extend the FRP to regions of near zero moment (near supports in simply supported beams and to points of contraflexure in continuous beams) in order to mitigate end debonding.

In the case of a simply supported beam, stresses causing plate end debonding are directly related to the distance from a support (near zero moment region) to the end of the FRP strip. The best mitigation against plate end debonding is to extend the FRP strips nearly to the supports, which will also ensure a firm anchoring of the FRP (Sebastian, 2001). In placing the retrofit, the shorter the unretrofit length is, the higher the force (loading on beam) required to cause delamination is (Brosens and Van Gemert, 2001). Buyukozturk et al. (2004) also determined that debonding potential was shown to decrease, along with an increase in ductility, as the FRP strips were lengthened in the case of simply supported beams. Sebastian (2001) states that the stresses that will induce the mixed mode failure of end debonding are found to increase with increased distance between the FRP strip termination and the location of the supports.

When thin FRP strips are used for retrofit, the maximum tensile stress (normal to the FRP) and resultant tensile force are very small. As thicker FRP strips are used, these forces increase and mechanical anchoring systems must be added to resist the tensile forces that would cause

Mode I failure (Brosens and Van Gemert, 2001). Overall, such a practice uses additional unnecessary materials in an inefficient manner. Anchoring systems result in a higher application cost, and anchorage can interfere with the benefits obtained from using a flexible layer (Maeda et al. 2002). Therefore, minimizing FRP thickness is an effective and efficient mitigation against bond failure. The practice of tapering the thickness of the FRP in regions of lower moments can also be utilized to mitigate debonding potential (Harries et al., 2003). Finally, thinner strips are also more flexible, which reduces Mode I forces near locations of local bending in the FRP.

As stated previously, using materials with a lower modulus of elasticity is effective as mitigation for debonding. Using a stiff plate results in much less ductile behavior and will cause high stresses in the adhesive at the termination of the FRP (Sebastian, 2001). Stiffer plates will also resist local bending at cracked sections of the beam, increasing Mode I forces. These are all reasons why the more flexible FRP composite is chosen over steel. Oehlers (2001) also states that in cases of steel retrofitting, the steel will typically yield across a crack before debonding would occur, although this behavior is largely dependent on the ratio of steel reinforcing. Such behavior is inefficient as the steel retrofit would yield prior to the existing concrete failure. Brosens and Van Gemert (2001) state that, "for (FRP) sheets, the risk of [plate end debonding] is much lower than for steel plates." Decreasing the stiffness of the FRP laminate will also allow an increase in the FRP strain limit (Task Group on Bond, 2005).

Avoiding low span-to-depth ratios (short shear span) is another effective means of mitigation for plate end debonding (Kotynia and Harries, 2006). Midspan debonding, on the other hand, is usually observed for higher span-to-depth ratios as longer shear spans result in higher moments for the same applied loading.

2.6 DESIGN OF FRP RETROFITS TO ADDRESS DEBONDING

The dimensions of the member to be strengthened and the FRP are relevant to FRP strengthening performance. The FRP width-to-member width ratio (b_f/b) affects how load is distributed between the two materials and how efficiently they are used. Section properties will also play a role as the cross-sectional strain gradient will affect shear transfer (Task Group on Bond, 2005).

As with all design, loading on the member will affect FRP performance depending on whether the load is static or dynamic and whether it is monotonic or cyclic in nature. The applied shear-to-moment ratio and moment gradient are also factors affecting behavior and are a function of whether the loads are concentrated or distributed on the span (Task Group on Bond, 2005).

When predicting the maximum allowable load on an FRP strengthened RC beam, many approaches are currently being proposed. In all approaches it is important to have an understanding of the concrete/FRP interfacial shear and normal stresses, as these are the cause of most debonding failures (Smith and Teng, 2000). It is also important to design with a maximum allowable FRP tensile strain in mind which should be sufficiently low to ensure that debonding will not occur.

Concrete softening has been observed to occur when concrete is subject to shear forces. However, when addressing this behavior, mathematical models of retrofit beam behavior become complex. It is therefore suggested that energy-based fracture mechanics (neglecting softening behavior) be used as this will "bring some good understanding of the mechanics of FRP-strengthened structures that is useful for FRP reinforcing design" (Yuan et al., 1999). Here, an interfacial fracture energy (G_f) approach is suggested, as discussed below.

2.6.1 Current Recommended Design Practices

ACI 440.2R (ACI, 2002) provides an equation for the maximum FRP strain to mitigate debonding failure:

$$\varepsilon_{fub} = \kappa_m \varepsilon_{fu} \tag{2.1}$$

Where ε_{fu} is the FRP design rupture strain and the value of κ_m is:

$$\kappa_m = \begin{cases} \dfrac{1}{60\varepsilon_{fu}}\left(1 - \dfrac{nE_f t_f}{2{,}000{,}000}\right) \le 0.90 \quad for\ nE_f t_f \le 1{,}000{,}000 \text{ lb/in.} \\ \dfrac{1}{60\varepsilon_{fu}}\left(\dfrac{500{,}000}{nE_f t_f}\right) \le 0.90 \quad for\ nE_f t_f > 1{,}000{,}000 \text{ lb/in.} \end{cases} \quad \text{(US units)} \tag{2.2}$$

$$\kappa_m = \begin{cases} \dfrac{1}{60\varepsilon_{fu}}\left(1 - \dfrac{nE_f t_f}{360{,}000}\right) \le 0.90 \quad for\ nE_f t_f \le 180{,}000 \text{ N/mm} \\ \dfrac{1}{60\varepsilon_{fu}}\left(\dfrac{90{,}000}{nE_f t_f}\right) \le 0.90 \quad for\ nE_f t_f > 180{,}000 \text{ N/mm} \end{cases} \quad \text{(SI units)} \tag{2.2}$$

where n = number of plies of FRP

E_f = FRP modulus of elasticity

t_f = FRP thickness

The ACI equation does not account for concrete strength, any internal steel reinforcement, adhesive layer properties or the FRP width to member width ratio (b_f/b). The equation is also markedly unconservative for design work (Task Group on Bond, 2005).

fib Bulletin 14 (2001) suggests the direct use of shear-stress slip relationships in predicting debonding failure. It recommends critical bond stress and slip parameters, which have been determined from experimental analysis. Bulletin 14 then gives three approaches to predict debonding failure. The first approach determines the maximum allowable axial load in the FRP and the length required to anchor this load. It also introduces a k_b factor, which accounts for the

b_f/b ratio (see below). The second approach determines a critical (unfavorable) crack pattern and the bond (adhesive) stresses this pattern would cause. Bond stresses rise between flexural cracks and these stresses are then transferred to the FRP. This second approach determines the maximum stress the FRP can have transferred to it, and determines an anchorage length differently than the first approach. The first two approaches can be used to derive allowable tensile strain equations for the FRP in order that debonding is mitigated. The third approach is concerned with checking that the concrete can withstand the FRP/concrete interface shear stress resulting from loading. If the interface shear stress is kept below the concrete bond shear strength, then cracks will not develop to cause debonding, and strain in the FRP will cause no concern. The UK's Concrete Society TR55 (Concrete Society, 2004) uses an approach similar to the first approach in Bulletin 14, only with more generalized factors.

The Japan Society of Civil Engineers (2001) uses an FRP stress equation which includes an interfacial fracture energy (G_f) term for the FRP/concrete interface. G_f can be determined from experimental results, and therefore, many factors and aspects of design can be empirically accounted for with this approach. The ultimate stress found can then be used to derive the allowable FRP tensile strain. However, testing and experimentally determined values are not always conducive to the design process.

Teng et al. (2001) proposed an FRP stress limit equation which also uses a k_b factor and an equation for required anchorage length. Later, Teng et al. (2004) proposed a limiting FRP strain equation, with a revised k_b factor. Although both equations are highly empirical the results are generally conservative. It is noted, however, that it is difficult to separate the effects of the k_b factor from the impact of other parameters in the equations.

Because very low peeling stresses will still have a very high effect on bond behavior, it is believed that limiting the allowable strain in the FRP is the best way to design FRP retrofit for RC beams (Kotynia & Harries, 2006).

All of these different approaches for computing maximum allowable FRP strain to mitigate debonding failures are plotted in Figure 2.4. In each case, where appropriate, the strains are plotted using the upper ($b_f/b = 1$; solid lines) and lower bound values ($b_f/b = 0$; dashed lines) of the parameter k_b. The importance of the k_b factor is very clear in the variation it offers the curves plotted in Figure 2.4. It is also noted that all curves fall below that of the ACI 440.2R curve (bold black curve), which is the current US standard.

Also shown in Figure 2.4 is some debonding data for some experimental beams (Harries and Kotynia, 2006). The important thing to note is the exceptional variability observed and the resulting non-conservative design resulting from many of the recommendations, particularly that of ACI 440.2R (bold black curve).

2.6.2 Recommended "Best Practice" for Mitigating Debonding

An assessment of existing bond models using available experimental data (Task Group on Bond, 2005) has resulted in the following recommendations:

"End peel" debonding should be addressed through specific requirements for anchorage and/or the location of the FRP curtailment. Thus, strain limits are not necessarily an appropriate approach to addressing end peel debonding in flexural members. End peel debonding is beyond the scope of the present work.

The use of allowable strain limits as an indirect way of evaluating in-span bonding is appropriate in a design context. Strain limits are easily incorporated into the design methods used for reinforced concrete members. The ACI Task Group on Bond (2005) recommends the adoption of the equation proposed by Teng et al. (2001) with a reduction to the leading

calibration factor, α. This reduction results in a conservative equation for strain limit to mitigate debonding:

$$\varepsilon_{fub} = \alpha k_b k_L \sqrt{\frac{\sqrt{f_c'}}{E_f n t_f}} \text{ (SI Units)} \qquad (2.3)$$

where f_c'= 28 day concrete compressive strength

$$k_b = \sqrt{2 - \frac{b_f}{b} \Big/ 1 + \frac{b_f}{b}} \qquad (2.4)$$

$$k_L = \begin{cases} 1 & L_b \geq L_{b\max} \\ \sin\left(\pi L_b / 2 L_{b\max}\right) & L_b < L_{b\max} \end{cases} \qquad (2.5)$$

The effective length of the FRP system is given in Equation 2.6; every effort should be made to ensure that $L_b > L_{b\,max}$:

$$L_{b\max} = \sqrt{\frac{E_f n t_f}{\sqrt{f_c'}}} \qquad \text{(SI units)} \qquad (2.6)$$

The α term in Equation 2.3 is an empirical constant dependent on loading and member geometry. Teng et al. (2001) recommend a value of α = 1.1. The ACI Task Group on Bond (2005) recommends that α = 0.9 results in generally conservative results. This relationship is adopted in the present work as it is most representative of available data.

It is noted that the Task Group (2005) report is a dynamic document affected by recent research and the need to establish consensus. As of November 2005, it is likely that Equation 2.5 will be removed in favor of a requirement that $L_b > L_{b\,max}$. Additionally the role of the b_f/b ratio in relation to midspan debonding remains unclear. Task Group consensus as of November 2005

favors removing Equation 2.4[3]. The findings of this study will contribute significantly to establishing the required consensus in this regard.

2.6.3 Factor Accounting for b_f/b Ratio

As is made clear in the previous sections, the ratio of FRP retrofit width (b_f) to beam soffit width (b) is believed to have a significant impact on the debonding behavior. Approaches to addressing this behavior are driven by the need to develop a factor (identified as k_b) by which to multiply the maximum allowable FRP strain (to set a limit for mitigating debonding). The k_b factor is a function of beam geometry and in its simplest form (Equation 2.7, below), represents an assumed 45^o "spreading" of shear stresses away from the edges of the FRP strip. This spreading is of course limited by the edges of the beam. However, this interpretation of the k_b factor is likely too simplistic, so the factor has been empirically revised by a number of researchers and documents, as shown below.

Lateral spreading of shear stresses likely contributes to the effect quantified by the parameter k_b. Equally, the confinement provided by the presence of concrete beyond the edges of the FRP strip also likely affects the value of this parameter. Quattlebaum (2003) has hypothesized that the k_b factor may also be calibrated to account for the significant shear lag effect present in thin elements (Timoshenko and Goodier, 1987). This effect will be briefly investigated in the present work.

Beyond simple load spreading, the value of k_b is essentially empirical. Values of k_b recommended by various sources are given below. In no case may b_f/b exceed 1 and the theoretical lower limit is $b_f/b = 0$ (no retrofit). For practical beam applications b_f/b will likely exceed 0.25. For slabs, this lower limit may be $b_f/s = 0.10$, where s, the spacing between FRP strips, replaces b.

[3] Dr. Harries is the chairman of the ACI Task Group on Bond and provides this information in the interest of clarity.

Teng et al. (2001):

$$k_b = \sqrt{2 - \frac{b_f}{b} \Big/ 1 + \frac{b_f}{b}} \tag{2.7}$$

fib (2001) and Concrete Society (2000):

$$k_b = 1.06\sqrt{2 - \frac{b_f}{b} \Big/ 1 + \frac{b_f}{400}} \geq 1.0 \quad \text{(b and } b_f \text{ in mm)} \tag{2.8}$$

Teng et al. (2004):

$$k_b = \sqrt{2.25 - \frac{b_f}{b} \Big/ 1.25 + \frac{b_f}{b}} \tag{2.9}$$

Quantifying the effect of b_f/b is a major objective of the present study.

2.6.4 Precautions

In calculations involving strain, it is important to know the intended location where strains are obtained or where limits are going to be applied. This is important in identifying strains at critical locations of the FRP. Local bending in the FRP is much more pronounced after steel yield, but is also slightly present before steel yield. If local bending in the FRP is occurring at cracks or if there is a mechanical restraint due to locking of concrete on opposite sides of a debonding failure plane, the strains in the middle of the FRP can be quite different from the strains present on the external surface of the FRP. Therefore, shear stresses of up to 200% in error have been shown, due to only obtaining strains from a single surface of the FRP (Sebastian, 2001). This effect is pronounced in proportion to the thickness of the FRP system.

When doing any type of repair or retrofit analysis it is important to consider the effects of the initial load (prior to FRP strengthening) on a member when designing the strengthening system. In practice, the FRP will generally be applied to deficient members, and therefore a cracked section analysis may be required (fib, 2001). Also, retrofit measures are usually only

active in resisting transient live loads, since the dead load of the structure is typically present during the retrofit procedure.

Finally, exposure to the environment is also important in determining a lasting design as the adhesives used in applying FRP to concrete (and to a lesser extent, the FRP itself) are highly susceptible to environmental degradation (Task Group on Bond, 2005).

"Bond layer resins tend to harden with age. The shear modulus of the resin (G_r) must be the [most critical] value likely to be obtained during the life of the structure" (Harmon et al., 2003).

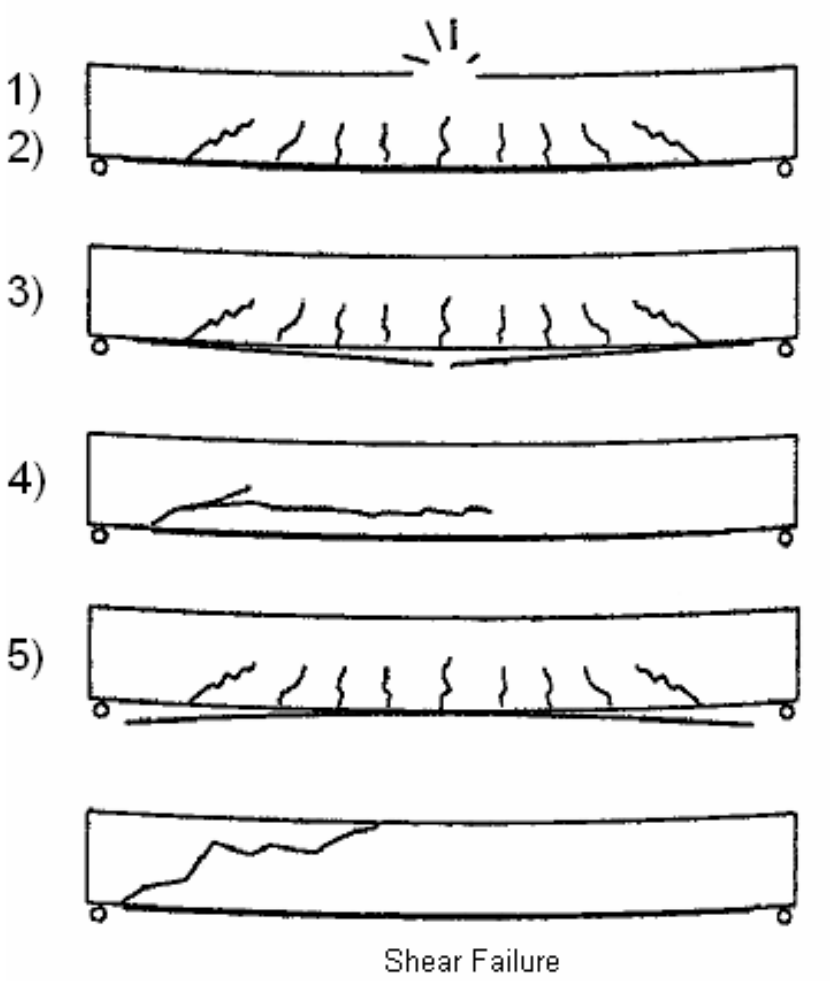

Figure 2.1 Limit states of CAA FRP applications (Buyukozturk et al., 2004).

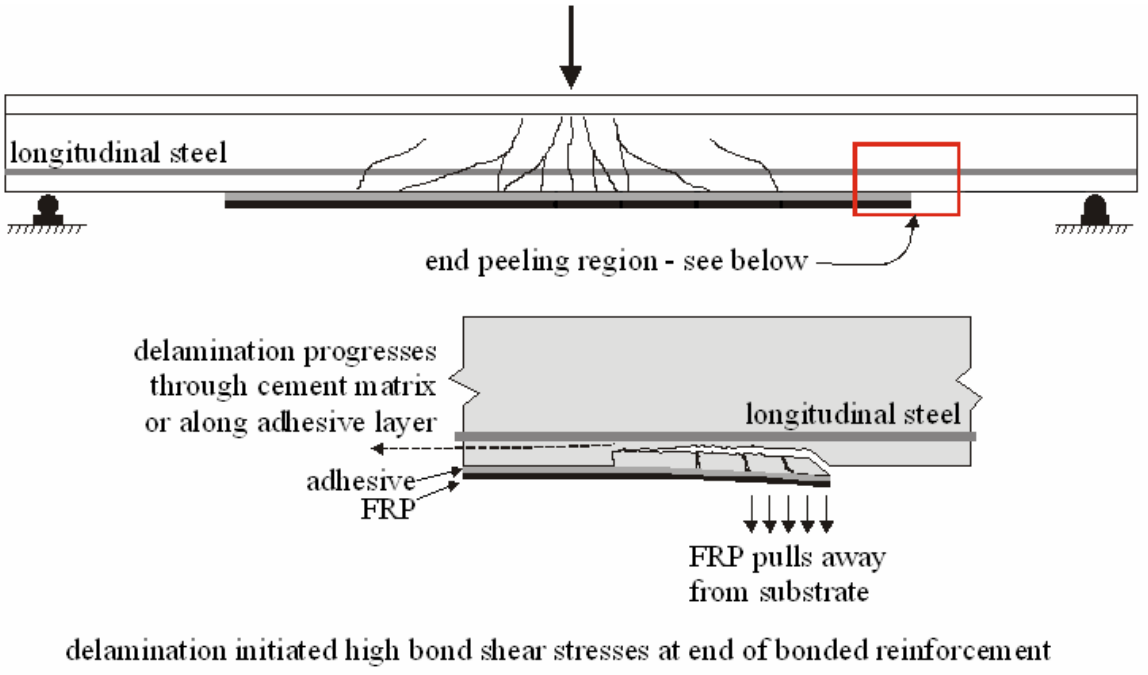

Figure 2.2 Concrete cover delamination typical of plate end debonding (figure adapted from Aidoo, 2004).

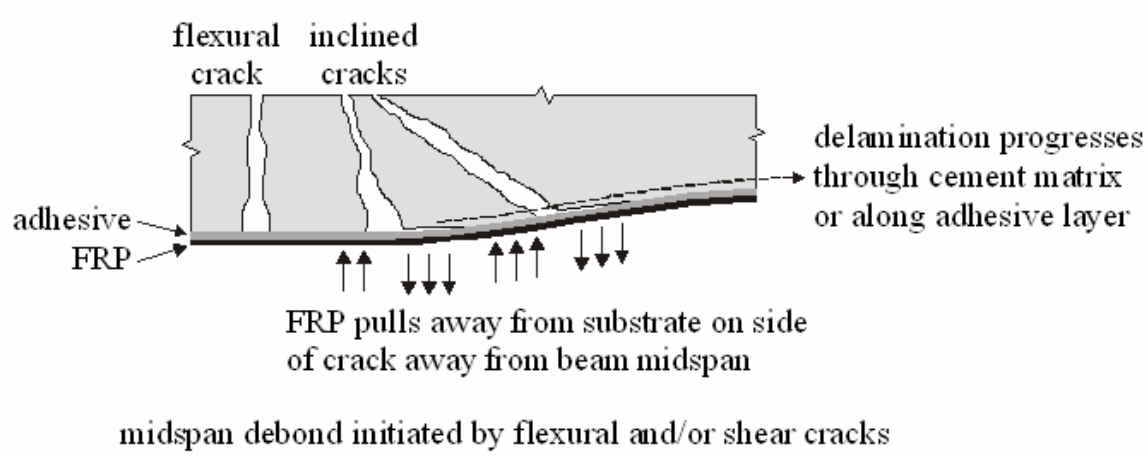

Figure 2.3 Intermediate crack induced (midspan) debonding (figure adapted from Aidoo, 2004).

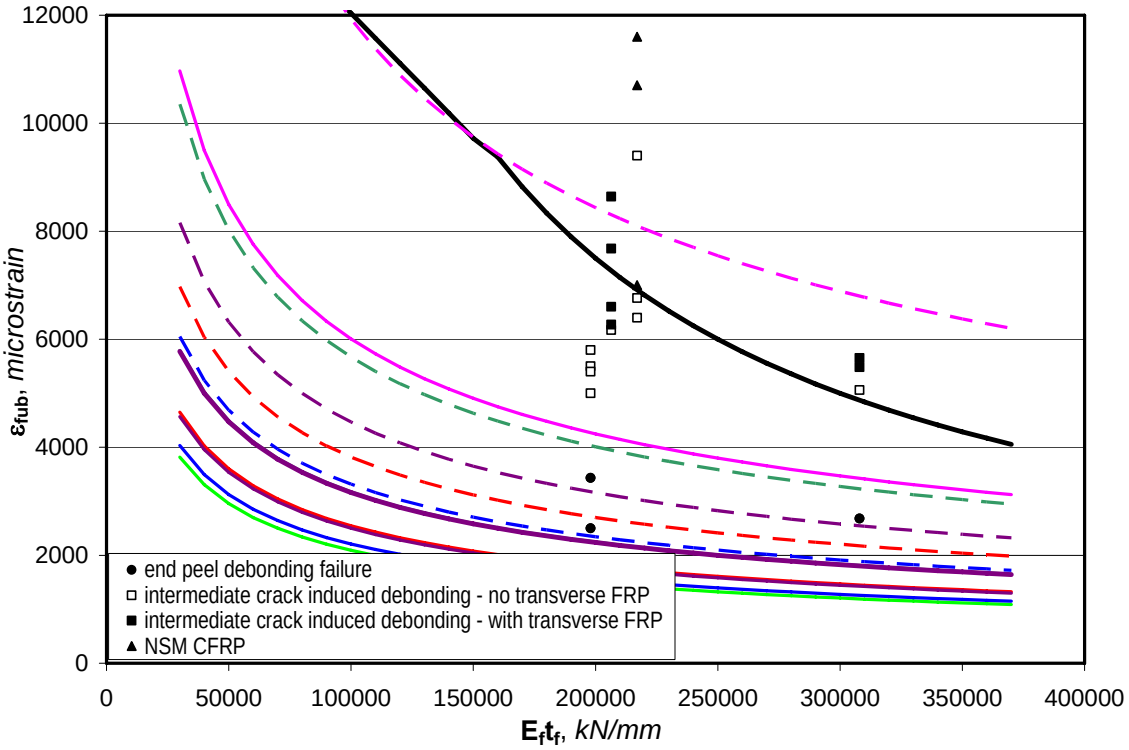

Figure 2.4 Various recommended limiting debonding strain relationships. Lines having the same color represent the same recommended relationships for the bounding cases of $b_f/b = 1$ (solid lines) and $b_f/b = 0$ (dashed lines). The ACI 440.2R relationship (Equation 2.1) is shown as the bold black curve.

3.0 EXPERIMENTAL PROGRAM

This chapter reports details of the entire experimental program. Primary results and definitions of the methods used to obtain these are also reported.

3.1 TEST SPECIMENS

Twenty-four identical reinforced concrete beams were cast from a single batch of Type I Portland cement concrete in the structural laboratory at the University of Pittsburgh (Figure 3.1). This work reports tests of nine of these including Specimen C, a control specimen which will be used in this and two other ongoing studies (Zorn, 2006 and Minnaugh, 2006). The beams were 10" (254 mm) deep, 6" (152 mm) wide and 186" (4730 mm) long. Eight beams were strengthened with various arrangements of carbon fiber reinforced polymer (CFRP) as described below, and one beam was left as an unretrofit control specimen (Specimen C).

Three #4 longitudinal steel reinforcing bars were used in each beam as primary flexural reinforcement resulting in a longitudinal tensile reinforcing ratio of 1.0%. An additional two #3 bars were provided as top bar reinforcing to allow the beams to be safely inverted for CFRP application and instrumentation. The beams were sufficiently long that no shear reinforcement was required (i.e.: V_c > maximum expected shear). The beam details are shown in Figure 3.2. The #4 reinforcing bars had a yield strength of 62.2 ksi (429 MPa) and a tensile strength of 96.8

ksi (667 MPa) as determined from tension tests conducted in compliance with ASTM E8 and reported in Table 3.1.

In addition to the beams, twenty-eight 6" (152 mm) diameter by 12" (305 mm) tall cylinders were prepared from the same batch of concrete. The beams and the cylinders were then cured under wet burlap and plastic sheeting for seven days. Twenty-eight day compressive strength (f_c') was determined to be 3384 psi (23.3 MPa). Following testing, cores were removed from some beams for *in situ* compressive strength testing. The compressive strength of concrete determined form cores tested at an age of 245 days was 5308 psi (36.6 MPa).

A commercially available 4" (102 mm) wide, 0.055" (1.4 mm) thick preformed unidirectional high strength carbon fiber (CFRP) strip system was used in this study (Fyfe, 2005). The material properties reported in Table 3.2 are those provided by the manufacturer. Two different commercially available adhesives were used in this study (SIKA, 2005). The adhesives were selected such that they had significantly different moduli. The Sikadur 30 product - the higher modulus adhesive – is a typically used product for CFRP retrofit measures. There are no known uses of Sikadur 23 – the lower modulus adhesive – in CFRP bonded retrofit applications. Nonetheless, as indicated by the results, Sikadur 23 provided excellent adhesive properties and appears to be suitable for FRP retrofit applications. Half of the retrofitted beams used the low modulus adhesive and the other half of the beams used the high modulus adhesive. Material properties of the adhesives are given in Table 3.3.

3.2 RETROFIT MEASURES

Eight different retrofit measures were examined in this research in that two different adhesive systems were used with each of four different CFRP strip arrangements. In order to

investigate the effect of the CFRP strip width-to-soffit width ratio, b_f/b, four different strip arrangements were used. Each strip arrangement was installed using both the low modulus adhesive and the high modulus adhesive. All beam dimensions remained constant between test specimens. The CFRP strip was cut and applied in widths of 1" (25 mm), 2" (51 mm), and 4" (102 mm) as shown in Figure 3.3. The case of two 1" (25 mm) wide strips having a clear spacing of 2" (51 mm) was also analyzed. Details of application are outlined in the following sections.

3.3 APPLICATION OF THE CFRP TO THE TEST SPECIMENS

The CFRP strips were applied to the soffits (tension face) of all test specimens except the control test specimen. In all retrofit cases, the CFRP was extended over the entire beam span to just short of the supports. In no cases did the CFRP extend over the supports. The manufacturer's instructions for installation were followed during the application of the adhesive and the CFRP. Retrofitting of the beams occurred after the beams had sufficiently cured (31 days) so as not to have an impact on the application process. All test specimens were turned upside-down and the application process occurred "down hand" as opposed to overhead which would likely occur in field application.

3.3.1 CAA Application of Preformed Composite Strip

The soffits of the beams were mechanically prepared with a wire brush to CSP3 (ICRI, 1997) and all loose material was removed with compressed air. The wire brush was used to expose the aggregate and remove surface laitance and dirt from the beam soffit in order to assure a satisfactory bond between the adhesive and concrete substrate.

The desired CFRP widths were cut from a 4" wide roll of CFRP. The strips were cut transversely to length with aviation snips and longitudinally with a utility knife and a straight edge. The

prepared CFRP strip, of approximately uniform width, was then cleaned of debris and stray fibers.

Following the manufacturer's specifications, the adhesives were mixed with the following epoxy resin to hardener ratios by weight:

Low Modulus Adhesive (Sikadur 23): 2:1

High Modulus Adhesive (Sikadur 30): 3:1

Adhesive was applied to the beam soffit and to the CFRP strip using a putty spatula. The CFRP strip was then applied to the beam soffit. The strip was pushed firmly into the adhesive to remove any voids in the adhesive and assure a uniform application. Hard rubber rollers were used to apply a uniform pressure and ensure a uniform adhesive thickness, squeezing excess adhesive out along the edges of the CFRP. The outer face of the CFRP strips was covered with masking tape, prior to the adhesive application, to ensure a clean surface for eventual strain gauge application.

3.3.2 Quality Control Verification of Adhesive Bond

Quality of adhesive bond to the concrete was assessed using a series of standard pull-off tests (ASTM D4541, 1995). These tests were conducted by a summer undergraduate intern and are reported here for completeness. Sixteen pull-off tests were conducted: four on each of the specimens having 4" (102 mm) CFRP applications (L4, H4 and L4F and H4F, reported by Zorn, 2006). In all cases the pull-off tests resulted in failure through the substrate concrete indicating a sound adhesive bond. The average pull-off capacity for the specimens having the H adhesive was 413 psi (2.85 MPa) and the average pull-off capacity for the specimens having the L adhesive was 384 psi (2.65 MPa). The tensile capacity of the concrete that may be used for design is estimated to be $4\sqrt{f_c'} = 232$ psi $\left(0.33\sqrt{f_c'} = 1.60 \text{ MPa}\right)$. The reported bond strengths of the

adhesive materials are provided in Table 3.3. These observations indicate that the adhesive was sound in all cases and pull-off was governed by the substrate concrete capacity. The *in situ* adhesive capacity may be reported as "at least" the test values reported.

3.4 SPECIMEN DESIGNATION

Test specimens were designated as follows:

XY

where X indicates the adhesive used (Table 3.3):

C = unretrofit control specimen

L = low modulus adhesive (Sikadur 23)

H = high modulus adhesive (Sikadur 30)

and Y indicates the retrofit detail (Figure 3.3):

1 = single 1" (25 mm) wide CFRP strip

2 = single 2" (51 mm) wide CFRP strip

2x1 = two 1" (2 x 25 mm) wide CFRP strips

4 = single 4" (102 mm) wide CFRP strip

3.5 TEST SETUP

All nine specimens were tested monotonically to failure under mid-point bending. Loading was applied by an MTS hydraulic actuator with a maximum capacity of 50 kips (222 kN) and a maximum stroke of 4" (102 mm). The test specimens were supported over a clear span of $178^{5}/_{8}$" (4537 mm). For all tests, 3" x 6" x ½" (76 mm x 152 mm x 13 mm) neoprene pads having a durometer hardness of 65-75, were used to support the beam ends, and in the middle of

the beam beneath the actuator as a loading pad. Under the neoprene pads at each support was a steel plate and rocker to produce a "simply supported" condition. A photograph of the test setup is shown in Figure 3.4.

3.6 INSTRUMENTATION

Nine instrumented beams were tested in this research. Each beam was instrumented with four electrical resistance strain gauges on the middle #4 reinforcing bar, numbered north to south: (1), (2), (3) and (4), as indicated in Figure 3.5. The eight retrofitted beams had an additional four electrical resistance strain gauges placed on the CFRP at the same axial locations along the beam as the reinforcing bar strain gauges. These were numbered north to south: (5), (6), (7) and (8) as shown in Figure 3.5. The two beams retrofitted with 4" wide CFRP strips had an additional four strain gauges added across the width of the CFRP to investigate the distribution of strain transversely across the strip. Strain gauges (9) and (10) were added at the location of strain gauge (5) and strain gauges (11) and (12) were added at the location of strain gauge (8). The strain gauge instrumentation is presented in Figure 3.5 and detailed strain gauge locator diagrams accompany each of the load vs. strain plots presented in Figures 3.14 thru 3.24.

Generally, many flexural cracks will form in the midspan of a beam, making it hard to determine exactly where cracks causing debonding will occur. This makes it difficult to determine the exact best place to put strain gauges on the FRP when collecting debonding data (Sebastian, 2001). Therefore, strain gauges will be put in the middle 36" (91.44mm) of all of the beams, as the middle of the beam, directly below the loading, is where flexural cracking is expected to begin.

The vertical deflection of test specimens C and L1 was measured at midspan using a linear variable displacement transducer (LVDT). The vertical deflection of the remaining test specimens, L2, L2x1, L4, H1, H2, H2x1 and H4, was measured using a draw wire transducer as shown in Figures 3.4 and 3.5. In all cases, vertical deflection at midspan was measured from the soffit of the specimen. Deflection data from the actuator's internal LVDT was also recorded and used to determine the compliance of the test setup and to correct midspan deflection data when necessary.

The 50 kip (222 kN) capacity load cell on the actuator recorded the applied load. Loads, deflections and strains were measured and recorded simultaneously using a PC-driven data acquisition system. Data was recorded at a rate of 2 samples per second for all monotonic tests.

3.7 TEST PROCEDURE

The nine reinforced beams were tested under mid-point bending over a clear span of $178^{5}/_{8}$" (4537 mm). One of the nine specimens was used as a control specimen, and was not retrofitted with CFRP. All nine specimens were tested monotonically under increasing midspan displacement to failure. Midspan displacement of the specimen was controlled to travel from near 0 to 4" (102 mm) in 30 minutes, providing a constant deflection rate of 0.13" (3.4 mm) per minute.

3.7.1 Specimen L4

Specimen L4 was used as a vehicle for the testing of an innovative instrumentation scheme which is part of a Carnegie Mellon University research effort (Kim et al., 2006). To accommodate this testing, the testing scheme for L4 was slower and required the loading to be held at various increments. In the case of L4, the loading was increased sequentially to 1000,

3000, 5000, 7000 and 9000 lbs (4.4, 13.3, 22.2, 31.1 and 40 kN), holding the load at these levels for approximately ten minutes while data was obtained. Following the 9000 lb level, the displacement was set to travel to 4" (102 mm) in 120 minutes, providing a constant deflection rate of approximately 0.025" (0.6 mm) per minute. This slower test procedure is not believed to have affected the results in any significant manner. It is possible that the resulting test displacements may be increased marginally under this slower test, although this cannot be verified.

3.8 TEST RESULTS

Figures 3.6 thru 3.13 show load vs. midspan deflection graphs for each retrofitted test specimen in comparison with the control specimen, Specimen C. Load vs. strain graphs are shown for each test specimen in Figures 3.14 thru 3.24. Coincident reinforcing bar and CFRP strains are shown plotted on the same axes. The strains at each location axially along the specimens are shifted from each other in the plots for clarity. Figures 3.19 and 3.24 show the transverse strain gradient in the 4" CFRP strips of specimens L4 and H4, respectively.

A summary of the key results for all test specimens is presented in Table 3.4. The following are definitions for the data reported in Table 3.4:

b_f/b: ratio of gross CFRP width to concrete substrate width (widths shown in Figure 3.3)

age: age, in days, at time of testing since test specimen was cast

cracking load: midspan loading at initiation of initial concrete cracking, as determined from first abrupt increase in reinforcing bar strain for each test specimen. A representative example of this determination is shown in Figure 3.25.

load at initial yield: midspan loading corresponding to the middle #4 tensile reinforcing bar attaining a strain of 2140 microstrain (yield strain value for reinforcing steel based on experimentally obtained yield stress data (see Table 3.1) and calculated assuming E = 29,000 ksi (200 GPa))

load at general yield: midspan loading at which general yield of the specimen occurred, defined as a significant change in stiffness of the load vs. deflection curve with observable nonlinearity. Since the stiffness of the load vs. deflection response decays gradually, general yield is determined as the intersection of the elastic tangent stiffness and the post-yield tangent stiffness as illustrated schematically in Figure 3.26.

strain in CFRP at general yield: maximum strain in CFRP at time of general yield deflection.

maximum load: maximum midspan loading carried by a test specimen during monotonic testing, as shown in Figure 3.26.

ultimate load: the greater of: the load corresponding to failure of the specimen, or the load at which the load carrying capacity falls below 80% of the maximum load obtained (see Figure 3.26).

ductility: ratio of the deflection at the ultimate load to the deflection at general yield.

maximum CFRP strain: the greatest strain in the CFRP observed. The strain in the corresponding reinforcing bar recorded at the same time is also indicated.

initiation of debonding: The FRP strain at which debonding apparently initiates as determined by comparing strain time histories (see Figure 3.27) of the CFRP strips and corresponding reinforcing bars. Additional knowledge of the debonding mechanism is also assumed as described in Chapter 2. It is hypothesized that debonding will initiate near midspan in the region between CFRP gauges (5) and (6) or (7) and (8). Debonding, once initiated, will propagate away

from the midspan toward the support. Thus, as the debonding propagates past the point of the outermost CFRP gauges, (5) or (8), the strains in these gauges should increase relative to their corresponding reinforcing bars, (1) and (4). This increase is due to the loss of shear transfer along the debonded region. The incremental stress usually transferred by the bond is now uniformly transferred across the debonded CFRP and is anchored beyond the debonded region. Observations of beam behavior and eventual complete debonding are used to verify the location of debonding identified by the strain data.

As an illustrative example, in Figure 3.27, CFRP strain gauge (5) and its corresponding reinforcing bar strain gauge (1) can be seen tracking each other; essentially both plots increase with increased deflections (as represented by the test time) at the same rate. This behavior indicates that plane sections are remaining plane and thus bond is sound at this location. CFRP strain gauge (8) and its corresponding reinforcing bar strain gauge (4) can also be seen tracking each other until about 800 seconds when the two plots begin to diverge from each other. This initial divergence is related to the yielding of the internal reinforcing steel near midspan at gauge (2) and then, at about 1050 seconds, at gauge (3). The rates of change of the strains in the reinforcing bar and CFRP are now independent of each other, indicating that plane sections are no longer plane and thus the CFRP has likely initiated debonding from the concrete substrate at this location. The CFRP strain value for the apparent initiation of debonding is reported as debonding passes CFRP strain gauge (8) at about 1200s (when the CFRP strain increases markedly) and the two plots (of strain gauges (8) and (4)) begin to significantly deviate from each other. Other activity noticed at this same time is the drop in strain in the corresponding rebar strain gauge (4). From this stage onward, CFRP gauge (8) tracks with the adjacent CFRP gauge (7). Debonding has occurred at both locations and thus the CFRP stress should be

relatively uniform between these locations. It is noted that although debonding has occurred, some stress transfer may still be affected through friction and aggregate interlock along the failure plane, explaining the minor differences between the adjacent debonded gauges.

All moments given in Table 3.4 are the midspan moments, determined from their corresponding midspan loading. The moments are determined from statics as PL/4 where 'L' is the clear span of the beam, 178⅝" (4537 mm), and 'P' is the midspan load. All deflections given in Table 3.4 are the midspan deflections measured at the corresponding midspan loading.

3.9 TYPICAL SPECIMEN BEHAVIOR

Qualitatively, all specimens exhibited similar behavior. Initial cracking of the concrete was observed at an applied load ranging from 550 to 750 pounds (2.45 to 3.34 kN) (Table 3.4). The theoretical cracking load of the concrete section, assuming concrete tensile capacity of $4.5\sqrt{f_c'}$ (U.S. units) is 586 pounds (2.61 kN). All specimens behaved in a linear manner having a flexural stiffness proportional to the amount of CFRP provided up to the initial yield of steel. As the specimens yielded, a softening of the flexural stiffness was observed. After general yield, the post yield flexural stiffness of the system is proportional to the amount of CFRP provided. During this post yield response, the propagation of debonding was evident as "popping" noises and occasional "wisps of concrete dust" were emanating from the CFRP/concrete interface region. This behavior was more evident in the H-specimens which have the high modulus adhesive, but was also evident in the L-specimens. Testing on the L1 specimen was stopped when excessive lateral deflections (resulting from uneven concrete crushing under the applied load) put the beam in danger of tipping, and therefore complete debonding did not occur in the specimen. Testing of the L4 specimen was also stopped before complete debonding occurred,

however significant local crushing of the compression concrete had occurred at the midspan loading point, as well as large shear cracks emanating from the load point to the north and the south. Testing of the L2x1 specimen was stopped due to shear failure and almost complete debonding of both strips south of the beam centerline. In all other retrofit beams, failure was relatively brittle and was characterized by a rapid complete CFRP debonding progressing toward one of the two supports. Shear and flexure cracks were present in all of the L-specimens, while the H-specimens appeared to only have cracking associated with flexure. The failure plane, in all cases, except that noted below, progressed through the cover concrete. Thus the debonded CFRP came away still bonded to the concrete as can be seen in Figure 3.28.

Except for the specimens mentioned earlier, the concrete attached to the L-specimens' CFRP typically extended up to the layer of the reinforcing steel in the region immediately adjacent midspan and included only a small thickness of cover concrete elsewhere. While the H4 specimen did have some failure at the reinforcement plane (seen under the actuator in Figure 3.28), its main failure plane was through the cover concrete immediately adjacent to the concrete/CFRP interface (seen to the left of the center line in Figure 3.28), as was the case with the other H-specimens. In some cases the failure plane was also through the CFRP at discrete locations as is noted below.

The two CFRP strips of H2x1 did not debond simultaneously, resulting in a plateau of reserve capacity as shown in Figure 3.12.

3.9.1 Interlaminar Failure in CFRP

Four specimens (H1, H2, H2x1 and H4), exhibited a final debonding failure that propagated through the cover concrete adjacent to the concrete/CFRP interface and then, near the specimen ends, progressed through the adhesive interface into the CFRP itself. Thus a thin layer of CFRP was left on the specimen as shown in Figure 3.29. This behavior was attributed to insufficient

resin in the CFRP strip itself – resulting in what is often called “dry fibers” and a resulting interlaminar failure. This condition results from the manufacturer trying to increase the fiber volume ratio (ratio of fiber to total volume of laminate) beyond that which is practical for the fiber type (approximately 0.70 in this case). This condition was verified by the CFRP supplier and has been observed in recent similar tests conducted elsewhere (personal correspondence between Dr. Harries and other researchers). Because the condition was only observed near the ends of the CFRP strips and only at the eventual final debonding, it is not believed to have affected the reported test results in any way. The CFRP manufacturer is reported to have recently reduced the fiber volume ratio for this product.

Table 3.1 Experimentally determined concrete and reinforcing steel material properties.

Specimen	28 Day Concrete Strength	Age at Time of Beam Test	Reinforcing Steel
	psi (MPa)	*days*	*ksi (MPa)*
C	f_c' = 3384 (23.3)	144	f_y = 62.2 (429) f_u = 96.8 (667)
L1		154	
L2		157	
L2x1		161	
L4		228	
H1		162	
H2		163	
H2x1		165	
H4		170	

Table 3.2 Manufacturer's reported properties of CFRP strips (Fyfe, 2005).

Property	ASTM test method	UC Strip
tensile strength, *ksi (MPa)*	D3039	405 (2792)
tensile modulus, *ksi (MPa)*		22500 (155138)
elongation at rupture		0.018
perpendicular strength, *psi (MPa)*		negligible
strip thickness, *in. (mm)*	na	0.055 (1.4)
widths used in testing, *in. (mm)*	na	1 (25); 2 (51); 4 (102)

Table 3.3 Manufacturer's reported properties of adhesive systems used (SIKA, 2005).

Property	ASTM test method	Sikadur 23	Sikadur 30
tensile strength, *ksi (MPa)*	D638	2.0 (14)	3.6 (25)
tensile modulus, *ksi (MPa)*		323 (2227)	650 (4482)
elongation at rupture		0.063	0.010
modulus of rupture, *ksi (MPa)*	D790	4.8 (33)	6.8 (47)
tangent modulus of elasticity, *ksi (MPa)*		471 (3247)	1700 (11721)
shear strength, *ksi (MPa)*	D732	3.0 (21)	3.6 (25)
bond strength, *ksi (MPa)*	C882	2.6 (18)	3.2 (22)
compressive strength, *ksi (MPa)*	D695	5.2 (36)	8.6 (59)
compressive modulus, *ksi (MPa)*		128 (883)	390 (2689)

Table 3.4 Summary of key results.

Specimen			C	L1	L2	L2x1	L4	H1	H2	H2x1	H4
b_f/b			0	0.17	0.33	0.33	0.67	0.17	0.33	0.33	0.67
age		days	144	154	157	161	228	162	163	165	170
First Cracking	load	kip	<0.66[1]	0.62	0.66	0.63	.75	0.55	0.64	0.64	0.65
	moment	k·in	<29.5	27.8	29.2	28.1	33.3	24.6	28.8	28.8	28.9
Initial Yield of Reinforcing	load	kip	5.91	6.05	6.78	5.99	7.31	6.16	6.38	6.63	8.44
	moment	k·in	264	270	303	267	326	275	285	296	377
	deflection	in.	0.980	1.070	1.000	0.842	1.455	0.984	0.948	0.893	1.078
General Yield	load	kip	6.96	8.12	8.61	9.08	10.68	7.94	8.80	9.20	10.44
	moment	k·in	311	363	384	406	477	355	393	411	466
	deflection	in.	1.180	1.350	1.320	1.350	1.492	1.320	1.360	1.300	1.400
	strain in CFRP	με	na	3150	3228	3483	3536	3400	3640	3764	3205
	rebar strain	με	na	2910	2627	6115	3591	2690	4428	11120	6667
Maximum Load	load	kip	6.98	8.96	9.96	10.23	11.65	8.47	9.79	10.15	11.07
	moment	k·in	312	400	445	457	520	378	437	453	494
	deflection	in.	1.423	2.453	2.061	2.352	2.340	2.158	1.878	1.974	1.717
	strain in CFRP	με	na	8218	6518	7872	6462	6160	6112	6853	4787
	rebar strain	με	2759	11559	13124	6624	14422	12446	14663	6034	9947
Ultimate Load	deflection	in.	3.077	3.343	2.239	2.549	2.844	2.408	2.176	2.210	1.865
	ductility		2.61	2.48	1.70	1.89	1.91	1.82	1.60	1.70	1.33
Maximum CFRP Strain	strain in CFRP	με	na	8370	6688	7878	6595	6466	6200	6863	4813
	rebar strain	με	15932	[3]	13167	6620	15337	12414	14812	6004	9952
Initiation of Debonding	strain in CFRP	με	na	5300	6688[2]	7878[2]	4540	2900	3550	3200	2850
	rebar strain	με	na	2600	[3]	[3]	2990	2300	2680	2790	2500

[1]For Specimen C, loading was started at 0.66 kips, which was above the first cracking load.
[2]No debonding was discernible from the data, therefore maximum strain in the CFRP was reported.
[3] Gauge reading exceeded maximum that may be recorded using the data acquisition system, approximately 15000 microstrain.

(a) Formwork with instrumented #4 tensile reinforcement and lifting hooks attached to #3 top reinforcement.

(b) Formwork with #4 tensile reinforcement instrumentation at midspan region of beam.

Figure 3.1 Beam specimen formwork prior to placing concrete.

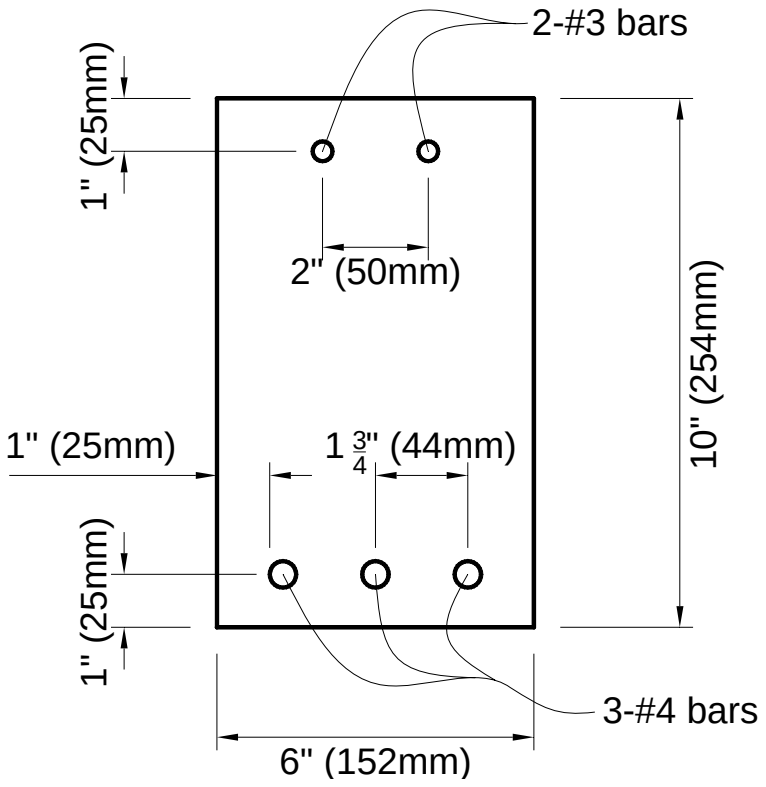

Figure 3.2 Detail of reinforced concrete beam specimens.

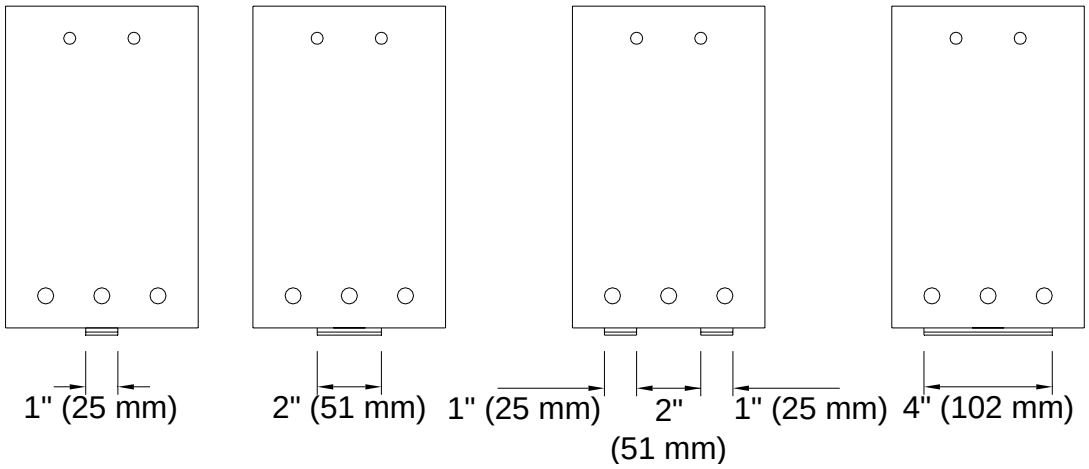

Figure 3.3 Detail of centered CFRP strips (a uniform adhesive layer approximately 1/16" (1.6 mm) thick was used in each case to adhere the CFRP).

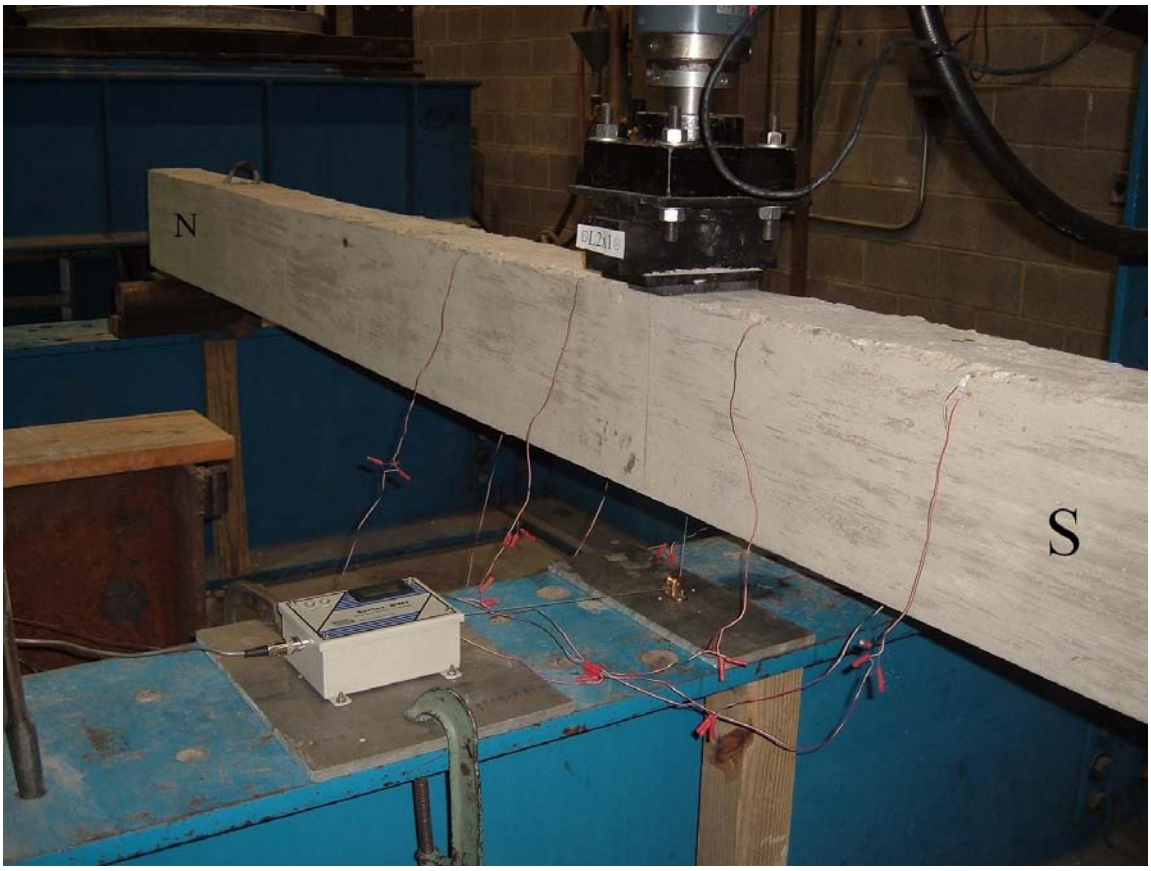

Figure 3.4 Test setup.

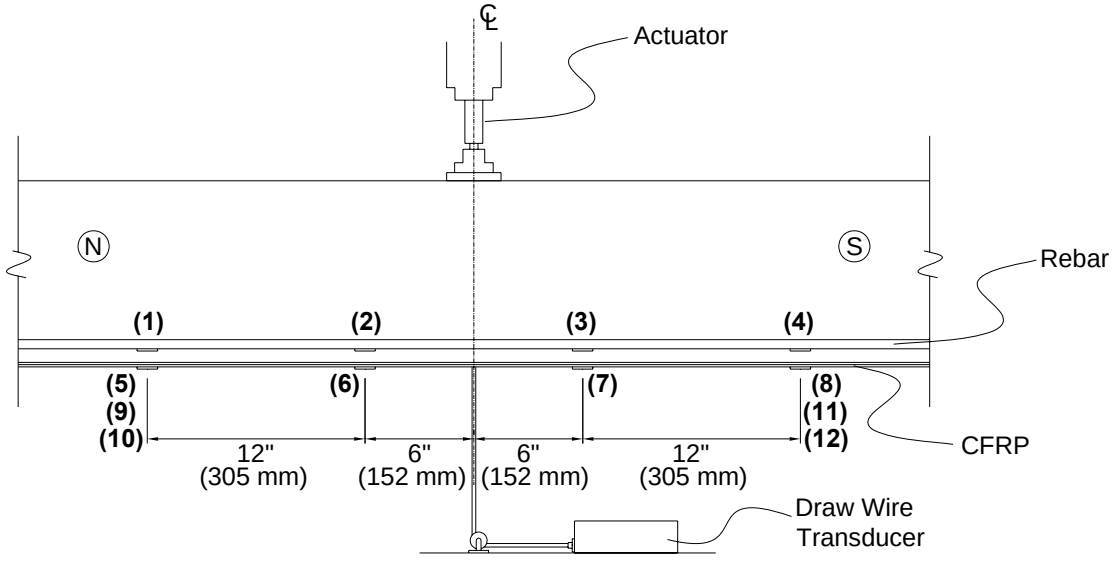

Figure 3.5 Instrumentation setup.

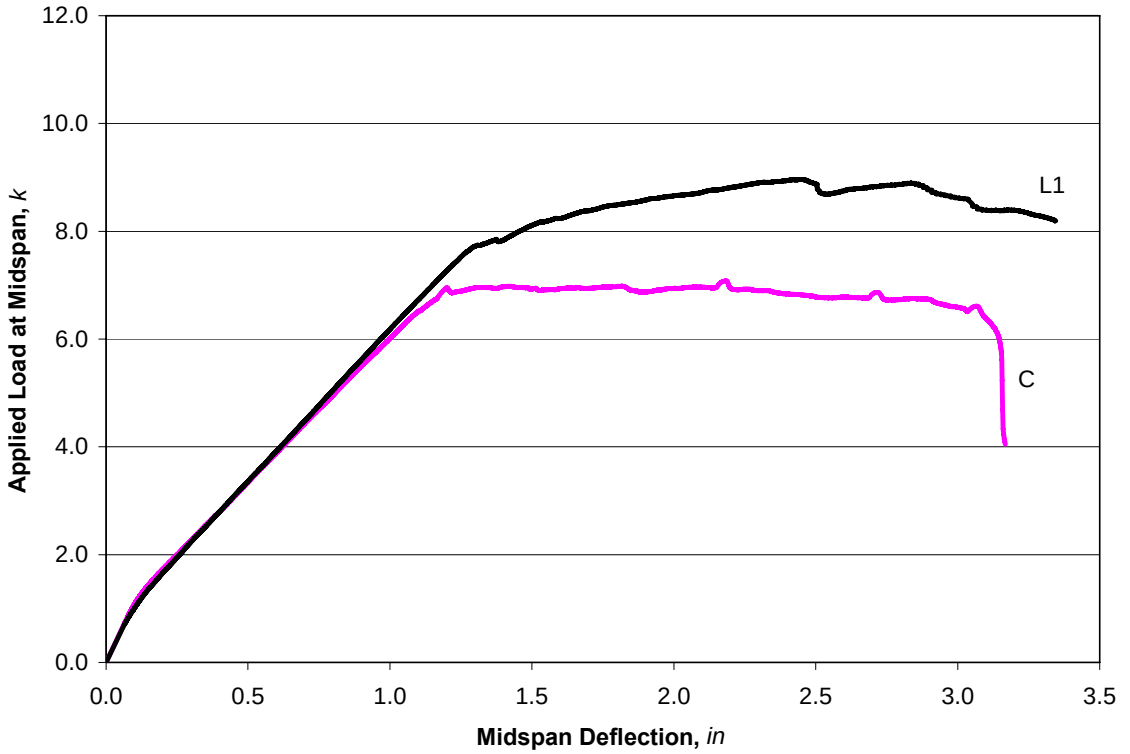

Figure 3.6 Test Specimens L1 and C.

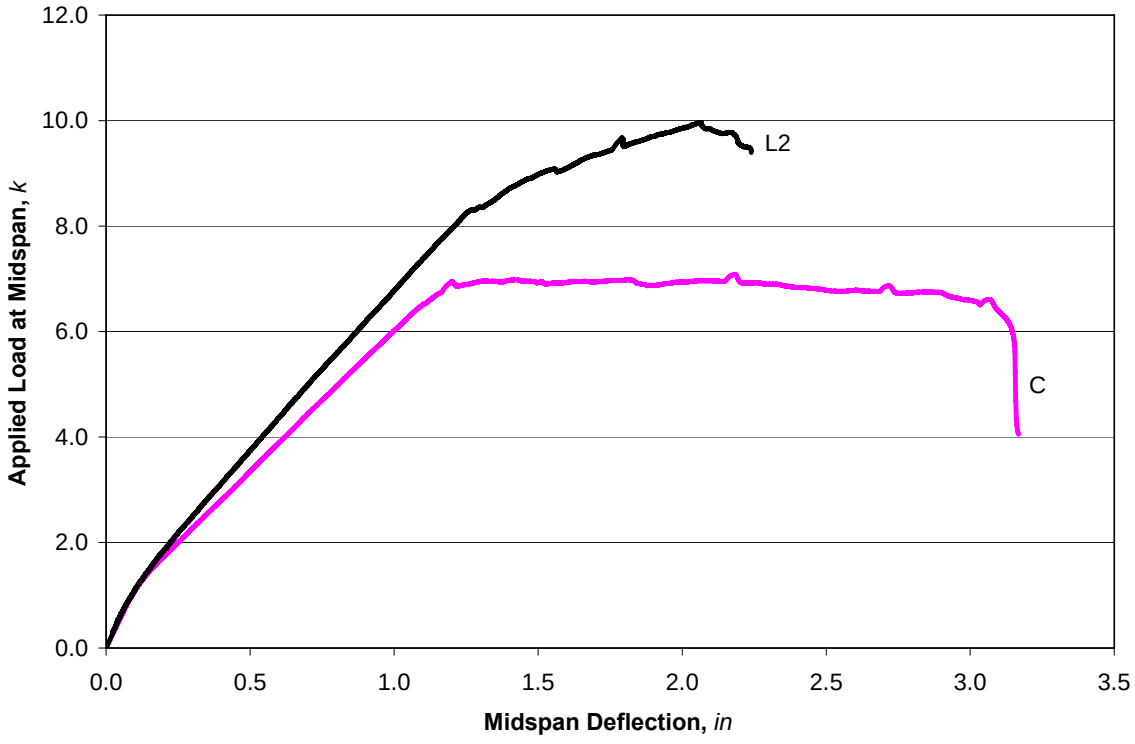

Figure 3.7 Test Specimens L2 and C.

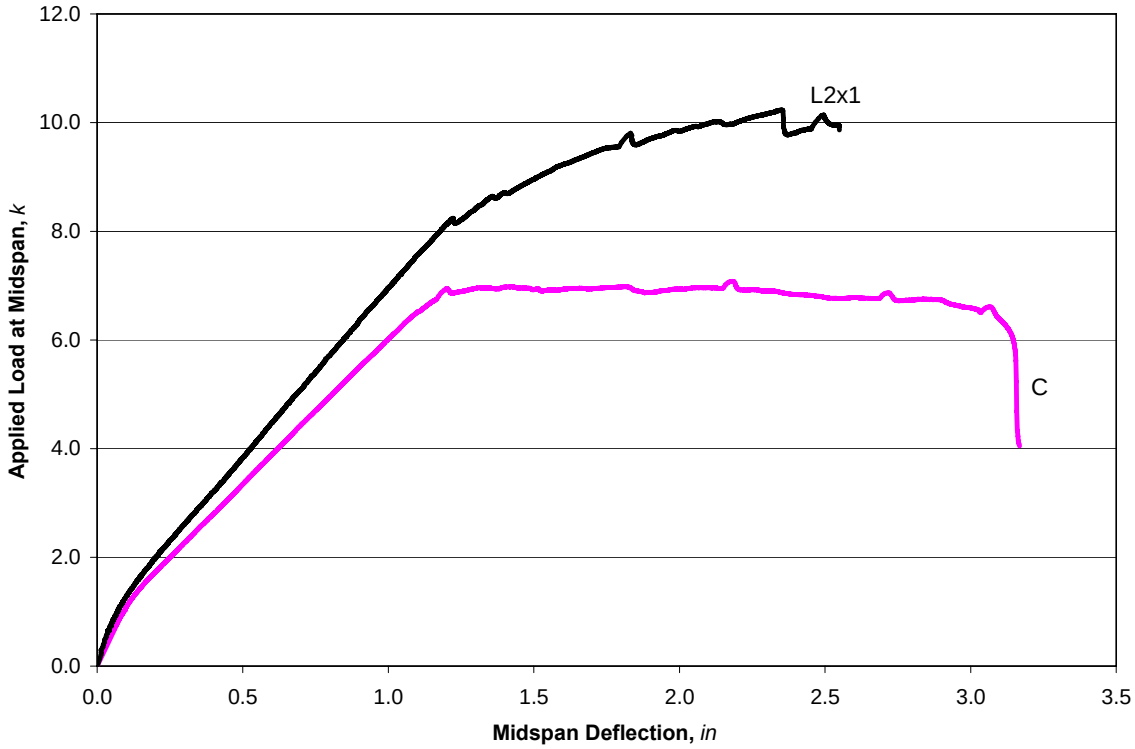

Figure 3.8 Test Specimens L2x1 and C.

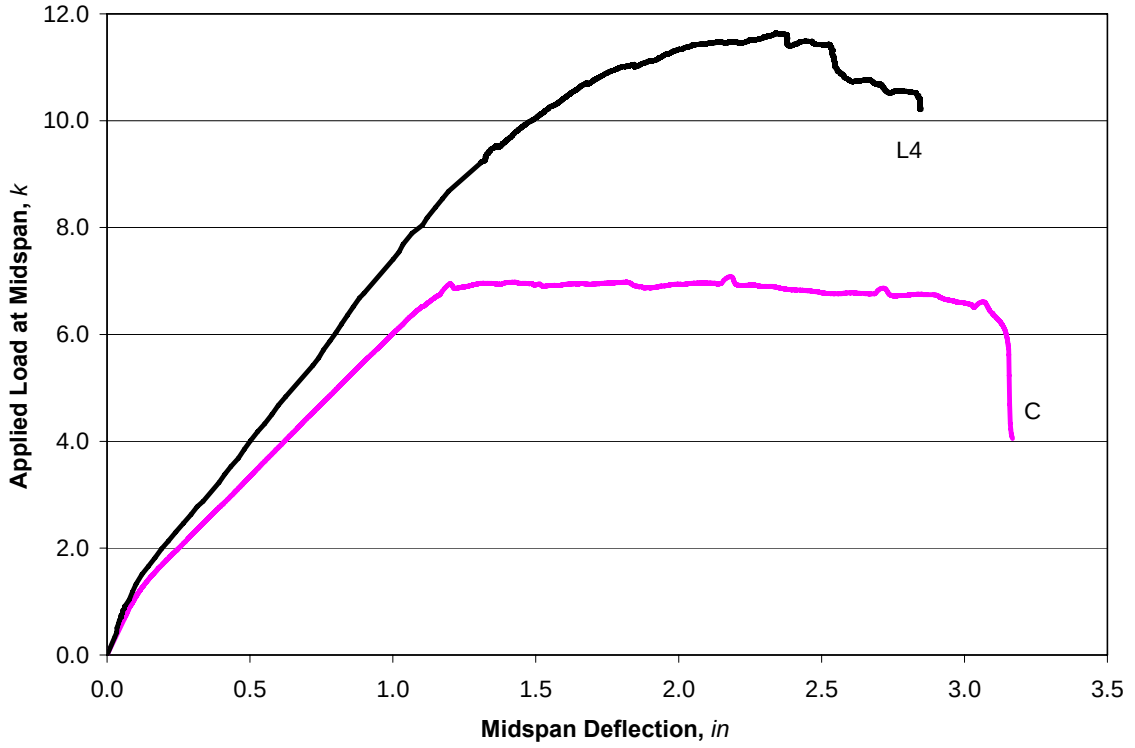

Figure 3.9 Test Specimens L4 and C.

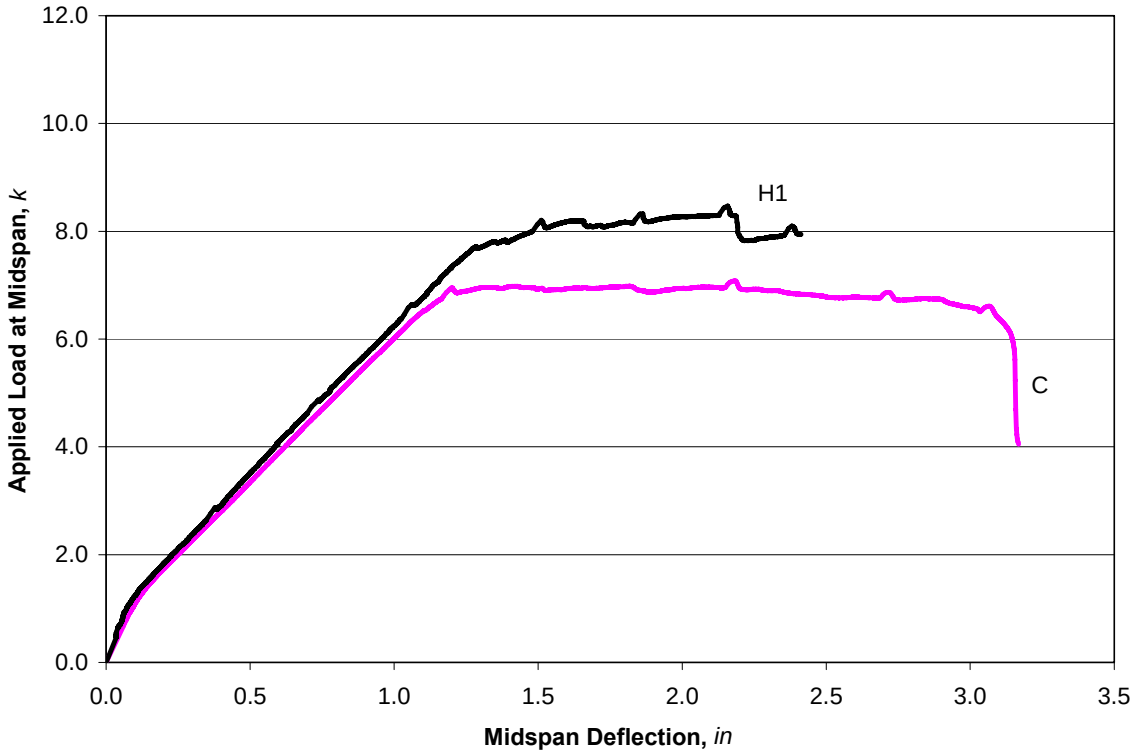

Figure 3.10 Test Specimens H1 and C.

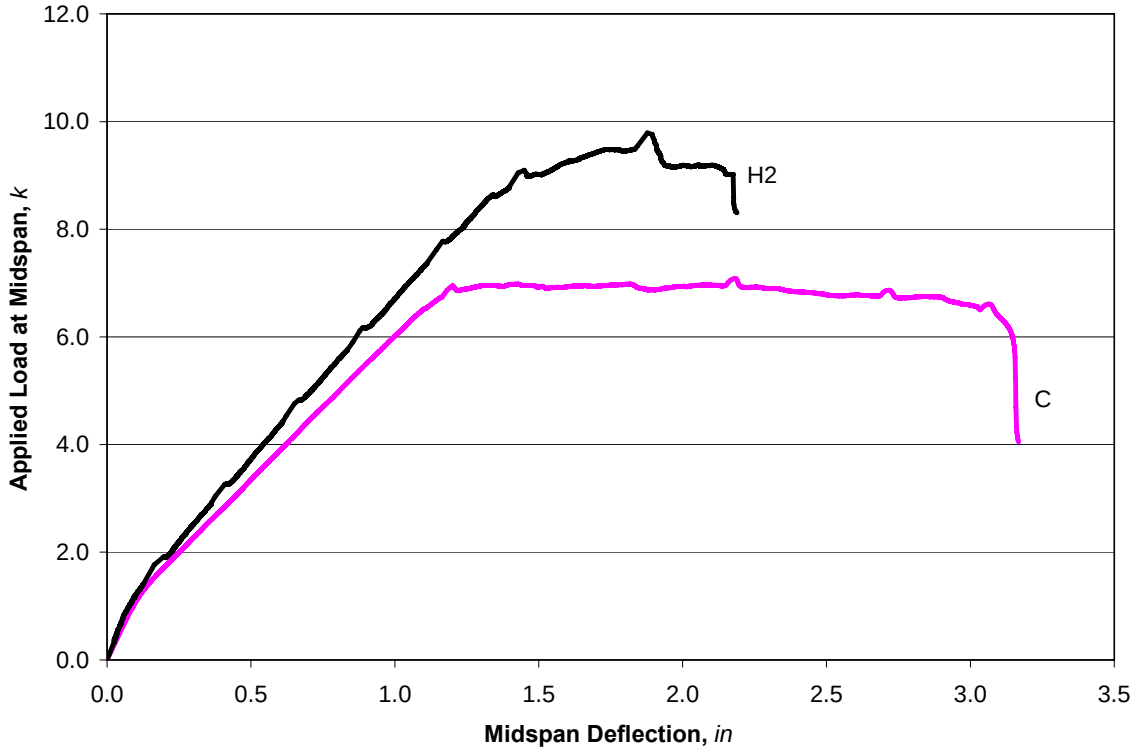

Figure 3.11 Test Specimens H2 and C.

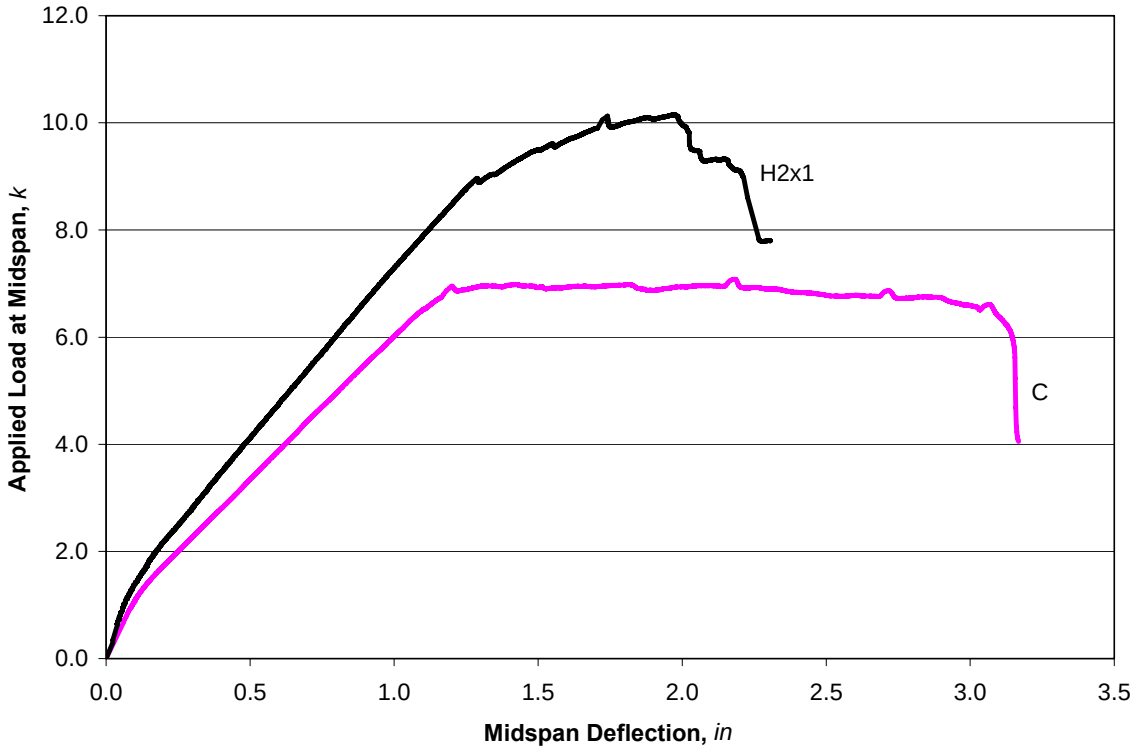

Figure 3.12 Test Specimens H2x1 and C.

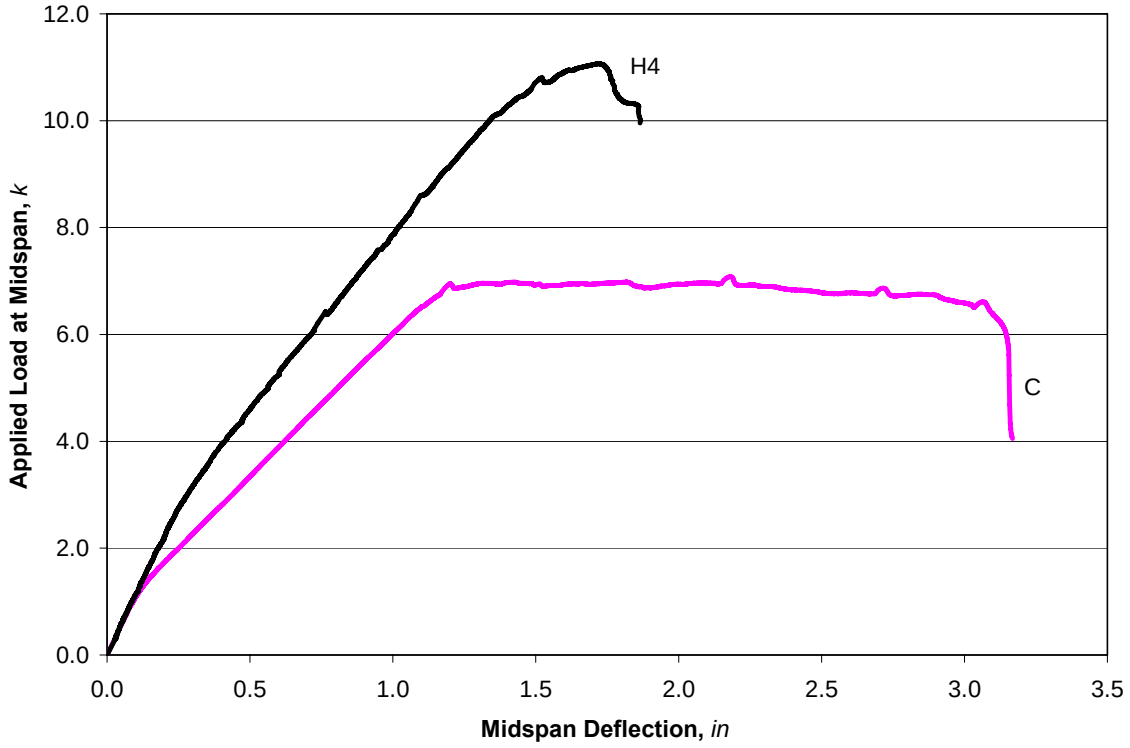

Figure 3.13 Test Specimens H4 and C.

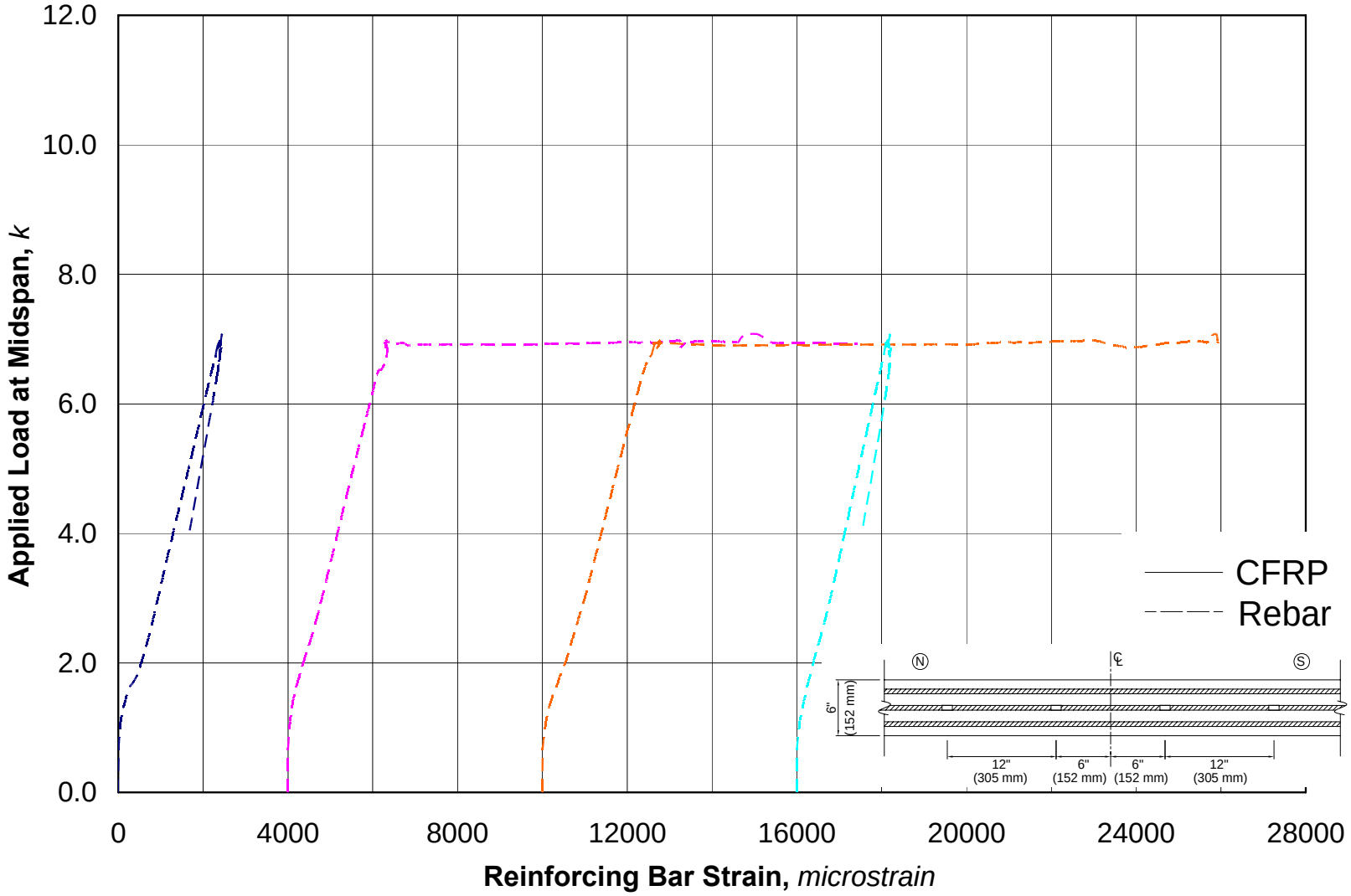

Figure 3.14 Test Specimen C.

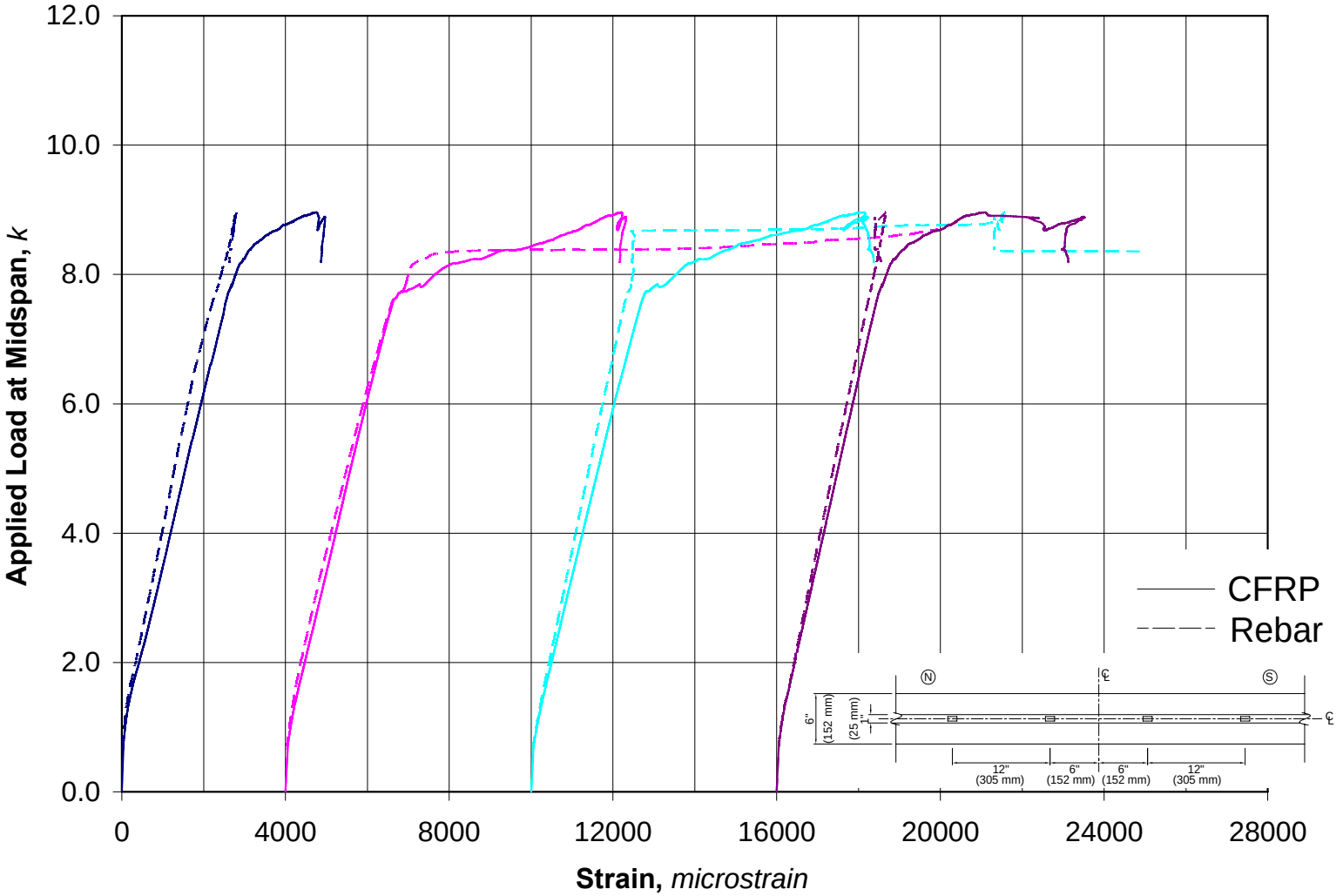

Figure 3.15 Test Specimen L1.

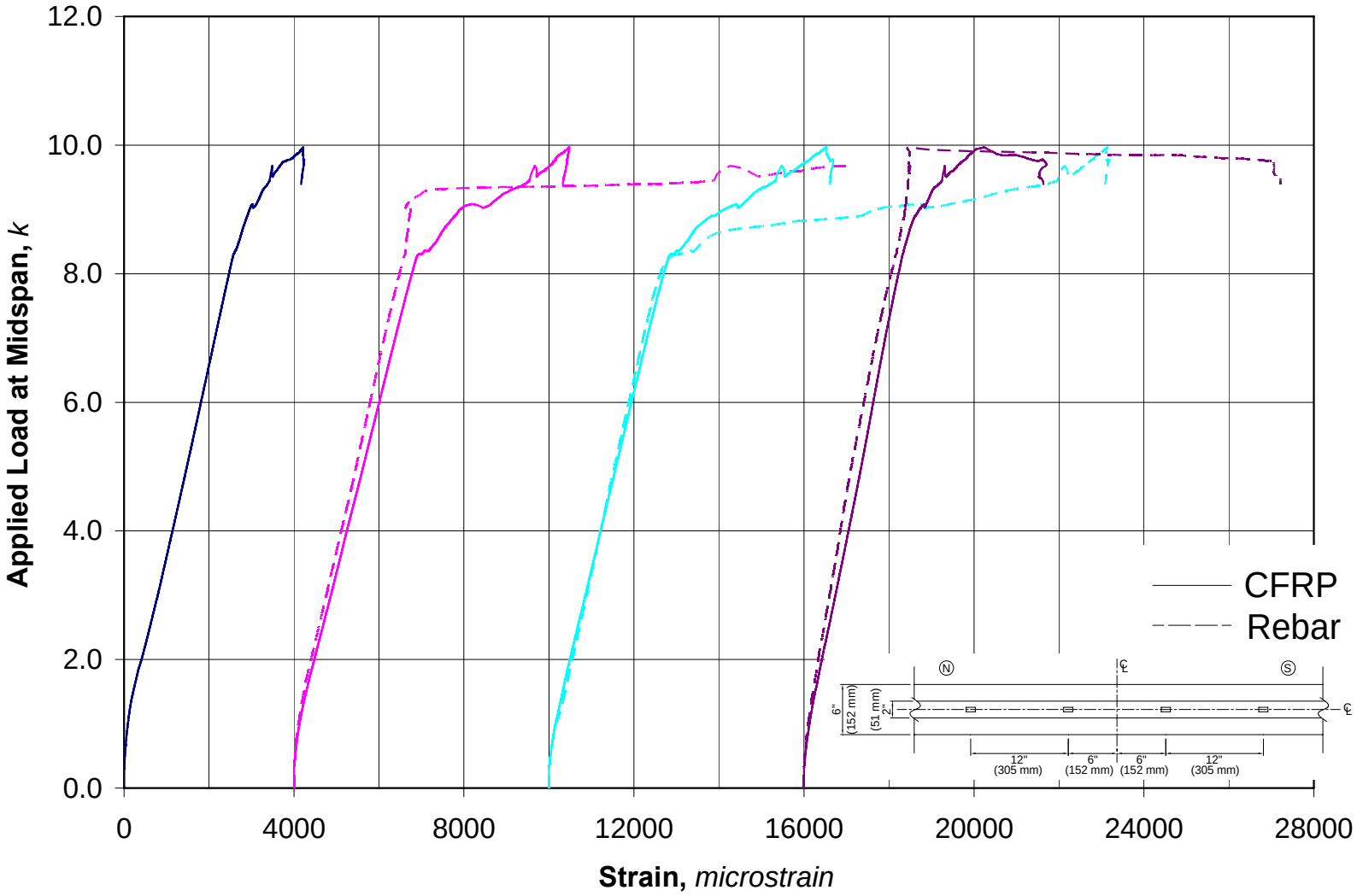

Figure 3.16 Test Specimen L2.

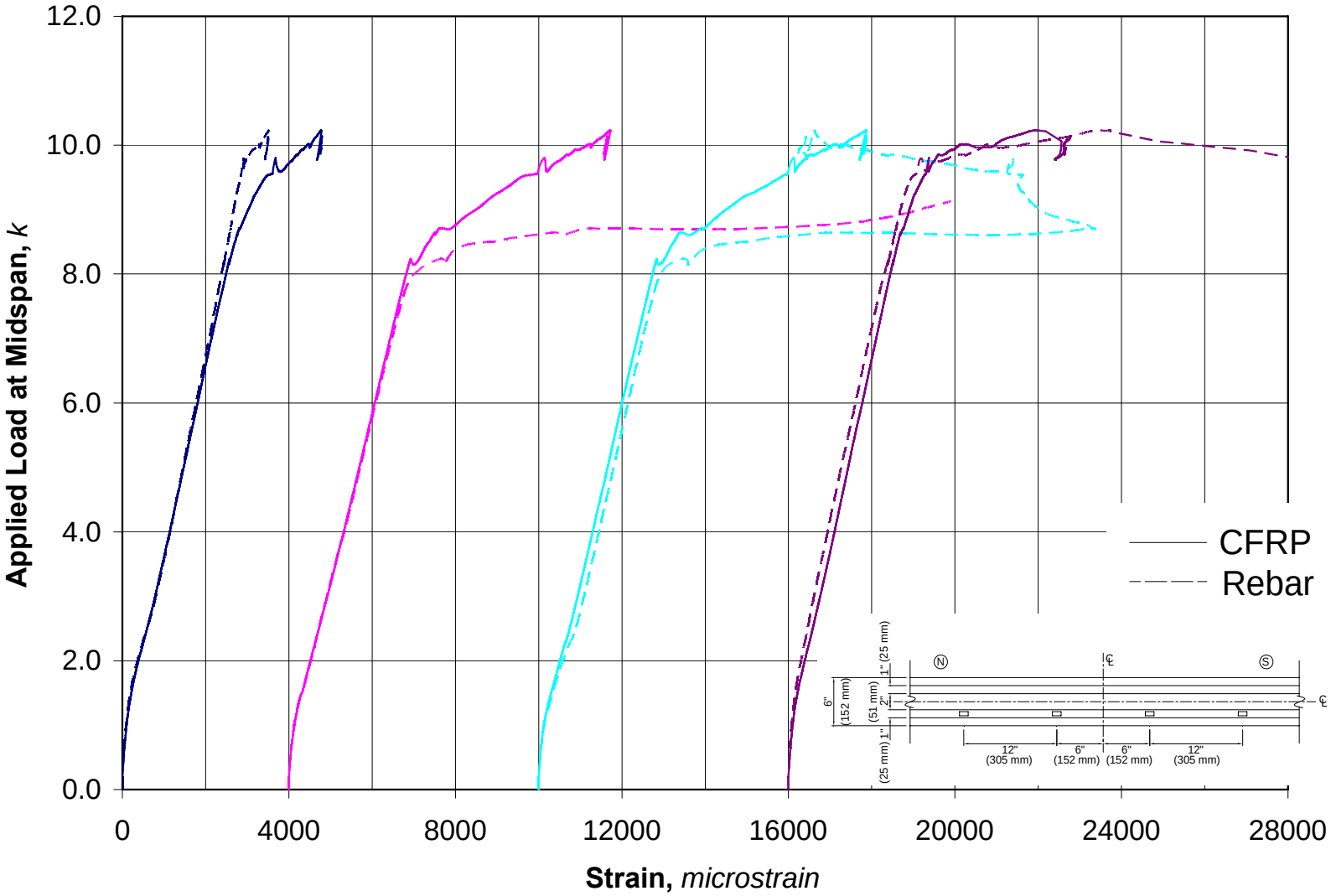

Figure 3.17 Test Specimen L2x1.

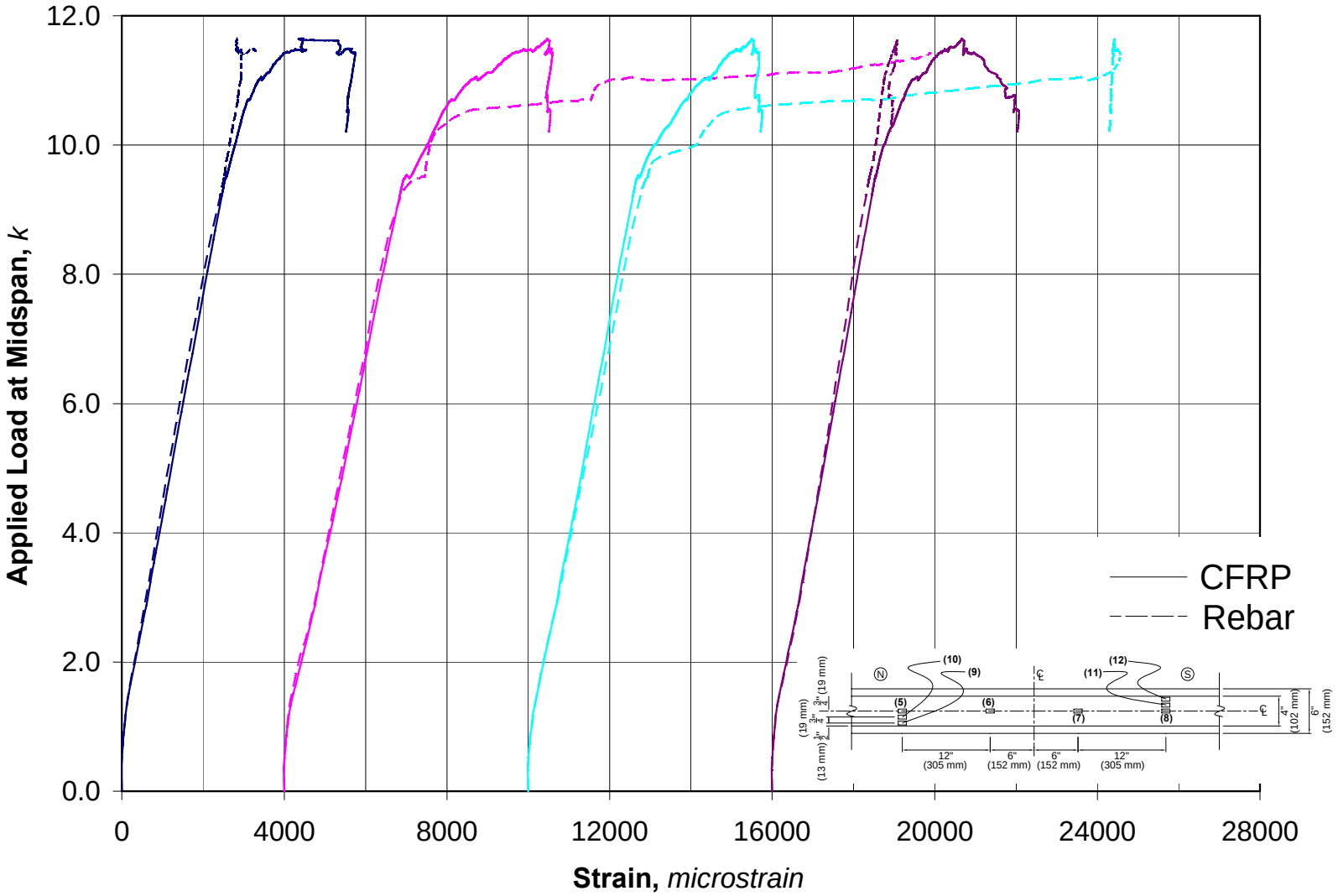

Figure 3.18 Test Specimen L4 strain gauges (1) thru (8).

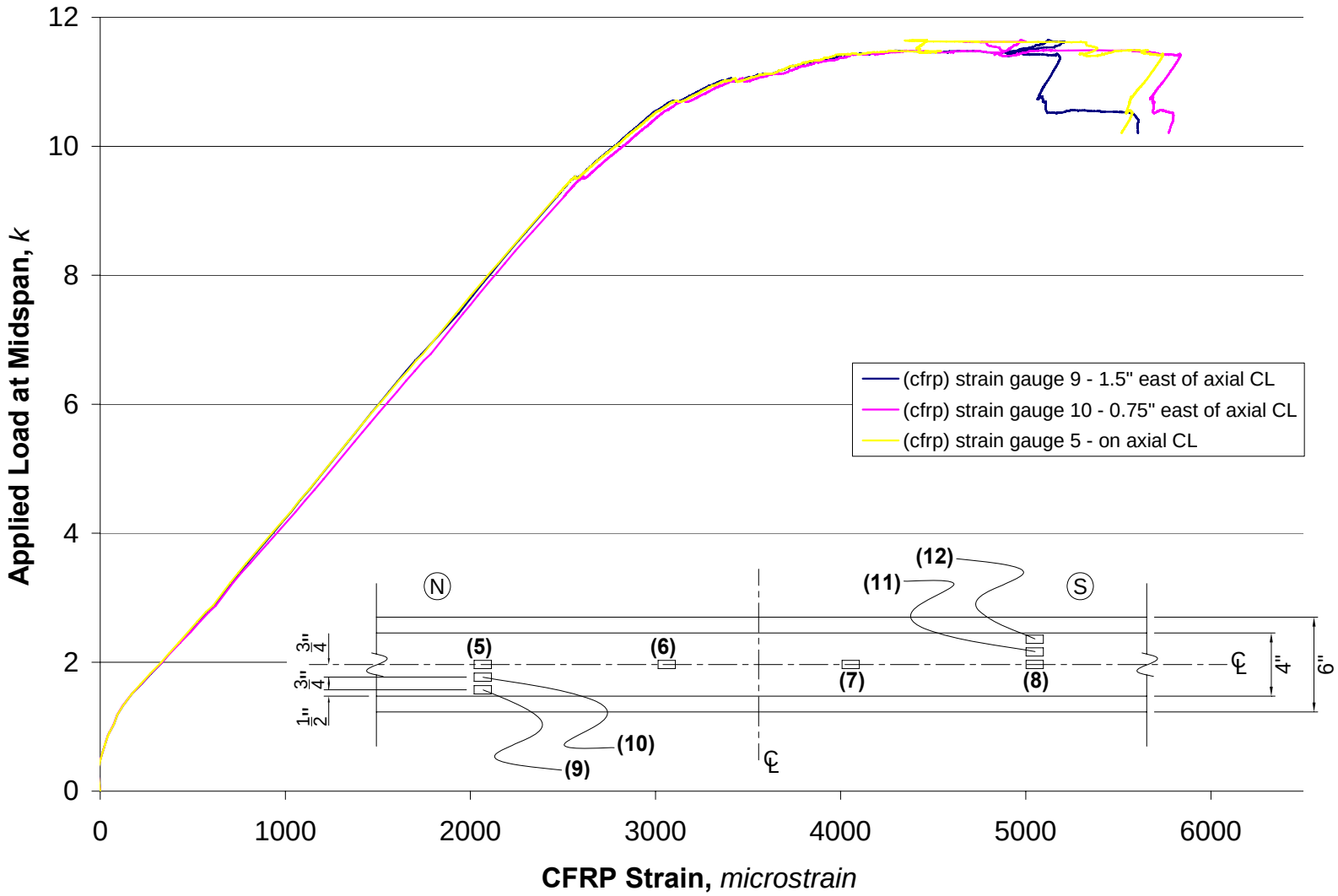

Figure 3.19(a) Test Specimen L4 - North strain gauges (9), (10) and (5).

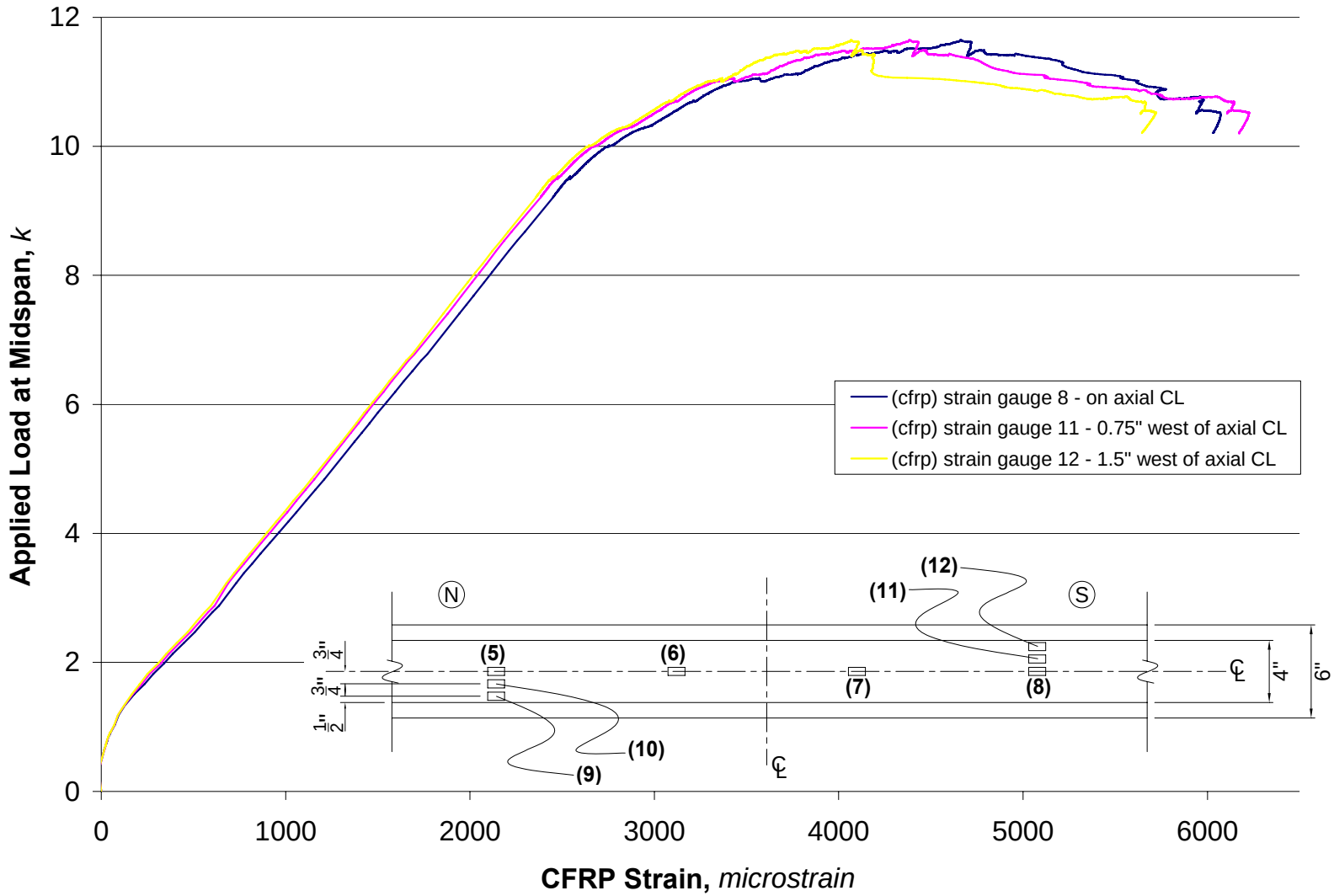

Figure 3.19(b) Test Specimen L4 - South strain gauges (8), (11) and (12).

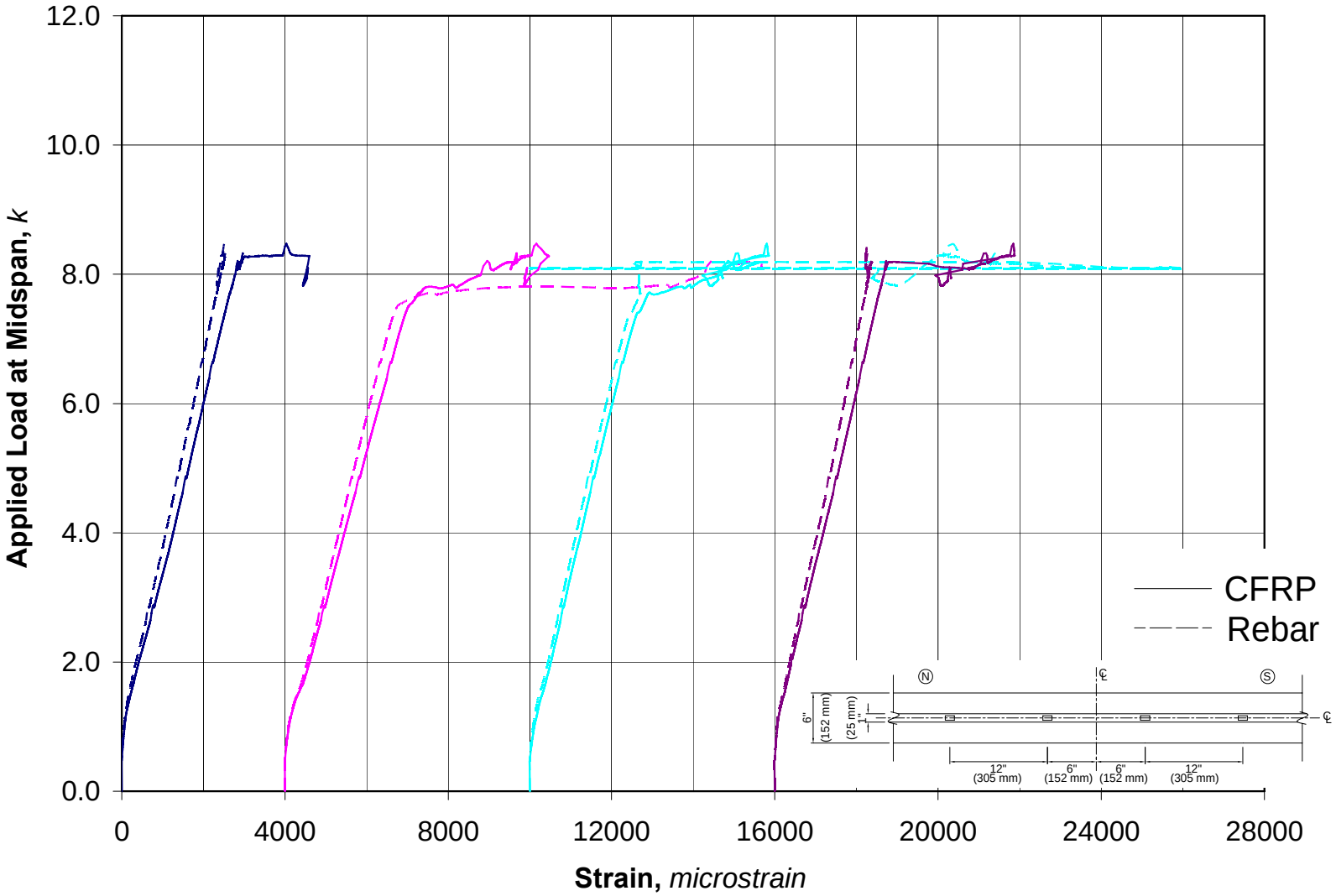

Figure 3.20 Test Specimen H1.

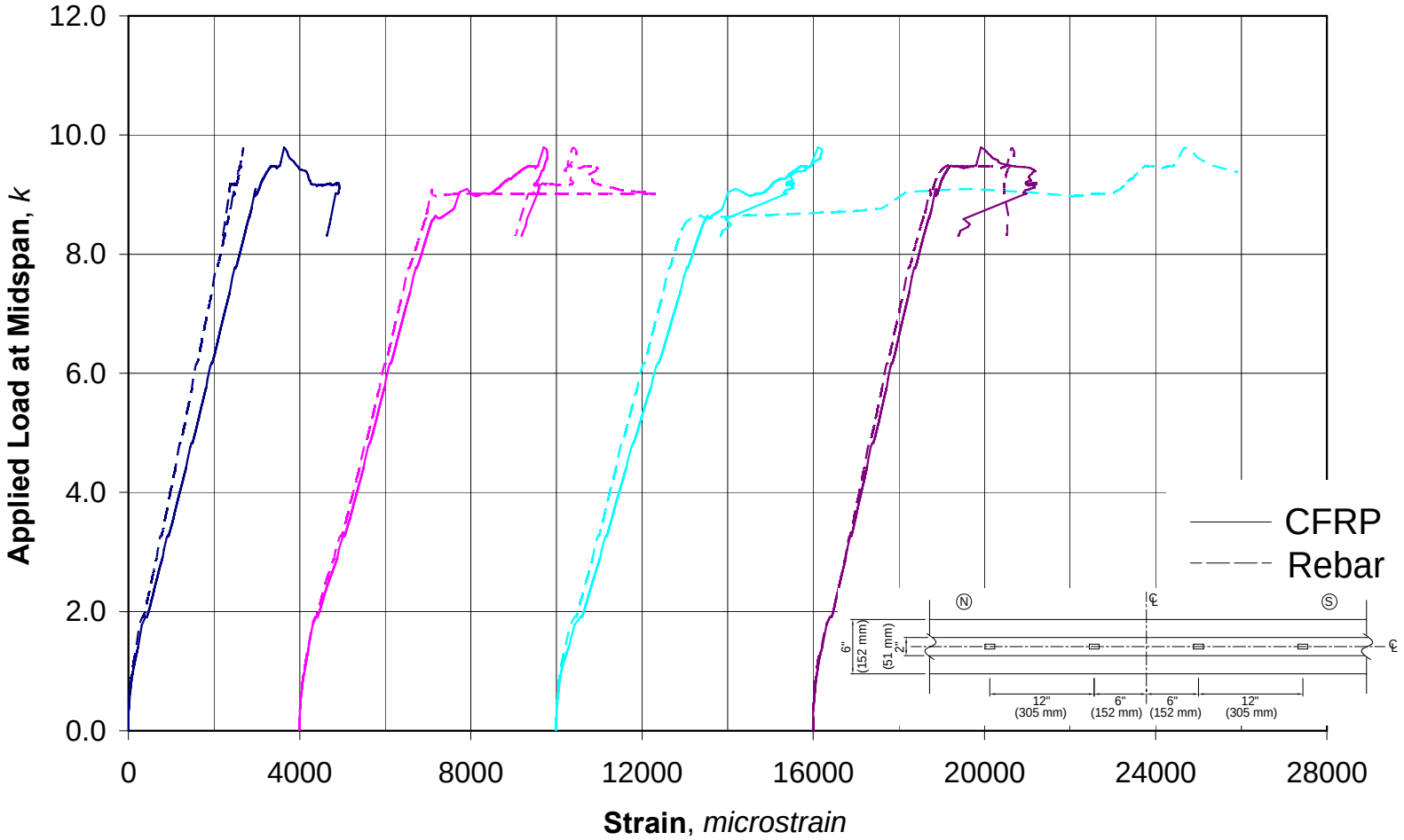

Figure 3.21 Test Specimen H2.

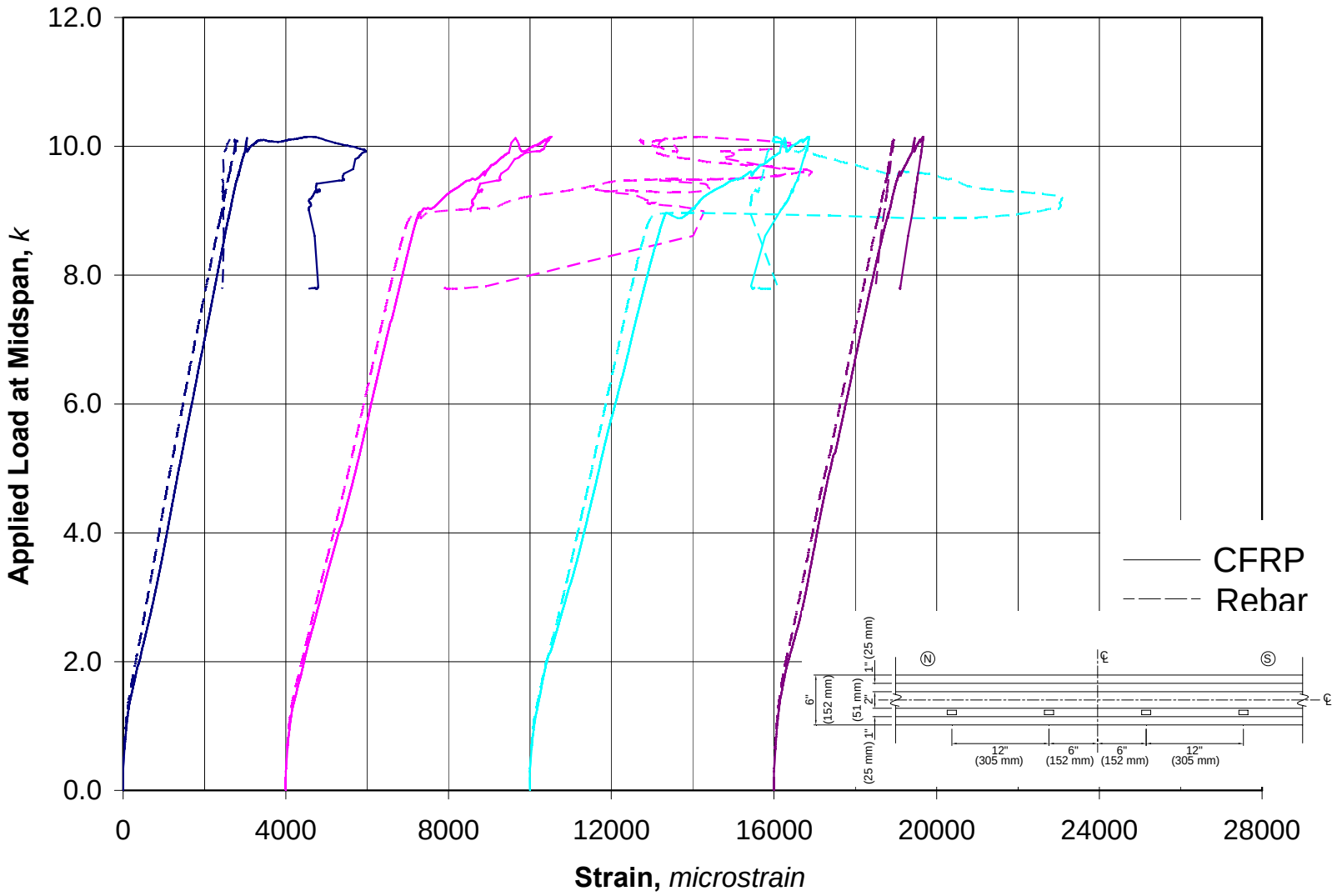

Figure 3.22 Test Specimen H2x1.

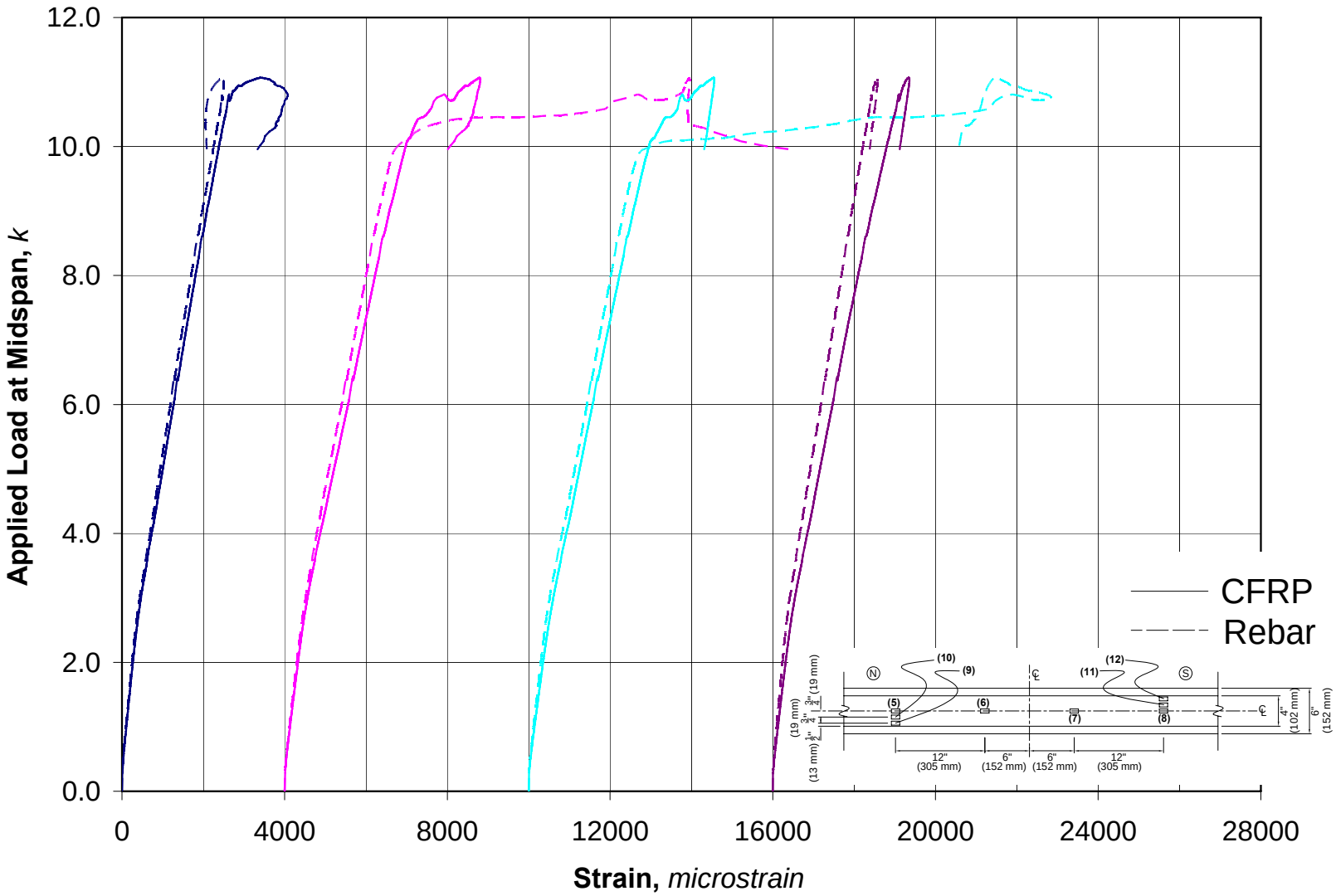

Figure 3.23 Test Specimen H4: strain gauges (1) thru (8).

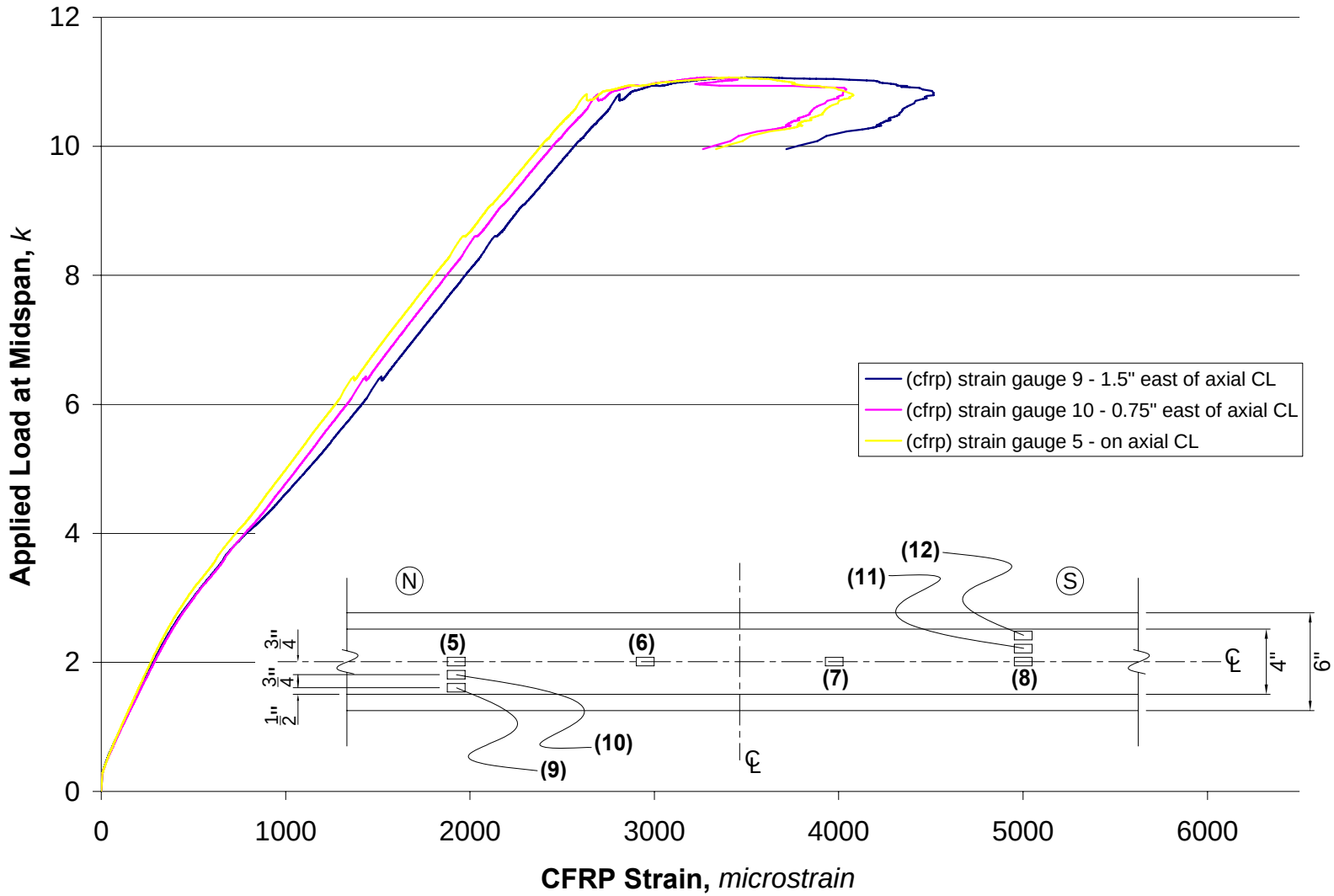

Figure 3.24(a) Test Specimen H4: North strain gauges (9), (10) and (5).

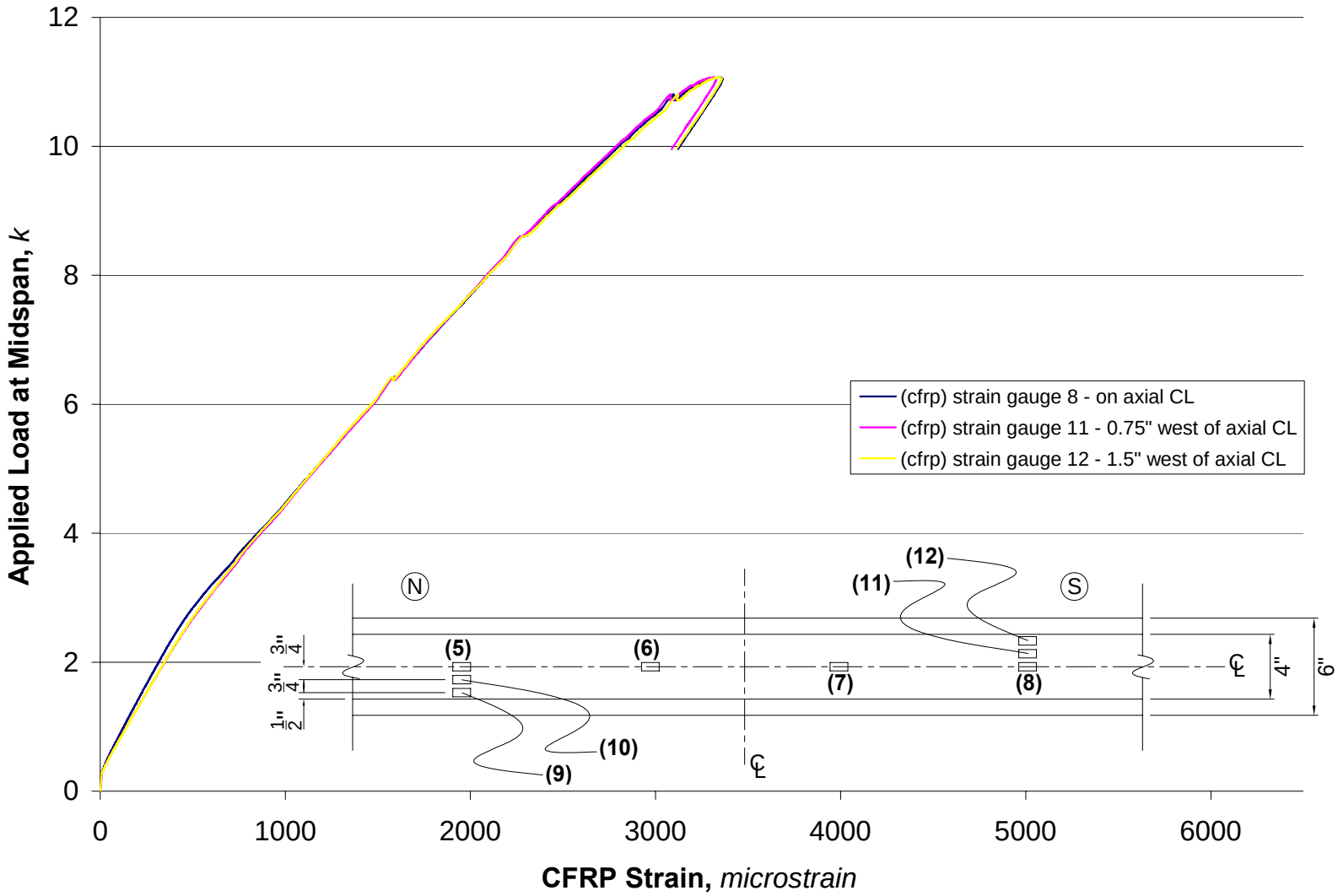

Figure 3.24(b) Test Specimen H4: South strain gauges (8), (11) and (12).

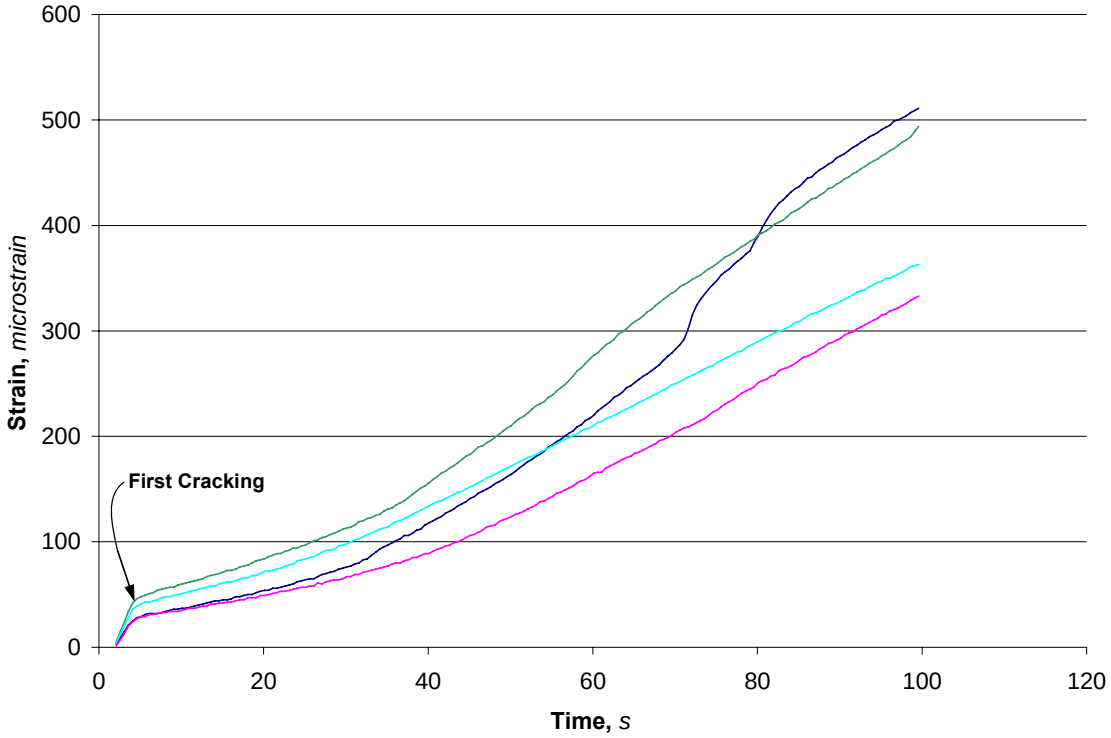

Figure 3.25 Example of determining first cracking.

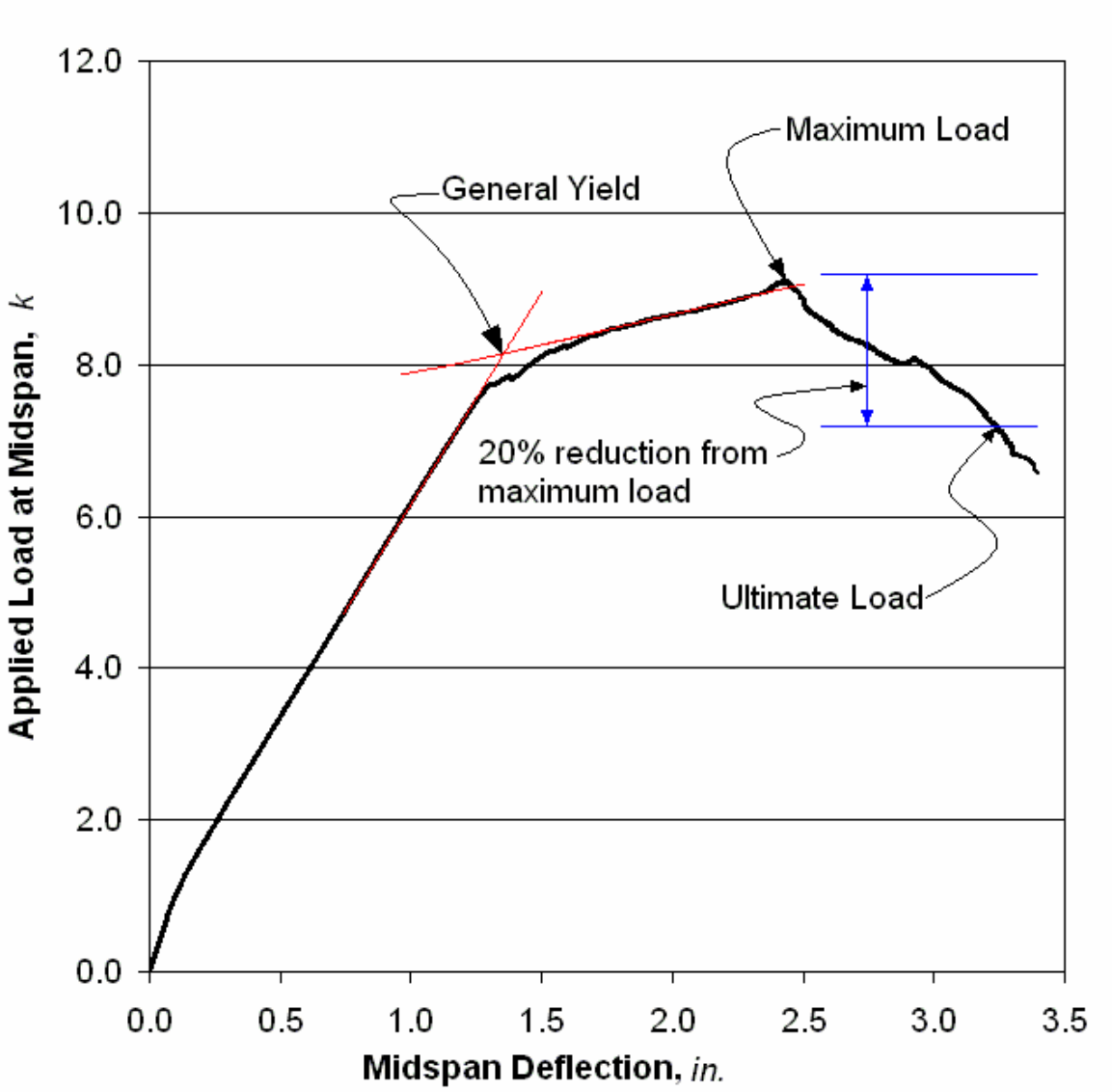

Figure 3.26 Determining general yield, maximum and ultimate loads.

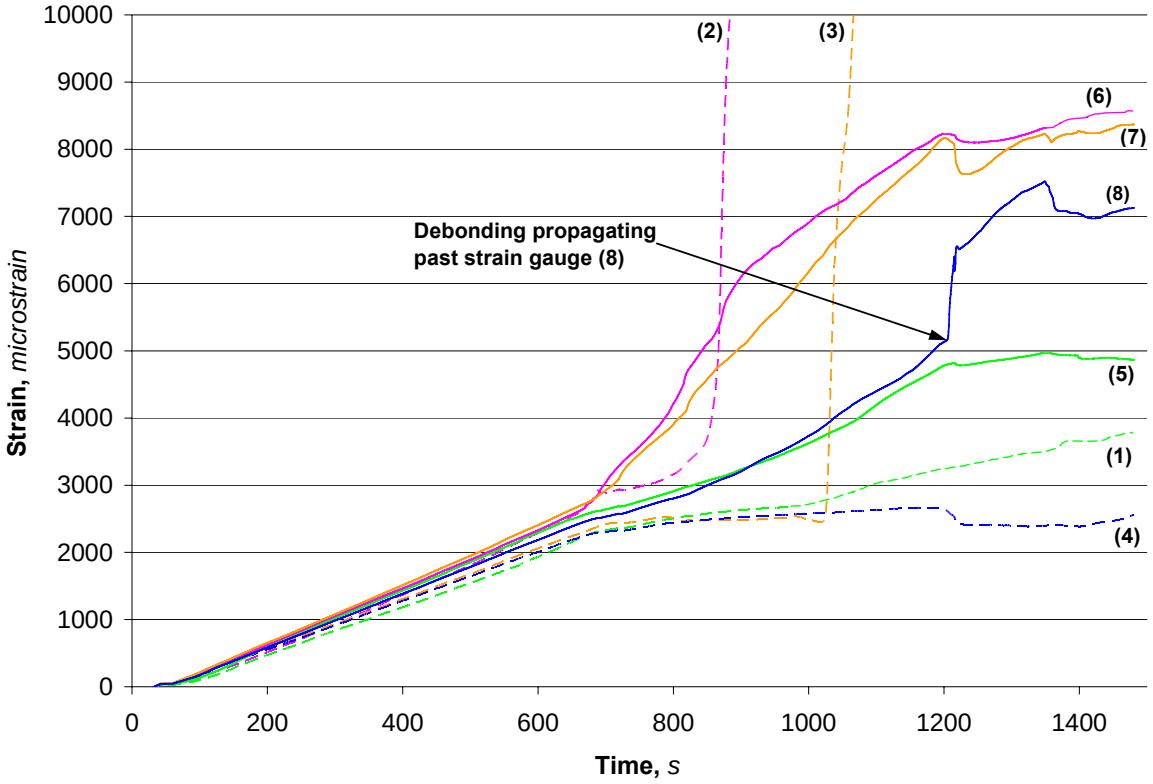

Figure 3.27 Determining initiation of debonding.

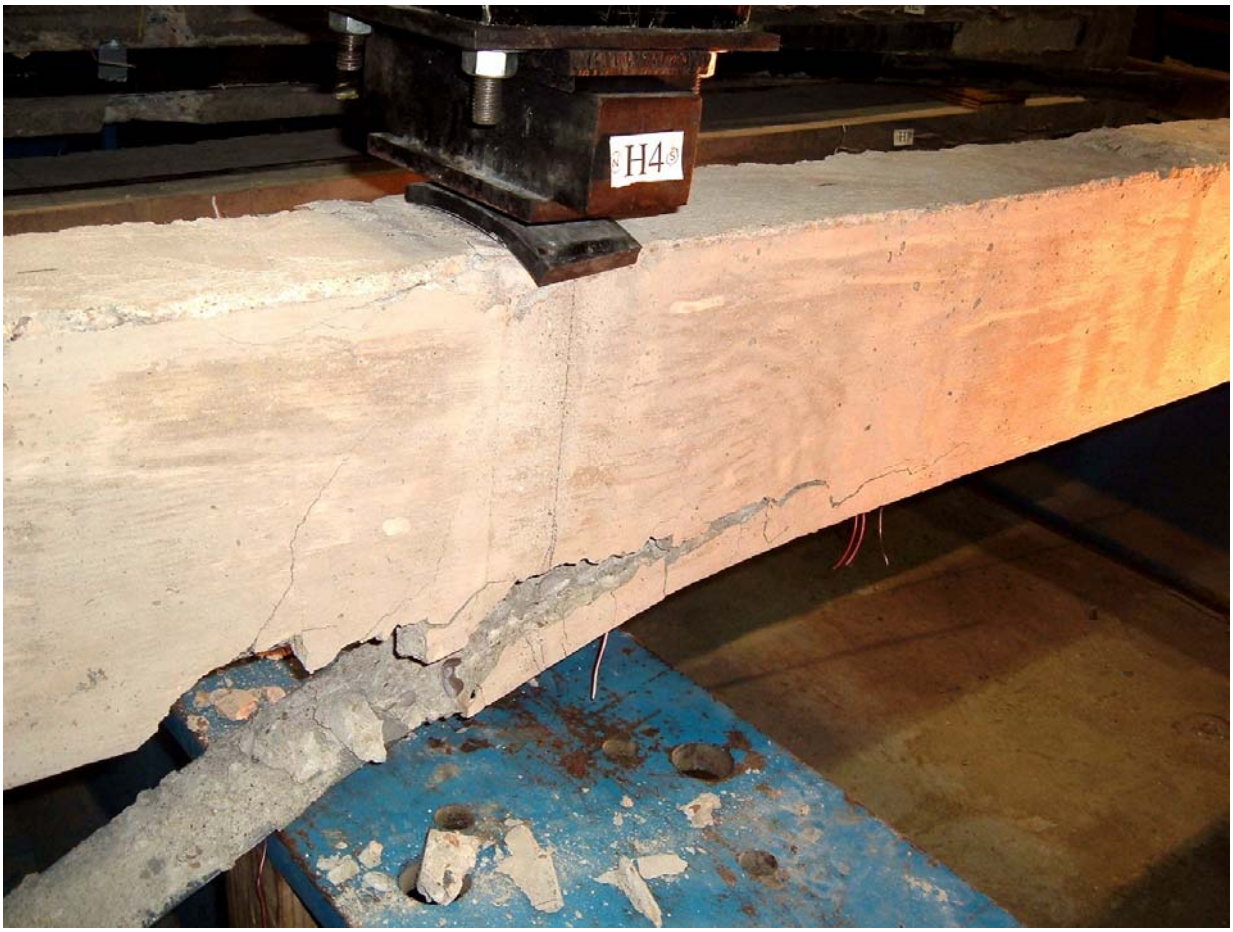

Figure 3.28 Failure thru the concrete cover (Specimen H4).

Figure 3.29 Interlaminar failure in CFRP (Specimen H1). Debonding began at midspan, propagating thru the concrete cover. The failure plane then "jumped" into the CFRP strip and then back into the concrete cover as can be seen to the right of this image.
The debonding propagated from left (midspan)-to-right (support) across the image.

4.0 EXPERIMENTAL RESULTS INTERPRETATION

This chapter reports interpretations of the experimental results reported in Chapter 3. Basis for these interpretations is also reported.

4.1 COMPARISON OF TEST SPECIMENS

Test specimen nomenclature is outlined in Section 3.4. Figures 3.6 thru 3.13 show the individual load deflection graphs for all eight retrofit test specimens compared to the control specimen. For direct comparison, all nine test specimen plots are represented here in Figure 4.1 on a single graph. A summary of the key results of this test program plot is given in Table 3.4 and definitions for all key result terms are given in Section 3.8. Initial cracking occurred at almost the exact same loading for all test specimens, varying over a range of about 200 lbs. (890 N). In Table 3.4, the general yield load increased with increasing CFRP retrofit width, b_f. Additionally, for b_f = 2" (51 mm), the 2x1 specimens, having 2 - 1" (25 mm) wide strips, exhibited slightly greater forces at general yield than the specimens having a single 2" strip. The displacements were essentially the same indicating a nominally stiffer response from the 2x1 retrofit. Also from Table 3.4 it can be seen that for like CFRP configurations, higher maximum loads were observed in the less brittle, lower modulus of elasticity adhesive (L-specimens). This observation is initially counterintuitive in that one would expect the stiffer adhesive to transmit greater shear forces and thus result in greater capacities. The reality is that softer resin allows for

a more efficient shear transfer and therefore larger strain values. The larger shear strains in the adhesive layer itself are relatively insignificant in this regard since the adhesive layer is very thin. Thus the observations of the present study support those of previous researchers (Section 2.3.2) in demonstrating a more efficient utilization of the CFRP with the more flexible adhesive layer. Similarly, equal or greater beam deflection ductilities were observed for the beams having the lower modulus adhesive. This observation is expected since the high modulus adhesive is more stiff and brittle. Properties of the adhesives used in this study are given in Table 3.4.

A summary of the key results, with all data normalized to the control specimen is, given in Table 4.1. A graphical representation of the normalized results analysis is given in Figure 4.2. These graphs plot the ratio of the test specimen over the control specimen versus the equivalent flexural reinforcement ratio ($\rho_{equivalent}$) of the test specimen:

$$\rho_{equivalent} = \frac{A_f E_f}{A_c E_s} + \frac{A_s}{A_c} \tag{4.1}$$

where A_c = gross area of concrete section; $A_c = hb$

A_f = cross sectional area of FRP; $A_f = t_f b_f$

A_s = cross sectional area of existing internal steel reinforcement

E_f = modulus of FRP material

E_s = modulus of steel reinforcement

For all specimens in this study, the second term in Equation 4.1 (A_s/A_c) is equal to 1%.

Figure 4.2 shows graphs for each of the four areas of analysis given in Table 4.1. In every plot it can be seen that the L specimens generally perform better than the H specimens. The improvement in load carrying response (Figures 4.1(a) and (b)) due to the softer adhesive is nominal. However the improvement in serviceability criteria (Figures 4.1(c) and (d)) is more significant when comparing low to high modulus adhesive. It is noted, however that since the

addition of CFRP increases the reinforcement ratio of these under-reinforced beams, the overall effect of the CFRP is to increase capacity and reduce deformation capacity as compared to the unretrofit control specimen; all data illustrates this expected behavior. It is very clear from Figure 4.2 that in every case the 2x1 specimens (shown as solid data points in Figure 4.2) were shown to perform better than their counterpart specimen of equal b_f/b ratio and adhesive type. Thus it is shown that the retrofit geometry has some influence on the overall retrofit performance and that multiple thinner strips may be preferable to fewer wider strips in terms of performance. This observation appears to support the hypothesis that the strips are able to engage a region of concrete wider than their own width (stress transfer spreading into the concrete). This observation will be discussed further below.

Finally, it can be seen in Figure 4.2 and Table 4.1 that there is a "law of diminishing returns" regarding the available retrofit. That is, doubling the CFRP does not double the extent of performance improvement (load carrying capacity) or degradation (deflection capacity). That is, the rate of performance change, itself, degrades with increasing CFRP provided.

4.2 PREDICTED DEBONDING BEHAVIOR

As stated in Section 2.6.2, the recommended critical strain above which debonding is likely, ε_{fub}, will be determined from the recommendation of Teng et al. (2001), given here as equation 2.3. In equation 2.3, the factor accounting for bond length, k_L, given here as equation 2.5, is taken as 1 for all test specimens since $L_b >> L_{bmax}$. Additionally, cover delamination (end peel debonding) has been effectively mitigated in all specimens by extending the CFRP close to the support along the relatively long shear span. As currently recommended by the Task Group on Bond (2005) the value $\alpha = 0.9$ will be used in applying equation 2.3. Even though relatively

low compressive strength values were obtained from the concrete cylinders tested 28 days after casting (as compared to that found from cores), this 28-day compressive strength of 3384 psi (23.3 MPa), given in Table 3.1, was still used in the strain equation (equation 2.3). The design equation for maximum allowable strain, ε_{fub}, given by Teng et al. (equation 2.3) is plotted in Figure 4.3 for the three b_f/b ratios used in this study: 0.167, 0.333 and 0.667. Also plotted in Figure 4.3 is the current ACI (2002) equation for maximum allowable strain, ε_{fub}, (equation 2.1) which is solely a function of the CFRP stiffness, $E_f t_f$. The observed values of the strain in the CFRP at the initiation of debonding are plotted for comparison to the maximum allowable values of strain predicted by equation 2.1 and 2.3. As noted in Table 3.4, the L2 and L2x1 data points in Figure 4.3 (solid triangles) exhibited even higher ε_{fub} values than those shown since no debonding was observed in these tests. In these two cases, the strain plotted is the maximum CFRP strain observed in the respective tests.

For the values of strain at initiation of debonding (obtained in this study and shown in Figure 4.3) the following conclusions can be drawn:

1. The ACI equation is generally non-conservative, overestimating the strain where debonding becomes likely by two fold for the high modulus adhesive (open shapes) and less so for the low modulus adhesive.
2. The equation recommended by Teng et al., including the k_b term, appears to provide appropriately conservative estimates of debonding for the specimens having low modulus adhesive, although remains unconservative for the high modulus adhesive.

It would be possible to recalibrate the Teng et al. recommendation by adjusting the α term. If this were to be done, it would appear that the α would include a function accounting for adhesive stiffness.

Finally, it has been proposed within the ACI Task Group on Bond (2005) that the k_b term should be neglected since the observed FRP debonding failure engages only a thin layer of concrete and the assumption of lateral spreading is inappropriate. The presented data, although limited, indicates that it is appropriate to include a term in the strain equation accounting for b_f/b. The following section discusses this further.

4.3 FACTOR ACCOUNTING FOR RETROFIT GEOMETRY, k_b

The k_b factor is discussed in Section 2.6.3 and is given by various researchers as a function of the ratio of FRP width to substrate width b_f/b.

In Figure 4.4, the three k_b equations given by equations 2.7, 2.8 and 2.9 are normalized to the calculated values for the single 2" (51 mm) strip test specimens and compared with the observed debonding strain values also normalized to the single 2" (51 mm) strip test specimens. In Figure 4.4, the vertical "predicted" axis is defined as:

$$\frac{k_{bspecimen}}{k_{b2}}$$

where $k_{bspecimen}$ = the value of k_b calculated for the specimen considered

k_{b2} = the value of k_b calculated for H2 or L2 (as appropriate)

Similarly, the horizontal "observed" axis is defined as:

$$\frac{\varepsilon_{fubspecimen}}{\varepsilon_{fub2}}$$

where $\varepsilon_{fubspecimen}$ = the debonding strain for the specimen considered

ε_{fub2} = the debonding strain for H2 or L2 (as appropriate)

The trivial case of specimens L2 and H2 are not shown, although through this normalization the appropriateness of the k_b calculations may be assessed.

Extremely similar results were found for each of the three equations proposed for determining k_b. For Specimens L1 and H1, the observed trend is contrary to the predicted increase in debonding strain. For Specimens L4 and H4, however, the predictions underestimate the observed degradation of behavior resulting from the wider strips. Finally, the predictions of k_b are unable to differentiate between, and thus underestimate the beneficial effect, of using the L2x1 and H2x1 FRP arrangements as compared to the single strip of L2 and H2. This result indicates that the difference in debonding shear from specimen to specimen was actually greater than the ratio of k_b values would imply. Therefore, not only is the ratio of b_f/b (as represented by k_b) a contributing factor to bond behavior, its contribution may indeed be underestimated in some cases. The improved behavior of the 2x1 specimens also suggests that additional factors are also affecting this behavior. The contrary observations for Specimens L1 and H1 require further study but may indicate that there is an optimal value for the b_f/b ratio.

Assuming plane sections remain plane, specimens with the same gross CFRP strip width and the same modulus adhesive should behave similarly until debonding initiates. This comparison cannot easily be made with the L2 and L2x1 specimens as initiation of debonding in these specimens was not discernible from the data, but it can made with the H2 and H2x1 specimens where initiation of debonding was determined as described in Section 3.8. The load and deflection responses of these specimen pairs are shown in Figure 4.5. In the two graphs

(especially with the H specimens) it can be seen that that 2x1 specimens are the better performing of the $b_f/b = 0.333$ specimens.

Figures 3.19 and 3.24 show the strain data obtained laterally across the test specimens retrofitted with 4" (102 mm) strips. Figure 4.6 more clearly shows the lateral strain gradient at the maximum load, at the general yield deflection and at an arbitrarily selected load of 5 kips. The figure reports the strains on the east half of the CFRP north of the beam centerline and the strains on the west half of the CFRP south of the beam centerline (strain gauge diagrams for the L4 and H4 specimens are given in Figures 3.18, 3.19, 3.23 and 3.24). On both the north and south sets of strain gauges there is a gauge placed on the centerline, causing 2 points on the graph at the beam soffit centerline in Figure 4.6. Figure 3.24(a) clearly shows the difference in lateral strain 18" (457 mm) north of the midspan centerline. Up until the maximum CFRP strain is achieved, strains are seen to increase with distance away from the axial centerline, at a given loading. This is expected due to shear lag effects near the edges of the beam. There is a small difference in lateral strain 18" (457 mm) south of the midspan centerline (Figure 3.24(b)) as the strains remain rather uniform across the section throughout testing. The strains at this location however, contradict expected behavior as the strain gauge closest to the soffit edge reports the highest strains only for a small part of testing from about 5 kips (22 kN) to about 7.5 kips (33 kN). This specimen failed with debonding on the north end of the beam where the expected strain results were present. Only in some instances of Figure 4.6 can higher strain values be seen at the edges of the CFRP as expected. It is believed that the strain gauges were not placed close enough to the edge to truly capture shear lag behavior and thus further investigation is required.

Table 4.1 Analysis of Key Results Summary (as illustrated in Figure 4.2).

Specimen:	L1	L2	L2x1	L4	H1	H2	H2x1	H4
ratio of general yield load to control general yield load:	1.17	1.24	1.30	1.53	1.14	1.26	1.32	1.50
ratio of maximum load to control maximum load:	1.28	1.43	1.47	1.67	1.21	1.40	1.45	1.59
ratio of max load deflection to control max load deflection:	1.72	1.45	1.65	1.65	1.52	1.32	1.39	1.21
ratio of ductility deflection to control ductility deflection:	1.09	0.73	0.83	0.92	0.78	0.71	0.72	0.61

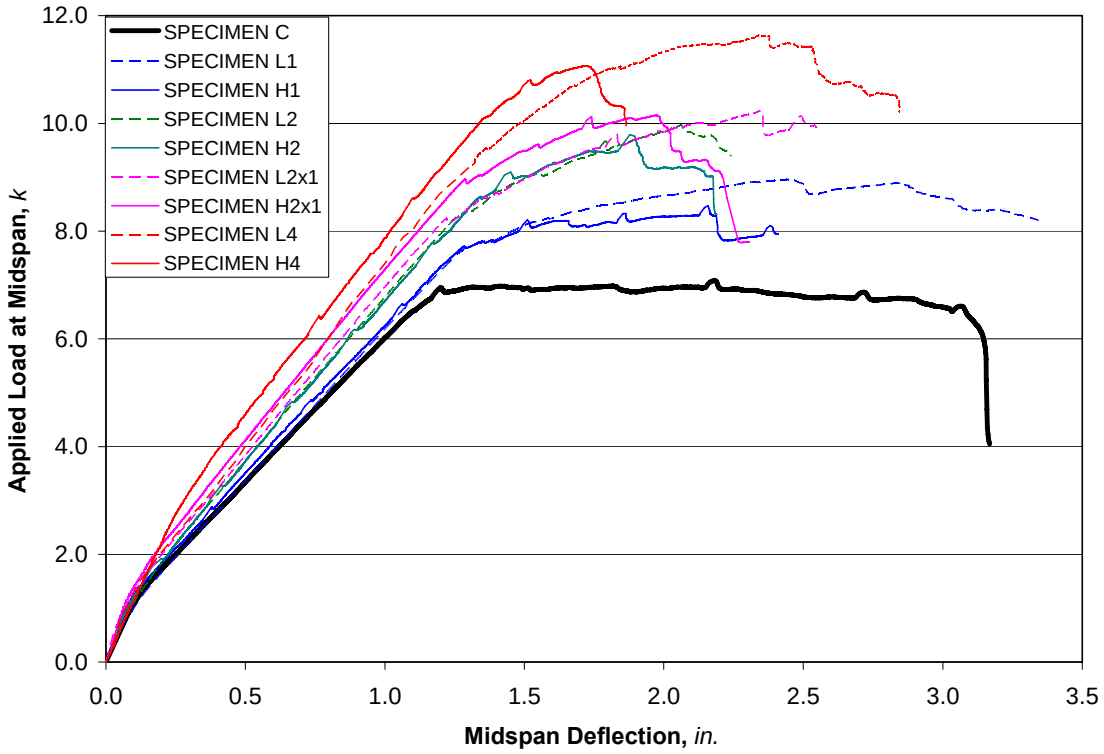

Figure 4.1 Load vs. Deflection for all test specimens.

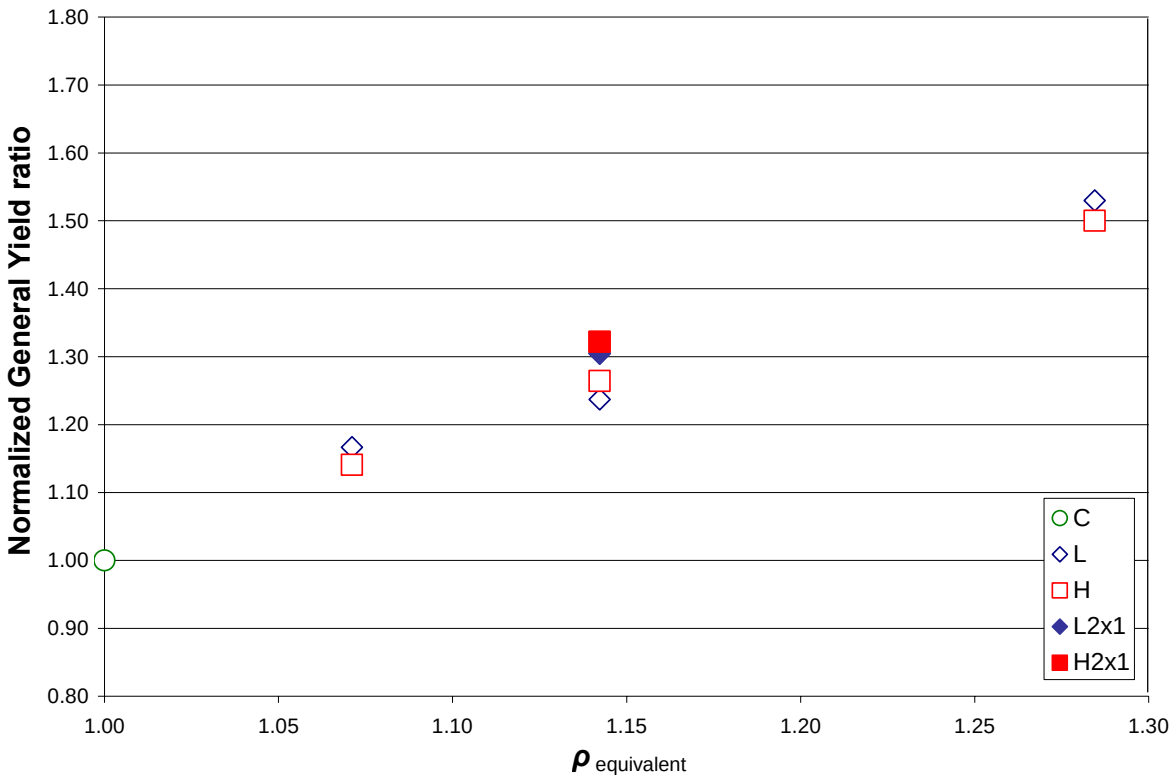

(a) Normalized General Yield ratio vs. Equivalent Steel Reinforcement ratio ($\rho_{equivalent}$).

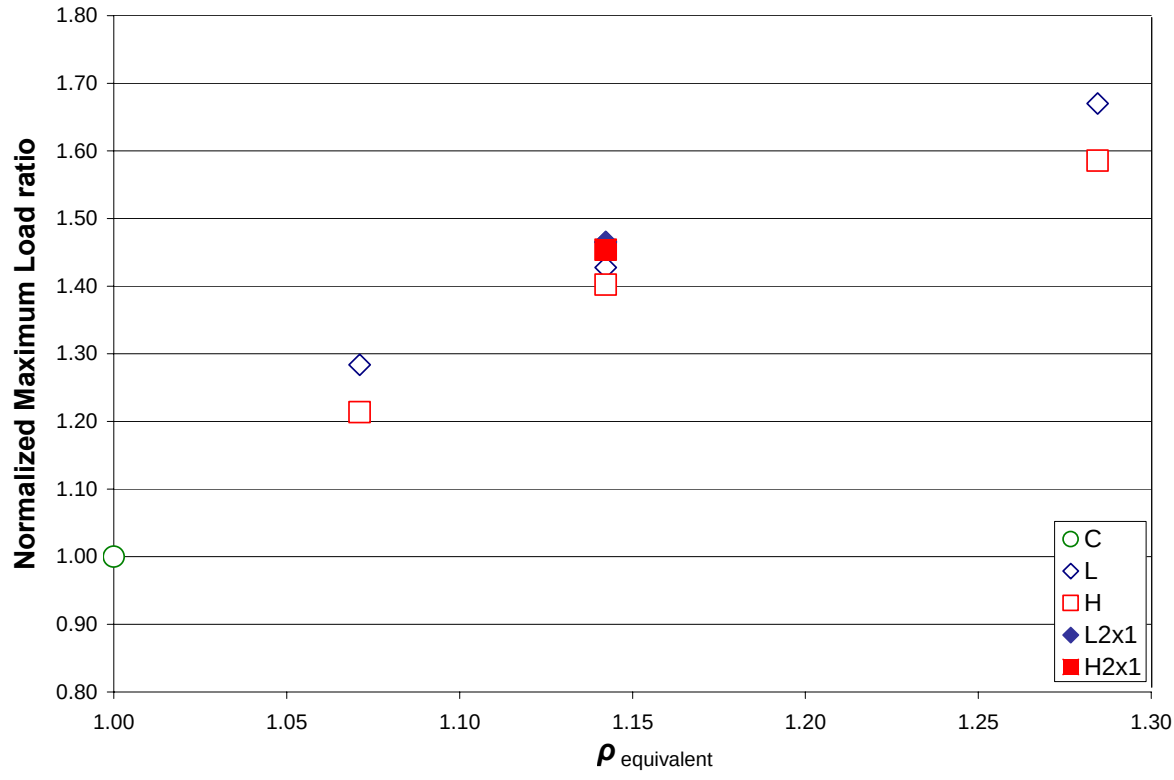

(b) Normalized Maximum Load ratio vs. Equivalent Steel Reinforcement ratio ($\rho_{equivalent}$).

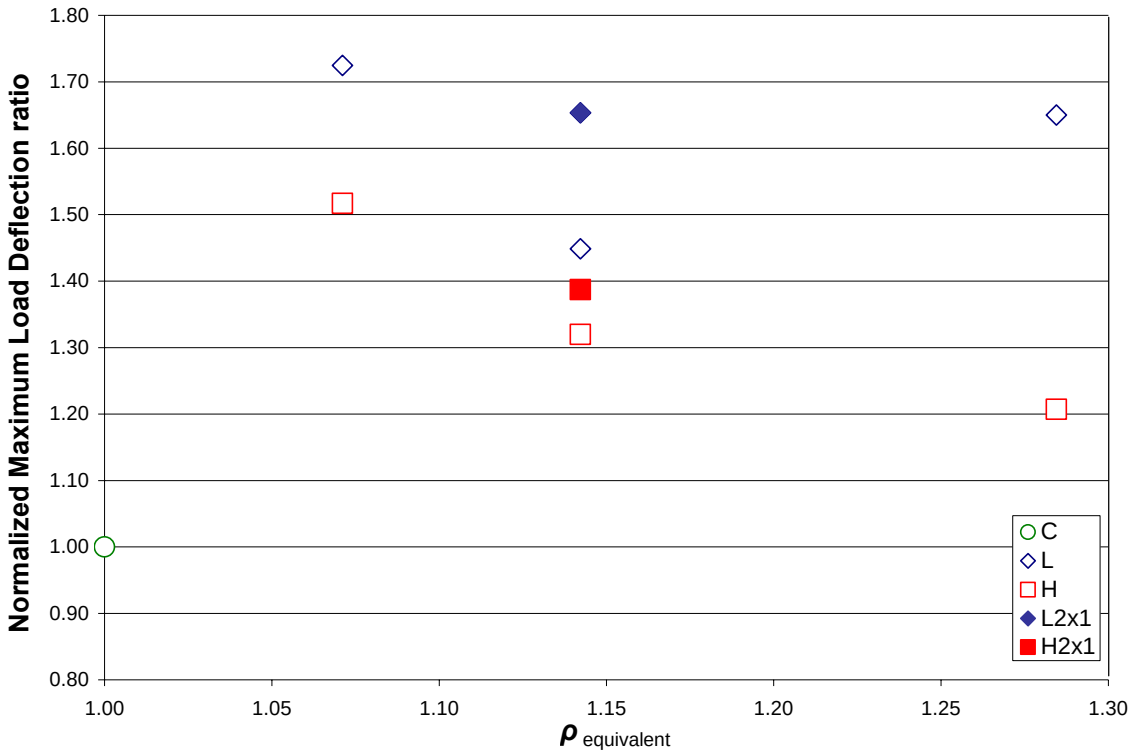

(c) Normalized Maximum Load Deflection ratio vs. Equivalent Steel Reinforcement ratio ($\rho_{equivalent}$).

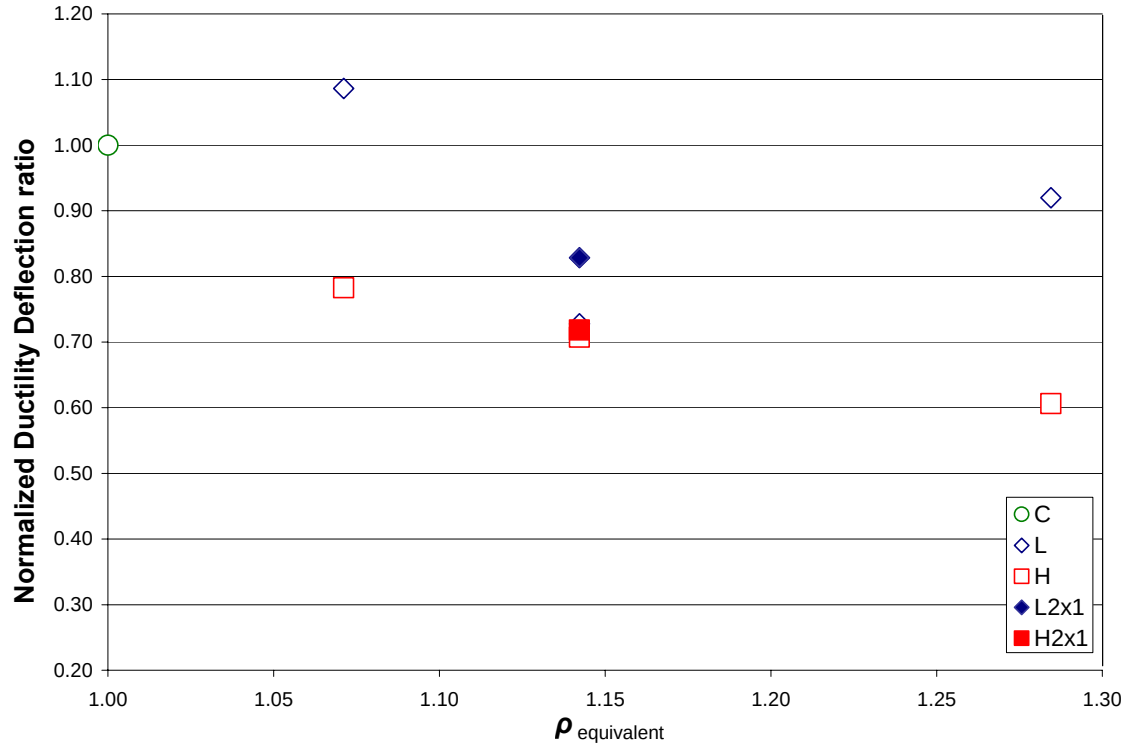

(d) Normalized Ductility Deflection ratio vs. Equivalent Steel Reinforcement ratio ($\rho_{equivalent}$).

Figure 4.2 Analysis of key results: ratio of retrofit test specimens to control specimen.

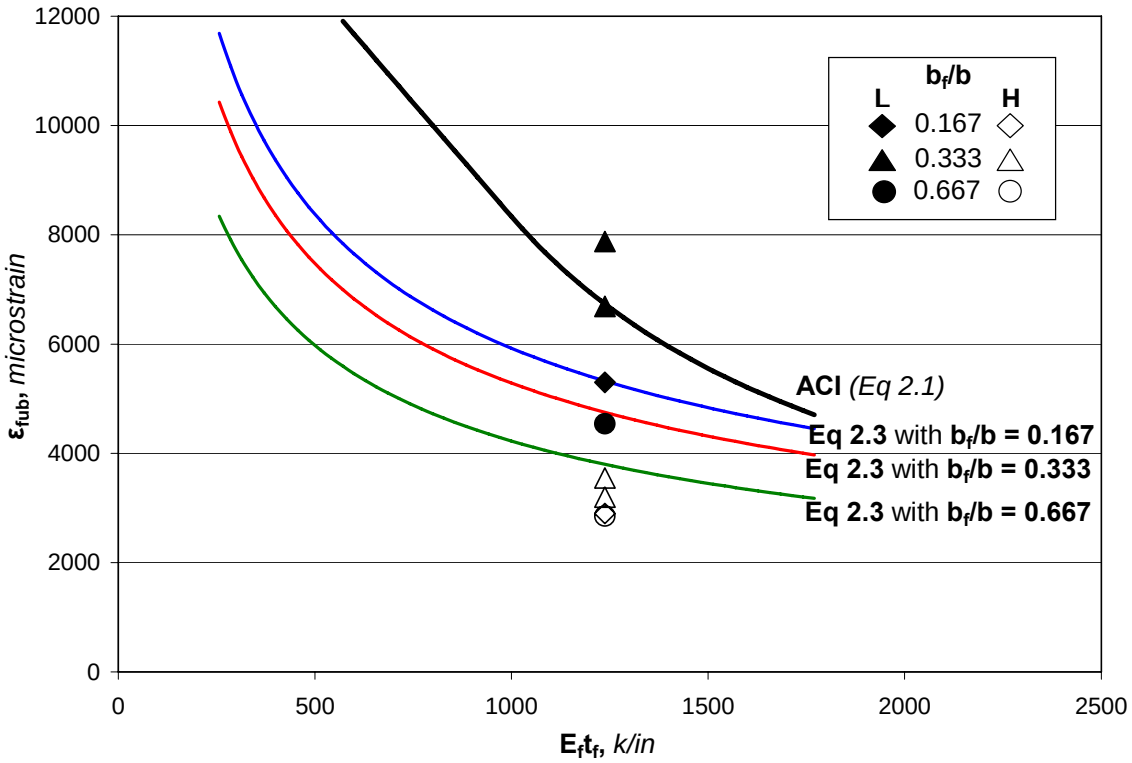

Figure 4.3 Observed strain vs. $E_f t_f$ for tested b_f/b values, compared with available strain equations.

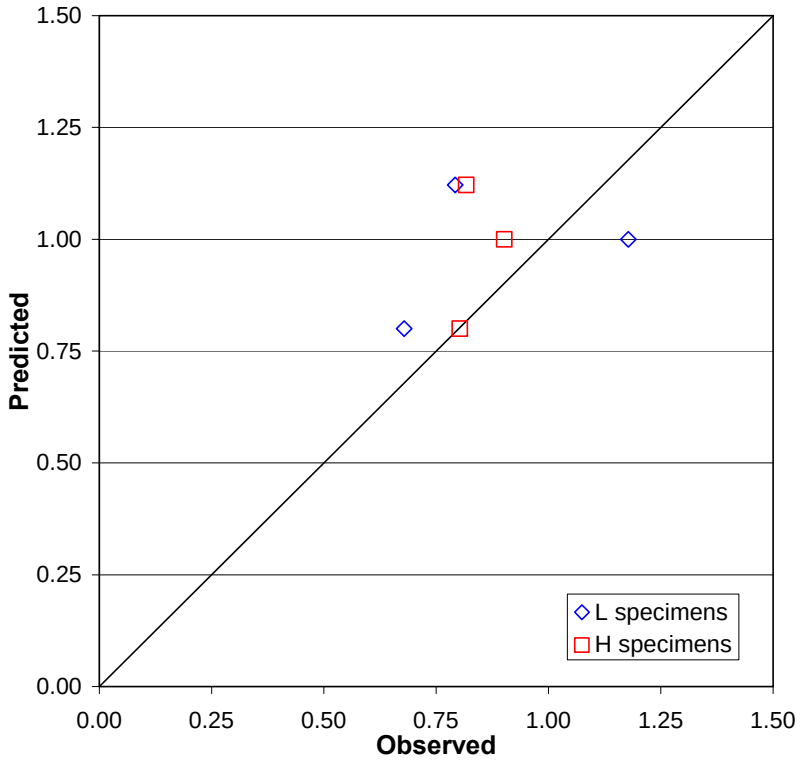

(a) Normalized effect of b_f/b based on Equation 2.7.

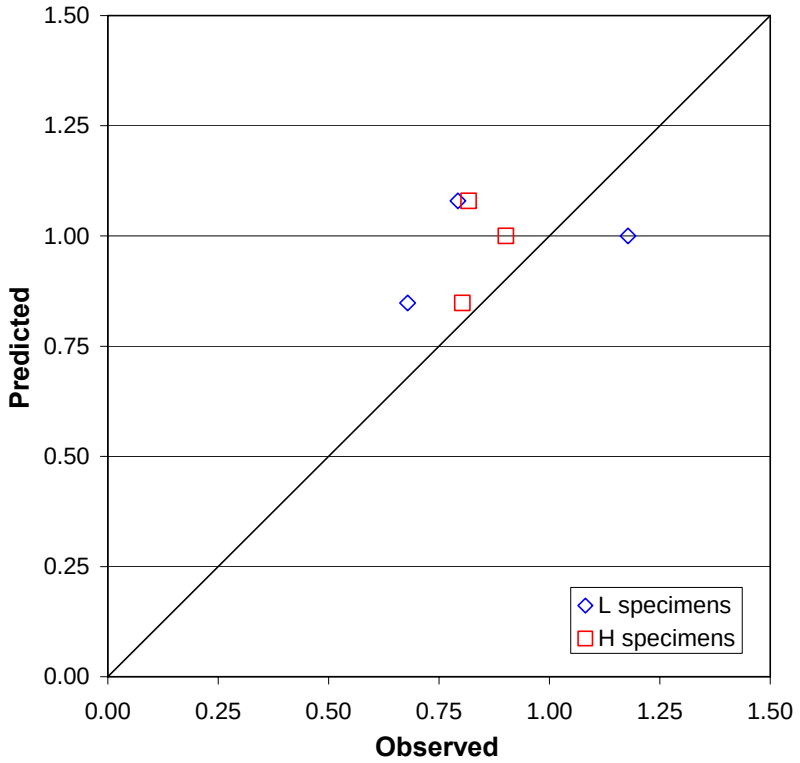

(b) Normalized effect of b_f/b based on Equation 2.8.

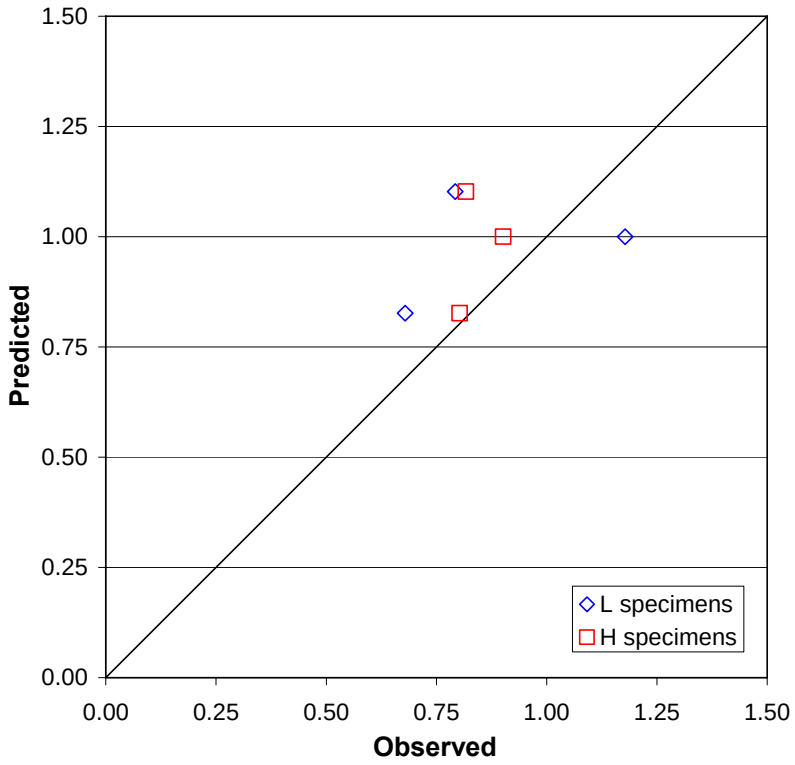

(c) Normalized effect of b_f/b based on Equation 2.9.

Figure 4.4 Normalized Predicted vs. Observed k_b-values.

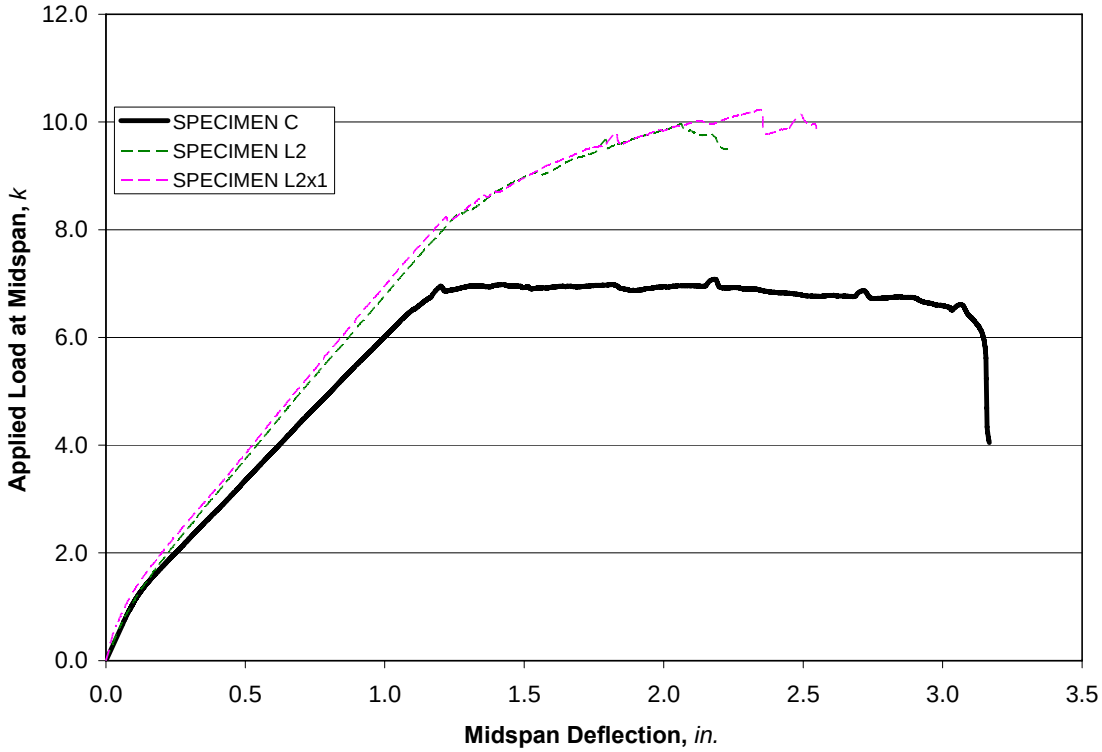

(a) Load vs. Deflection for L2 and L2x1 test specimens.

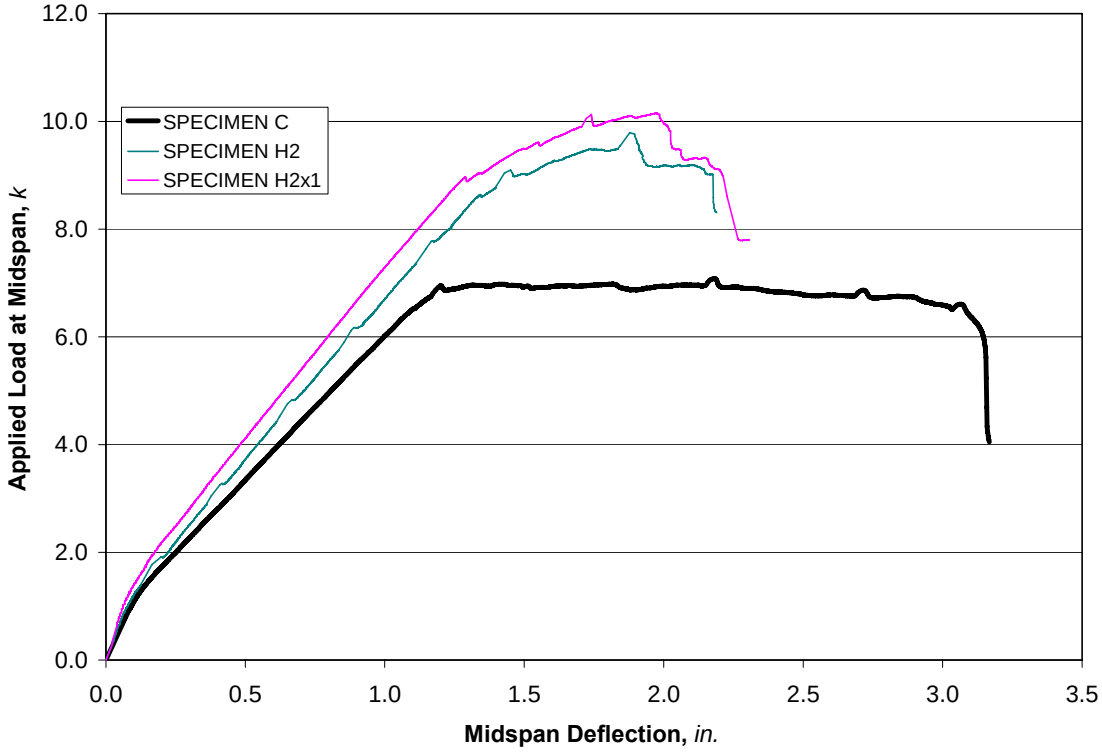

(b) Load vs. Deflection for H2 and H2x1 test specimens.

Figure 4.5 Comparison of b_f = 2" (51 mm) specimens.

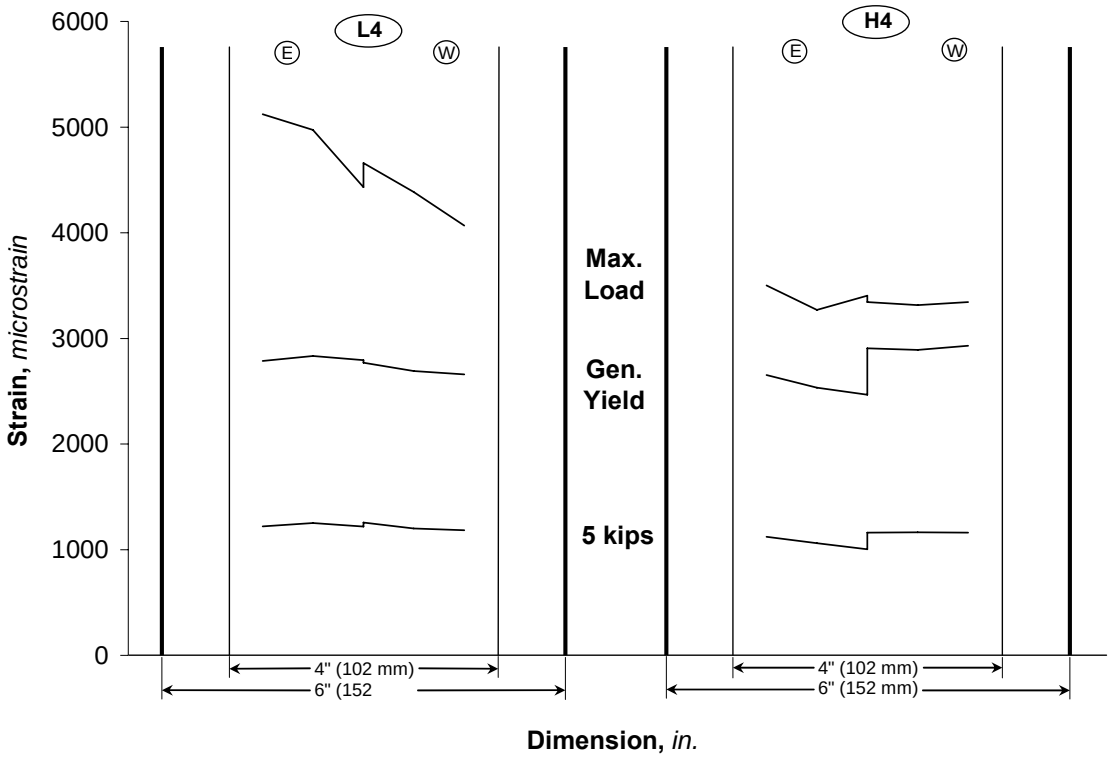

Figure 4.6 Beam Soffit Strain Gradients.

5.0 SUMMARY, CONCLUSIONS AND RECOMMENDATIONS

This chapter reports and discusses conclusions of the experimental program. A summary of the test procedure and continuing needs/areas for future work are also presented.

5.1 SUMMARY OF TEST PROGRAM

Nine test specimens were tested, each 10" (254 mm) deep, 6" (152 mm) wide and 186" (4730 mm) long. Eight beams were strengthened with various arrangements of carbon fiber reinforced polymer (CFRP) and one beam was left as an unretrofit control specimen (Specimen C). All beams had three #4 longitudinal steel reinforcing bars as primary flexural reinforcement resulting in a longitudinal tensile reinforcing ratio of 1.0%.

A commercially available 4" (102 mm) wide, 0.055" (1.4 mm) thick preformed unidirectional high strength carbon fiber (CFRP) strip system was used in this study. Additionally, two commercially available adhesives, with significantly different moduli, were used in this study. Material properties of the higher modulus adhesive system are typical of those traditionally used in such CFRP applications. The lower modulus adhesive had a modulus approximately half of that of the high modulus adhesive. Half of the retrofitted beams used the low modulus adhesive and the other half of the beams used the high modulus adhesive.

In order to investigate the effect of the CFRP strip width-to-soffit width ratio, b_f/b, four different strip arrangements were used. Each strip arrangement was installed using both the low

modulus adhesive and the high modulus adhesive. The CFRP strip was cut and applied in widths of 1" (25 mm), 2" (51 mm), and 4" (102 mm). The case of two 1" (25 mm) wide strips having a clear spacing of 2" (51 mm) was also tested. The CFRP strips were applied to the soffits (tension face) of all test specimens except the control test specimen. In all retrofit cases, the CFRP was extended over the entire beam span to just short of the supports.

Quality of adhesive bond to the concrete was assessed using a series of standard pull-off tests (ASTM D4541, 1995). In all cases the pull-off tests resulted in failure through the substrate concrete indicating a sound adhesive bond.

All nine specimens were tested monotonically to failure under mid-point bending. The test specimens were supported over a simply supported clear span of $178^{5}/_{8}$" (4537 mm). Each beam was instrumented with four electrical resistance strain gauges on the middle #4 reinforcing bar. The eight retrofitted beams had an additional four electrical resistance strain gauges placed on the CFRP at the same axial locations along the beam as the reinforcing bar strain gauges. The two beams retrofitted with 4" wide CFRP strips had an additional four strain gauges added across the width of the CFRP to investigate the distribution of strain transversely across the strip. The vertical deflection at midspan of test specimens and the applied midspan load were also recorded. Midspan displacement for these monotonic tests was controlled to travel from near 0 to 4" (102 mm) in 30 minutes, providing a constant deflection rate of 0.13" (3.4 mm) per minute.

5.2 CONCLUSIONS

All specimens tested in this program exhibited intermediate crack induced debonding behavior. The observed failures were generally bond-induced although concrete crushing was observed in all cases. The following conclusions have been drawn from this work:

1. Increased general yield and maximum loads (and therefore, increased flexural capacity) were observed with increasing CFRP retrofit material area (as measured by strip widths, b_f). The rate of increased capacity however, decreases with increasing CFRP area.
2. Related to the previous point, deflection capacity was observed to generally decrease with increasing CFRP retrofit widths, b_f.
3. For the two cases tested with $b_f/b = 0.333$, the 2x1 specimens showed greater maximum load capacity and also had greater deflection capacity indicating that the retrofit geometry has some influence on the overall retrofit performance and that multiple thinner strips may be preferable to fewer wider strips in terms of performance. Thus the FRP width-to-substrate width ratio, b_f/b, is shown to affect intermediate crack induced debonding behavior.
4. In general, higher general yield and maximum loads were observed in the less brittle, lower modulus of elasticity adhesive (L-specimens). Higher deflections were also found with the L-specimens at general yield and maximum loads.
5. The ACI equation intended to mitigate debonding failure by limiting the allowable strain in the FRP (the limiting strain is referred to as ε_{fub}) is generally non-conservative, overestimating the strain where debonding becomes likely by two fold for the high modulus adhesive and less so for the low modulus adhesive.
6. The equation for estimating ε_{fub} recommended by Teng et al. (2001), including the modifying k_b term, appears to provide appropriately conservative estimates of debonding for the specimens having low modulus adhesive although remains unconservative for the high modulus adhesive. This indicates that the nature of the adhesive should be included in the calculation of limiting strain.

7. Proposed values for the coefficient k_b which accounts for the b_f/b ratio were found to be inconsistent with the observed results. In some cases, the difference in debonding shear from specimen to specimen was actually greater than the ratio of k_b values would imply, in others a contrary trend was observed. Nonetheless, it appears that the ratio of b_f/b (as represented by k_b) is a contributing factor to bond behavior although other geometric parameters of the retrofit also contribute to the observed behavior.
8. Cover delamination (end peel debonding) was effectively mitigated in all specimens by extending the CFRP close to the support along the relatively long shear span.
9. Shear lag effects transversely across the CFRP strip were not observed with the instrumentation provided. Any such effect is therefore confined to the edge regions of the CFRP strip which were not instrumented in this study.

5.3 RECOMMENDATIONS

In practice, the higher modulus adhesive (H specimens) used in this study is close to what is generally recommended in the field for FRP application. This work has shown that the current ACI recommendation for calculating critical strain (ε_{fub}) is significantly unconservative when using such an adhesive. This observation leads to the following recommendations:

1. The more accurate equation proposed by Teng et al. (2001) be adopted for determining critical strain:

$$\varepsilon_{fub} = \alpha k_b k_L \sqrt{\frac{\sqrt{f_c'}}{E_f n t_f}} \tag{5.1}$$

2. The use of lower modulus adhesive systems, provided that they demonstrate sufficient bond strength, be promoted in bonded FRP applications.

Nonetheless, for use in a design context, Equation 5.1 requires proper calibration. The following recommendations are made in this regard:

3. It has been suggested that the k_b factor may be neglected for the case of intermediate crack induced debonding since this factor is understood to account for load spreading into the concrete and no such spreading is observed in an FRP delamination failure. The results of this study, however, indicate that there is an effect which may be attributed to the b_f/b ratio. The present factor accounting for this effect appears inadequate and further study is required to understand and quantify this effect.
4. In addition to b_f/b, the beneficial effect of a larger number of thinner strips making up b_f should be incorporated into the k_b factor.
5. The calibration of Equation 5.1 should recognize the contribution of adhesive stiffness. Further study over a wider range of adhesive properties is necessary to quantify this effect.

Other factors, some of which are discussed in Chapter 2, beyond those studied in the present work will also affect FRP delamination behavior. Thus significantly further study – to establish a sound data base of test results over a wide range of parameters – is required.

Finally, the activities of this study have shown that the determination and monitoring of debonding FRP is very difficult in the laboratory – and likely more difficult in the field. It is recommended that improved methods be developed to detect debonding. A pilot application of such a novel debond detection scheme was applied to Specimen L4 in the present study and is reported elsewhere (Kim et al., 2006).

REFERENCES

Ahmed, O., Van Gemert, D., Vandewalle, L. (2000). "Improved Model for Plate-End Shear of CFRP Strengthened RC Beams." *Cement and Concrete Composites 23* (2001), pp 3-19.

Aidoo, J. (2004) *Flexural Retrofit of Reinforced Concrete Bridge Girders Using Three CFRP Systems*, Ph.D. Dissertation, Department of Civil and Environmental Engineering, University of South Carolina, 197 pp.

Ali, M.S., Oehlers, D.J., Sung-Moo, P. (2001) "Comparison between FRP and Steel Plating of Reinforced Concrete Beams." *Composites: Part A 32*, pp1319-1328.

American Concrete Institute (ACI) Committee 440 (2002), *ACI 440.2R-02 Guide for the Design and Construction of Externally Bonded FRP Systems for Strengthening Concrete Structures*. 45 pp.

Brosens, K., Van Gemert, D. (2001) "Anchorage of externally bonded reinforcements subjected to combined shear/bending action." CICE2001, International Conference on FRP Composites in Civil Engineering, 12-14 Dec, 2001 Hong Kong.

Buyukozturk, O., Gunes, O., Karaca, E. (2004) "Progress on Understanding Debonding Problems in Reinforced Concrete and Steel Members Strengthened Using FRP Composites." *Journal of Construction and Building Materials*, Vol 18, pp. 9-19.

Concrete Society 2000. *Design Guidance on Strengthening Concrete Structures Using Fibre Composite Materials* Technical Report 55, The Concrete Society, London, 70 pp.

Federation Internationale du Beton (fib) (2001). *fib Bulletin 14: Externally Bonded FRP Reinforcement for RC Structures*.

Fyfe, 2005 Technical Product Data Sheet http://www.fyfeco.com/products/misc.html, accessed December 1, 2005.

Harmon, T.G., Kim, Y.J., Kardos, J., Johnson, T., Stark, A. (2003). "Bond of Surface-Mounted Fiber-Reinforced Polymer Reinforcement for Concrete Structures." *ACI Structural Journal* (Sept-Oct 2003), Title no. 100-S57, pp 557-564.

Harries, K.A., Harmon, Giurgiutiu (2003). "Collaborative Research – Debonding Behavior and Performance Assessment of Adhesively Bonded FRP Materials Using Multi-Method Instrumentation Scheme." *Outline of Proposed Collaborative Research Submission to NSF*.

International Concrete Repair Institute (1997). Concrete Surface Profile Chips. ICRI, Sterling, VA.

Japan Society of Civil Engineers (JSCE) (2001), *Recommendations for the Upgrading of Concrete Structures with use of Continuous Fiber Sheets*. Concrete Engineering Series 41,250 pp. (available in English on CD)

Kaminska, M.E. and Kotynia, R. (2000) Experimental Research on RC beams strengthened with CFRP strips, *Report No. 9*. Department of Concrete Structures, Technical University of Lodz. 55 pp.

Kim, S.D., In, C.W., Cronin, K., Sohn, H, and Harries, K.A. 2006. Active Sensing for Disbond Detection in FRP Strengthened RC Beams, *Proceedings of the 24th International Modal Analysis Conference (IMAC)*, St. Louis, Jan-Feb 2006.

Kotynia, R., Harries, K. A. (2006) "Strain Efficiency and Limit States of Externally Bonded and Near-Surface Mounted CFRP-Strengthened RC Members." *Composites B* (under review)

Kotynia, R. and Kaminska, M.E. (2003) Ductility and failure mode of RC beams strengthened for flexure with CFRP, *Report No. 13*. Department of Concrete Structures, Technical University of Lodz. 51 pp.

Maeda, T., Komaki, H., Tsubouchi, K., Murakami, K. (2002). "Strengthening Effect of Carbon Fiber Sheet Adhesion Method Using Flexible Layer." *Transactions of the Japan Concrete Institute*, Vol.23, pp185-192.

Mays, G.C., Hutchinson, A.R. (1992) *Adhesives in Civil Engineering*. Cambridge University Press.

Minnaugh, P. (2006). *Experimental Behavior of Steel Reinforced Polymer Retrofit Measures*. MS Thesis, University of Pittsburgh Department of Civil and Environmental Engineering, May 2006.

Mohamed Ali, M.S., Oehlers, D.J., Park, S. (2001) "Comparison between FRP and Steel Plating of Reinforced Concrete Beams." *Composites: Part A 32* (2001), pp 1319-1328.

Oehlers, D.J. (2001). "Development of Design Rules for Retrofitting by Adhesive Bonding or Bolting either FRP or Steel Plates to RC Beams or Slabs in Bridges and Buildings." *Composites: Part A 32* (2001), pp 1345-1355.

Quattlebaum, J.B., (2003). "Comparison of Three CFRP Flexural Retrofit Systems under Monotonic and Fatigue Loads." *MS Thesis*, Department of Civil and Environmental Engineering, University of South Carolina, Columbia, SC.

Saadatmanesh H., Ehsani, M.R. (1990). "Fiber Composites Can Strengthen Beams", *Concrete International*, 12(3), 65-71.

Sebastian, W.M. (2001). "Significance of Midspan Debonding Failure in FRP-Plated Concrete Beams." *Journal of Structural Engineering* (July 2001), pp792-798.

Sikadur, 2005 Technical Product Data Sheet, http://www.sikaconstruction.com/con/con-prod-name.htm#con-prod-Sikadur23LoModGel, accessed December 1, 2005.

Smith, S.T., Teng, J.G. (2000). "Interfacial Stresses in Plated Beams." *Engineering Structures 23* (2001), pp 857-871.

Smith, S.T., Teng, J.G. (2001). "FRP-Strengthened RC Beams. I: Review of Debonding Strength Models." *Engineering Structures 24* (2002), pp 385-395.

Smith, S.T., Teng, J.G. (2001). "FRP-Strengthened RC Beams. II: Assessment of Debonding Strength Models." *Engineering Structures 24* (2002), pp 397-417.

Task Group on Bond (2005). "Current Recommendations and Guidelines for Mitigating Debonding Failures in Adhesively Bonded, Externally Applied FRP Applications." *ACI 440F* (May 2005), Version 1.0, pp 2-12.

Teng, J.G., Smith, S.T., Yao, J. and Chen, J.F. 2001. Intermediate Crack Induced Debonding in RC Beams and Slabs, *Construction and Building Materials*, Vol. 17, No. 6-7, pp 447-462.

Teng, J.G., Lu, X.Z., Ye, L.P. and Jiang, J.J. 2004. Recent Research on Intermediate Crack Induced Debonding in FRP Strengthened Beams, *Proceedings of the 4th International Conference on Advanced Composite Materials for Bridges and Structures*, Calgary 2004.

Timoshenko, S. P., and Goodier, J. N. (1987 reissue). *Theory of Elasticity, 3rd Edition*.

Yuan, H., Wu, Z., Yoshizawa, H. (1999). "Theoretical Solutions on Interfacial Stress Transfer of Externally Bonded Steel/Composite Laminates." *Structural Eng/Earthquake Eng JSCE* (2001), Vol. 18, No. 1, pp 27-39.

Wan, B., Sutton, M., Petrou, M.F., Harries, K.A., and Li, N. (2004) Investigation of Bond between FRP and Concrete Undergoing Global Mixed Mode I/II Loading, *ASCE Journal of Engineering Mechanics*, Vol. 130 No. 12 pp 1467-1475.

Zorn, A. (2006). *Effect of Adhesive Stiffness and CFRP Geometry on the Behavior of Externally Bonded CFRP Retrofit Measures Subject to Fatigue Loads*. MS Thesis, University of Pittsburgh Department of Civil and Environmental Engineering, May 2006.